TECHNICAL REPORT STANDARD TITLE PAGE

1. Report No.	2. Government Accession No.	3. Recipient's Catalog No.
FHWA/IN/JTRP-2003/5		

4. Title and Subtitle	5. Report Date
Simplified Shear Design of Prestressed Concrete Members	August 2003
	6. Performing Organization Code

7. Author(s)	8. Performing Organization Report No.
Robert J. Frosch and Tyler S. Wolf	FHWA/IN/JTRP-2003/5

9. Performing Organization Name and Address	10. Work Unit No.
Joint Transportation Research Program 1284 Civil Engineering Building Purdue University West Lafayette, IN 47907-1284	
	11. Contract or Grant No. SPR-2798

12. Sponsoring Agency Name and Address	13. Type of Report and Period Covered
Indiana Department of Transportation State Office Building 100 North Senate Avenue Indianapolis, IN 46204	Final Report
	14. Sponsoring Agency Code

15. Supplementary Notes

Prepared in cooperation with the Indiana Department of Transportation and Federal Highway Administration.

16. Abstract

Design methods for the shear resistance of reinforced and prestressed concrete beams are based on empirical evidence. Due to different approaches in their development different equations are used to calculate the shear strength of reinforced and prestressed concrete. Recent research conducted by Tureyen has proposed a simplified shear model for reinforced concrete which is primarily based upon mechanics and corresponds well with a wide range of test results. The objective of this research was to determine the applicability of the shear model to prestressed concrete.

The applicability of the shear model was evaluated by a comparison of its results with the results of a database of 84 specimens which failed in shear. This analysis indicated that the shear model is applicable to prestressed sections. The shear model was simplified to develop an equation which is suitable for design office use. This equation is consistent with that proposed by Tureyen for reinforced concrete and unifies the design of these sections. As most prestressed sections designed are either T or I in shape, the research also investigates the use of the simplified design equation for these sections. Based on a comparison with test results, it is shown that the simplified design equation works well and provides a consistent factor of safety.

A design example is presented to illustrate the differences between the proposed design equation and the current ACI 318 and AASHTO 16th Edition provisions. Differences resulting from the different design methods are highlighted and discussed. As the proposed design equation requires calculation of the neutral axis depth, a simple hand-calculation procedure is also developed to approximate this value for prestressed sections. Finally, recommendations are provided for the proper implementation of the proposed method in design practice.

17. Key Words	18. Distribution Statement
prestressed concrete, reinforced concrete, shear, shear strength, structural concrete.	No restrictions. This document is available to the public through the National Technical Information Service, Springfield, VA 22161

19. Security Classif. (of this report)	20. Security Classif. (of this page)	21. No. of Pages	22. Price
Unclassified	Unclassified	94	

Form DOT F 1700.7 (8-69)

Final Report

FHWA/IN/JTRP-2003/5

SIMPLIFIED SHEAR DESIGN OF PRESTRESSED CONCRETE MEMBERS

By

Robert J. Frosch
Principal Investigator
Professor of Civil Engineering

and

Tyler S. Wolf
Graduate Research Assistant

School of Civil Engineering
Purdue University

Joint Transportation Research Program
Project No. C-36-58EE
File No. 5-13-5
SPR-2798

Conducted in Cooperation with the
Indiana Department of Transportation
and the
Federal Highway Administration

Purdue University
West Lafayette, IN 47907
August 2003

TABLE OF CONTENTS

LIST OF TABLES

LIST OF FIGURES

ACKNOWLEDGEMENTS

This work was supported by the Joint Transportation Research Program (JTRP) administered by the Indiana Department of Transportation (INDOT) and Purdue University through contract SPR-2798. The support of the Indiana Department of Transportation (INDOT) and the Federal Highway Administration (FHWA) are thankfully recognized. The authors would like to thank Dr. Tommy Nantung from the INDOT Division of Research for serving as the project administrator. In addition, thanks are extended to John Jordan and Keith Hoernschemeyer for their participation and thoughtful comments throughout this project as members of the Study Advisory Committee.

NOTATION

A	=	area of concrete cross-section, in^2
A_c	=	area of concrete cross-section resisting shear transfer, in^2
A_{eff}	=	effective area to resist shear, in^2
A_s	=	area of steel, in^2
b	=	width of section, in.
$b_{eff,v}$	=	effective flange width, in.
b_w	=	web width, in.
b_i	=	width of cross-section at location of slice, in
c	=	distance from extreme compression fiber to neutral axis depth, in.
c_{npt}	=	distance from extreme compression fiber to neutral axis depth calculated as if the section were not prestressed, in.
d	=	distance from extreme compression fiber to centroid of longitudinal tension reinforcement, in.
e	=	distance from the centroid of the tension reinforcement to the centroid of the cross-section, in.
E_c	=	modulus of elasticity of concrete, psi
E_r	=	modulus of elasticity of reinforcement, psi
E_s	=	modulus of elasticity of steel, psi
f_c'	=	specified compressive strength of concrete, psi
f_{pc}	=	compressive stress in concrete (after allowance for all prestress losses) at centroid of cross section resisting externally applied loads or at junction of web and flange when the centroid lies within the flange, psi
f_{pe}	=	compressive stress in concrete due to effective prestress forces only (after allowance for all prestress losses) at extreme fiber of section where tensile stress is caused by externally applied loads, psi
f_{per}	=	bottom fiber stress ratio
	=	f_{pe} / f_c'
f_{ps}	=	stress in prestress strand, psi
f_{pe}	=	effective prestress force, psi

f_t = tensile strength of concrete, psi

H = overall height of a given section, in.

jd = distance between the resultants of the internal compressive and tensile forces on a cross section, in.

K = modifier of $\sqrt{f_c'}$, which represents the critical average shear stress

M_{cr} = moment causing flexural cracking at section, in.-lb

M_{max} = maximum factored moment at section due to externally applied loads, in.-lb

P = effective prestress force, lb

= $A_s f_{se}$

n = modular ratio

= E_r / E_c

S_b = section modulus with respect to the bottom fiber of a cross section, in^3

t_f = flange thickness, in.

ν = multiple of the cracking moment

V_c = nominal shear strength provided by concrete, psi

V_{calc} = calculated nominal shear strength, lb

V_{ci} = nominal shear strength provided by concrete when diagonal cracking results from combined shear and moment, lb

$V_{ci,equation}$ = nominal shear strength based upon neutral axis calculated using Equation 5.4, lb

V_{cw} = nominal shear strength provided by concrete when diagonal cracking results from excessive principal stress in web, lb

V_d = shear force at section due to unfactored dead load, lb

V_{flex} = shear force which would cause a flexural failure, lb

V_i = factored shear force at section due to externally applied loads occurring simultaneously with M_{max}, lb

V_{ih} = Shear transferred at a horizontal slice, lb

V_n = nominal shear strength, lb

V_p = vertical component of effective prestress force at section, lb

V_{test} = shear force that failed specimen, lb

α = integer to modify the effect of the applied moment

β = constant to modify t_f

γ = constant to modify b_w

Δx = length of cross-section above a crack, in.

ε = strain

ε_0 = strain to define the secant modulus of elasticity

ε_s = steel strain

λ = modifier of $c_{elastic}$ which accounts for prestressing level and applied moment

ρ = reinforcement ratio

= A_s / bd

ρ_{eff} = effective reinforcement ratio

= $\rho E_r / E_s$

σ = flexural stress, psi

σ_i = flexural stress at the location of a horizontal cut, psi

$\sigma_{\max}$ = maximum flexural stress on the compression zone, psi

σ_s = steel stress, psi

τ = shear stress, psi

τ_{avg} = average shear stress on the compression zone, psi

= V / bc

τ_{cr} = shear stress at which tensile failure occurs, psi

τ_i = shear stress at the location of a horizontal cut, psi

θ = angle from vertical accounting for flange contribution, degrees

ζ = total effective overhang, in.

CHAPTER 1
INTRODUCTION

1.1 General

The behavior of structural concrete beams subjected to shear has been investigated since the advent of reinforced concrete. Due to the number of variables involved, a general shear theory has been evasive. Consequently, design has been based on empirical evidence. This basis has provided a multitude of design equations for the design of structures in shear. For instance, the ACI 318 Building Code (ACI 318-02) provides five different equations to evaluate the concrete contribution to shear resistance, V_c, for nonprestressed members and three different equations to evaluate V_c for prestressed members. To calculate V_c according to the AASHTO design specifications is dependant on the version of specifications used. In general, the 16th edition (AASHTO 1998) conforms to the ACI building code. However, the AASHTO LRFD (AASHTO LRFD 2002) bridge design specifications have introduced substantially different provisions for shear design and produced a new method that designers must consider.

The AASHTO LRFD specifications are based on the Modified Compression Field Theory (MCFT) and on Strut-and-Tie modeling. There are advantages to the LRFD method, such as unified treatment of nonprestressed reinforced members and prestressed members. However, the LRFD provisions have been identified as being complex, requiring time-consuming iterations, producing illogical answers in some situations, and providing excessive amounts of reinforcement for certain cross-sections (NCHRP 2002). ACI 318 and AASHTO 16th edition, while generally providing ease in calculation, have also been identified as having many shortcomings including lack of conservatism for lightly reinforced cross-sections, for sections utilizing high strength concrete (Tompos 2000; Tureyen and Frosch 2002), and large sections (Reineck et al. 2003).

1.2 Mechanisms of Shear Transfer

One of the primary reasons a unified shear strength calculation procedure has yet to be developed is the complexity of the resistance mechanics involved. There are many factors that contribute to the strength of structural concrete, and it is difficult to determine the contribution of each component. There has been considerable disagreement regarding these components and their contribution to shear resistance. ACI-ASCE Committee 445 (Committee 445 1998) discusses the six main shear resistance components which are currently considered.

a) *Uncracked Concrete and Flexural Compression Zone:* Shear force can be transferred through the uncracked compression zone by inclined principal tensile and compressive stresses. Integrating the shear stress distribution over the uncracked compression zone provides the shear resistance of the uncracked portion of the section.

b) *Interface Shear Transfer:* Also known as aggregate interlock, it is the force caused by aggregate protruding from the crack surface preventing relative slippage of the concrete sections. The protruding aggregate provides friction while normal forces prevent relative slippage of the concrete sections.

c) *Dowel Action of Longitudinal Reinforcement:* Along with a tensile force, longitudinal reinforcement provides a vertical force preventing slippage of the concrete sections. Dowel action, however, is limited by the tensile strength of the concrete cover containing the reinforcement.

d) *Residual Tensile Stresses across Cracks:* After a crack has formed in a beam, all of the concrete in the plane of the crack has not lost its ability to resist tension. Concrete can bridge small cracks and still provide some tensile strength across the crack width. ACI-ASCE Committee 445 indicates that these forces can exist until cracks exceed widths of 0.002-0.006 in. (0.05-0.15 mm).

e) *Arch Action:* When the geometry of the beam and placement of the load allow, the force from the load may transmit directly from the point of application to the reaction of the beam. This direct compression strut, coupled with the longitudinal reinforcement, creates tied arch action which helps resist shear. Arch action is primarily prevalent in beams with shear span to beam depth (a/d) ratios less than 2.5. When arch action does not contribute to shear resistance, shear is considered to be transferred by "beam action".

f) *Web Reinforcement:* Transverse reinforcement, called stirrups, resist shear by traversing cracks. Web reinforcement not only resists shear, but also prevents cracks in the concrete from extending. When the concrete cannot carry tension, due to a crack, the web reinforcement solely transfers the shear across the crack.

1.3 Modes of Failure

The most common method to determine the mode of a beam failure is by observing the crack patterns during and after loading. These crack patterns reveal the shear flow to the reaction. The mode of failure is a function of many different variables dependant on a specific beam. Documentation of experimental data (Sozen, Zwoyer and Siess 1959; Tompos 2000) has listed these four categories as the most common modes of failure.

a) *Flexure-Compression (FC):* Flexure-compression failures are the result of having a beam with higher shear strength than flexural strength. Failure occurs at the point of maximum flexural stress where the compressive strain exceeds its capacity.

b) *Flexure-Shear (FS):* A flexure-shear failure, shown in Figure 1.1, is the result of a crack which begins as a flexural crack, but as shear increases, the crack begins to

"turn over" and incline towards the loading point. Failure finally occurs when the concrete separates and the two planes of concrete slide past one another. This mode of failure is common in beams which do not contain web reinforcement.

Figure 1.1: Flexure-Shear Failure

c) *Shear-Compression (SC):* Shear compression failures, shown in Figure 1.2, typically occur in beams which contain adequate web reinforcement. In this mode, the crack propagates through the section until it begins to penetrate the compression zone. This crack causes a redistribution of compressive forces in the compression zone onto a smaller area. When the compressive strength is exceeded, a shear compression failure occurs. This type of failure is common in deep beams, where arch action is prevalent. The compressive strut caused by arch action prevents a diagonal tension crack from propagating into the compression zone.

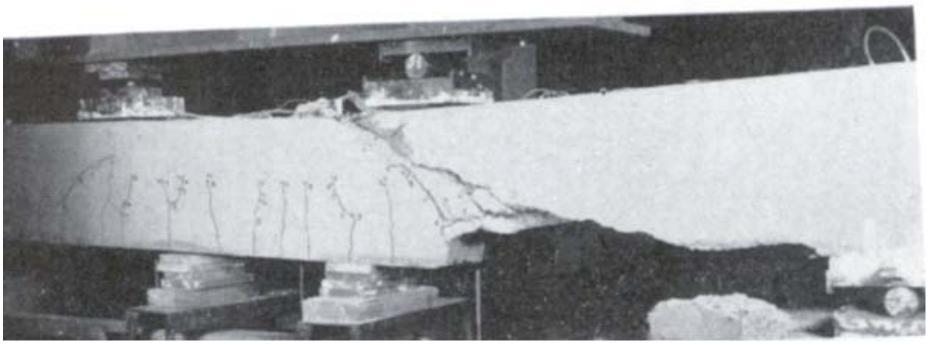

Figure 1.2: Shear-Compression Failure (Sozen, Zwoyer and Siess 1959)

d) *Web-shear (WS):* Before a section cracks from flexure, it is possible to exceed the tensile strength of the concrete at the point of maximum shear stress. This mode is primarily observed in sections with thin webs. Failure occurs at the

location of peak shear stress, as shown in Figure 1.3. While, the mechanics of this failure are identical to flexure-shear, failure is brittle and occurs with little or no warning.

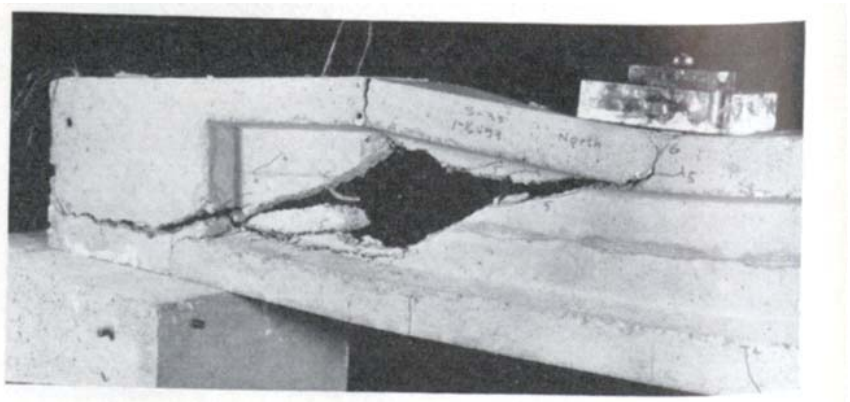

Figure 1.3: Web-shear Failure (Sozen, Zwoyer and Siess 1959)

1.4 Factors Influencing Shear Strength

There are many factors which influence the shear strength of concrete. Some of these variables are currently taken into account in the ACI Building Code and in the AASHTO 16th edition while some are not directly considered.

a) *Axial Force:* Shear failures are commonly due to tensile failure of the concrete. While axial compression can delay the onset of critical tension in the section, axial tension can hasten the failure. Compression, such as provided by an axial force or prestressing tendons, provides an increase in shear strength.

b) *Tensile Strength of Concrete:* The interaction between shear and flexural stresses causes diagonal tension in a concrete cross-section. When the tensile stresses exceed the tensile strength of concrete, shear cracks occur. Therefore, as the tensile strength of the concrete is increased, there is a corresponding increase in the shear strength of the section. The tensile strength of the concrete is commonly related to the square root of the compressive strength, $\sqrt{f_c'}$, as shown in Figure 1.4.

c) *Longitudinal Reinforcement Ratio (r):* The longitudinal reinforcement ratio can affect shear strength in several ways. A low amount of steel may result in wider flexural cracks, resulting in reduced dowel action and aggregate interlock. Each of these factors can decrease the shear strength of the section. High values of r require a larger compression zone, raising the amount of shear which can be transferred by the uncracked concrete shear transfer mechanism, thus increasing shear strength (Committee 445 1998).

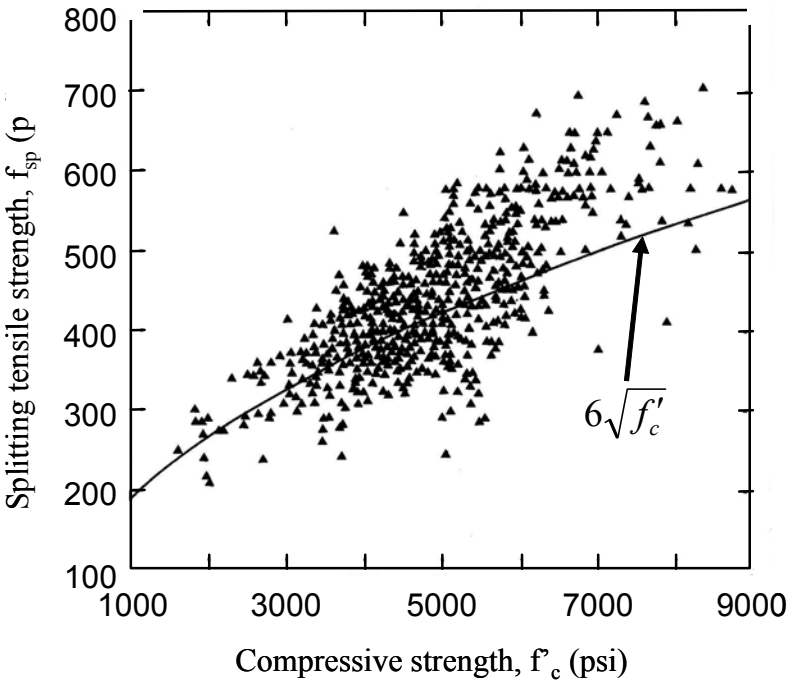

Figure 1.4: Split Test Results (MacGregor 1997)

d) *Shear Span-to-Depth Ratio (a/d)*: When the a/d ratio is less than approximately 2.5, the presence of arch action can increase the shear strength of a section. As this ratio grows larger, beam action is more likely to occur. As the a/d ratio continues to increase, the likelihood of a flexural failure increases. Large a/d ratios also cause cracks to become wider, making it more difficult to transfer shear across cracks via aggregate interlock and dowel action, thus decreasing shear strength (Committee 445 1998).

1.5 Design Methods

1.5.1 ACI-318 and AASHTO 16th Edition

Currently the ACI Building Code (ACI 318-02) and AASHTO 16th edition Specifications use the same methods for computing shear strength for both nonprestressed and prestressed members. For simplicity, ACI 318 will be used to refer to both of these specifications.

a) Reinforced Concrete:

1) *Shear Strength:* Although there are several equations used to design reinforced concrete for shear, the most commonly used equation is given by Equation 1.1 (ACI 318 Equation 11-3).

$$V_c = 2\sqrt{f_c'}b_w d \qquad \text{(Eq. 1.1)}$$

where:

f_c' : compression strength of concrete, psi

b_w: web width, in.

d: effective depth of cross-section, in.

Equation 1.1 was empirically derived from tests of reinforced concrete sections. The value $2\sqrt{f_c'}$ is the design average shear stress $\left(V/bd\right)$ of the concrete.

b) *Prestressed Concrete:*

1) *Web-shear*: The equation for web-shear strength, V_{cw}, is given in Equation 1.2 (ACI 318 Equation 11-12).

$$V_{cw} = (3.5\sqrt{f_c'} + 0.3f_{pc})b_w d + V_p \qquad \text{(Eq. 1.2)}$$

where:

f_{pc} : compressive stress at the centroid of the section resisting externally applied loads, psi

V_p : vertical component of effective prestressing force at section, lb

This equation was derived using a principal stress analysis of an uncracked section. Principal stresses are used to calculate the shear stress which causes a tensile failure in the concrete section. Using basic mechanics, the shear force which causes this shear stress is determined. This shear force is taken as the capacity of the concrete section. ACI 318 also discusses an alternative method to calculate web-shear strength using a principal stress analysis directly and a tensile strength limit of $4\sqrt{f_c'}$.

2) Flexure-Shear: Currently there are two equations in ACI 318 to calculate the flexure-shear strength of prestressed members. The most commonly used flexure-shear strength equation for prestressed concrete is shown in Equation 1.3 (ACI 318 Equation 11-10).

As explained in the ACI 318 commentary, the $V_i M_{cr}/M_{\max}$ term is the load required to cause a flexural crack at the point in question. The first term of the equation is the increment in shear which causes the flexural crack to turn over into a flexure-shear crack.

$$V_{ci} = 0.6\sqrt{f_c'}b_w d + V_d + \frac{V_i M_{cr}}{M_{\max}} \geq 1.7\sqrt{f_c'}b_w d \qquad \text{(Eq. 1.3)}$$

where:

V_d: shear force at section due to unfactored dead load, lb

V_i: factored shear force at section due to externally applied loads occurring simultaneously with $M_{\max}$, lb

M_{cr}: moment causing flexural cracking at section due to externally applied loads, lb-ft

$M_{\max}$: maximum factored moment at section due to externally applied loads, lb-ft

1.5.2 AASHTO LRFD

Recently, the AASHTO LRFD specifications adopted the Modified Compression Field Theory (MCFT) to calculate the shear strength of concrete. An advantage of the MCFT is its applicability to reinforced concrete as well as prestressed concrete. The MCFT examines average stresses, as well as local concrete and steel stresses, at crack locations. The angle of cracking in the section is assumed to be uniform and the uncracked concrete between these cracks is analyzed. In addition, contribution of aggregate interlock to shear strength is also quantified as a mechanism of shear transfer. Using compatibility and equilibrium relationships, this method calculates the shear strength of the section. Whereas, the original Compression Field Theory (CFT) ignored the residual tension stresses in the concrete, the Modified Compression Field Theory (MCFT) takes these stresses into account. MCFT considers these multiple mechanisms of shear transfer in the calculation of shear strength.

1.6 Current Design Expression Limitations

1.6.1 ACI and AASHTO 16th Edition

As evident from review of these shear design equations, the equations for reinforced and prestressed concrete are considerably different. These differences are due to the empirical nature of their development. Several limitations have been recently observed with the ACI 318 method of calculating shear strength for reinforced concrete sections. Experimental evidence has indicated that the method used by ACI 318 for nonprestressed sections can overestimate the shear strength of sections with low reinforcement ratios, high strength concrete, and large effective depths. When this method was derived, it was based on test data which did not include cross-sections of these types. Similarly, the equations for calculating shear strength of prestressed members are also based on empirical data. Therefore, extrapolation of these equations to conditions outside of the data used in their development is questionable.

1.6.2 AASHTO LRFD

The AASHTO LRFD shear design provisions have been identified as being complex; requiring time-consuming iteration, producing illogical answers in some

situations, and providing excessive amounts of reinforcement for certain cross-sections (NCHRP 2002). It also assumes a uniform cracking angle, which does not agree with data from past tests.

1.7 Recent Findings

For the calculation of shear strength, ACI 318 uses an effective area of $b_w d$ for the area in which shear is resisted. Figure 1.5(a) illustrates a beam which has formed flexure cracks during loading. Figure 1.5(b) shows a close-up of the hatched portion shown in 1.5(a) located between two cracks. In this figure, the tensile stress in the concrete below the neutral axis is ignored and the entire tensile force is provided by the reinforcement. If horizontal slices are taken along the depth of this section, the shear stress diagram shown in Fig. 1.5(c) is generated. This shape can be approximated as rectangular, considering a uniform shear over the depth of the beam, as shown in Figure 1.5(d). The effective area, $b_w d$, used in ACI-318 and AASHTO 16th edition was derived using this process.

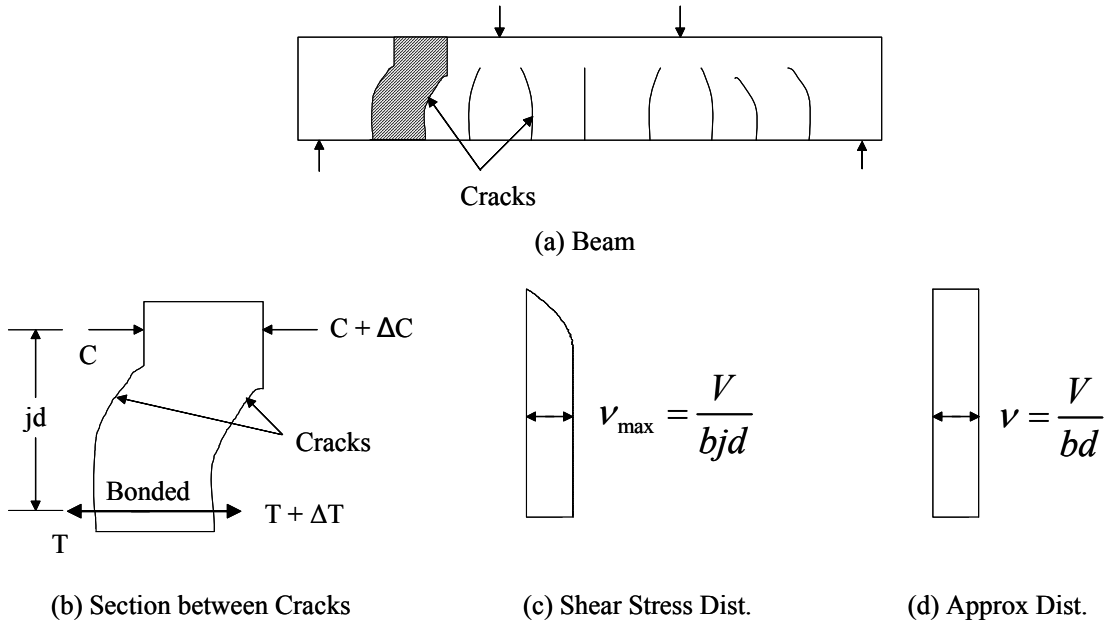

Figure 1.5: Shear Area Derivation

1.7.1 Shear Transfer in a Cracked Beam

Unlike ACI 318, recent research (Tureyen 2000; Tureyen and Frosch 2003) has recommended the use of $b_w c$ for the area of shear transfer. The model for this theory is also based on a cracked section. Figure 1.6(a) presents the compression zone above the neutral axis of a cracked section. The hatched portion below this area represents the neglected tension zone of the section. All tension is carried through the longitudinal reinforcement in the bottom of the section. Across the crack width, it is assumed that the tension reinforcement is unbonded. Therefore, the tensile force on each side of Dx must be equal.

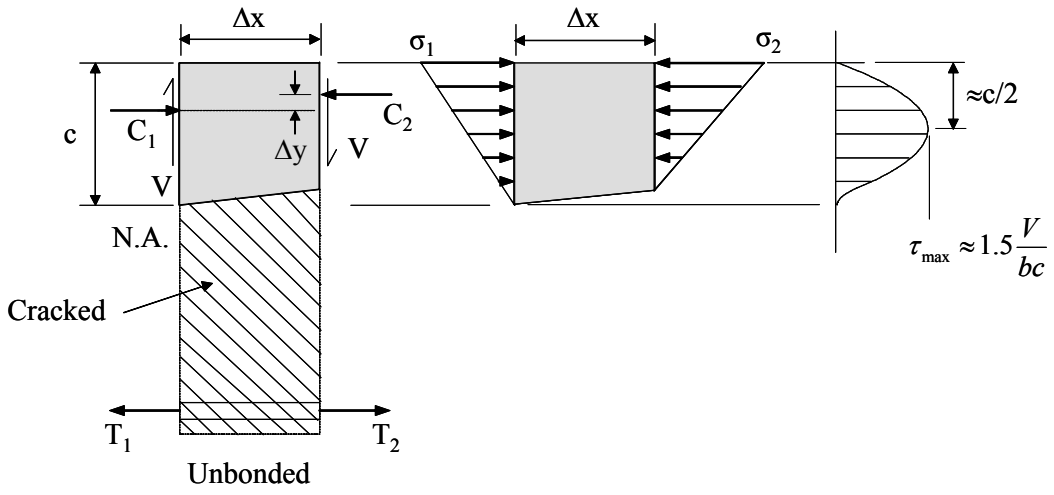

(a) Cracked Section (b) Flexural Stresses (c) Shear Stresses

Figure 1.6: Cracked Section

To maintain equilibrium, the compressive force on the concrete must be equal to the tensile force. The compression zone is subjected to flexural stresses on both sides as shown in Fig. 1.6(b). If this flexural stress distribution is integrated, the compressive resultants are generated to maintain the section in horizontal equilibrium. Because the tension force on each side is equal, the compressive forces must also be equal.

Analyzing the section in moment equilibrium, the section must resist the clockwise moment caused by VDx. The section can resist this moment by shifting the compressive force upward. This creates a moment CDy which must be equal and opposite of VDx. A reduced neutral axis depth and an increase in the top fiber concrete stress can accomplish this upward shift.

This difference in flexural stress creates the shear stress distribution shown in Figure 1.6(c), where the shear stress is zero below the neutral axis. Because all shear stress is distributed over the compression zone, the area to resist shear is taken as $b_w c$.

1.7.2 Shear Strength Model

Above a crack, each element is subjected to axial compression and shear stress as shown in Fig. 1.6. The state of stress on a typical element is shown on the Mohr's Circle given in Figure 1.7. The equation for the principal tension stress is presented in Equation 1.4.

$$-f_t = \frac{\sigma}{2} - \sqrt{\tau^2 + \left(\frac{\sigma}{2}\right)^2} \qquad \text{(Eq. 1.4)}$$

Analysis by Tureyen indicates that a maximum shear stress, τ_{max}, of $\frac{3}{2}\frac{V}{b_w c}$ is located at the center of the compression zone. Assuming a linear stress model, the flexural stress at this point is $\sigma_{max}/2$. Rearranging for the shear force V, the shear strength of the section, V_c, at which a tension failure occurs is presented in Equation 1.5.

$$V_c = \frac{2}{3} b_w c \sqrt{f_t + f_t \frac{\sigma_{max}}{2}} \qquad \text{(Eq. 1.5)}$$

where:

σ_{max} : maximum flexural stress along the depth of the section, psi

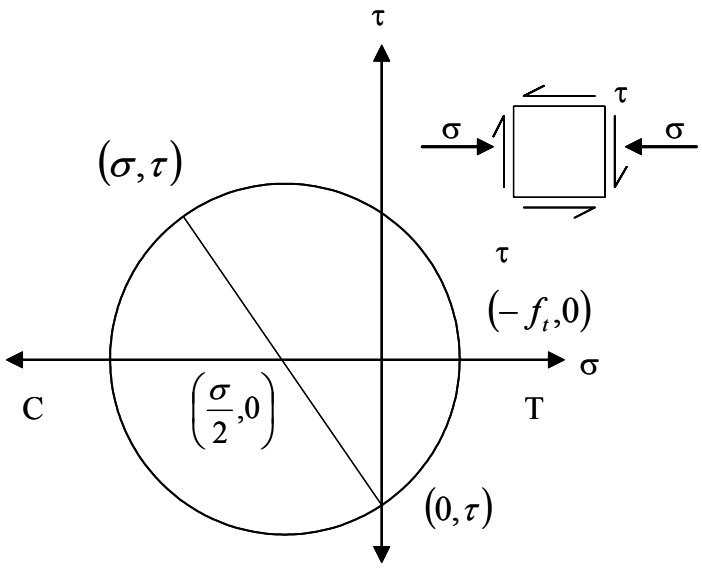

Figure 1.7: Mohr's Circle

1.7.3 Design Equation

Equation 1.5 was simplified by Tureyen using a tensile limit of $6\sqrt{f_c'}$. This equation was rearranged resulting in Equation 1.6.

$$V_c = K\sqrt{f_c'} b_w c \qquad \text{(Eq. 1.6)}$$

where:

$$K = \sqrt{16 + \frac{4\sigma_{max}}{3\sqrt{f_c'}}}$$

Tureyen recommended that the value of K could be simplified considering both the analytical and experimental results. As shown in Figure 1.8, the experimental values of K are fairly consistent across the range of effective reinforcement ratios. A value of 5

was selected to give a conservative, simple value for design as shown in Figure 1.8. The final design equation is shown in Equation 1.7.

$$V_c = 5\sqrt{f_c'}b_w c \qquad \text{(Eq. 1.7)}$$

This simplified equation does not appear to be influenced by variation of the reinforcement ratio, strength of concrete, or depth of the section. This is unlike ACI 318 which is influenced by these variables. Figure 1.9(a) illustrates the performance of the ACI 318 design expression with varying reinforcement ratio. Figure 1.9(b) illustrates the performance of Equation 1.7 considering the same test data.

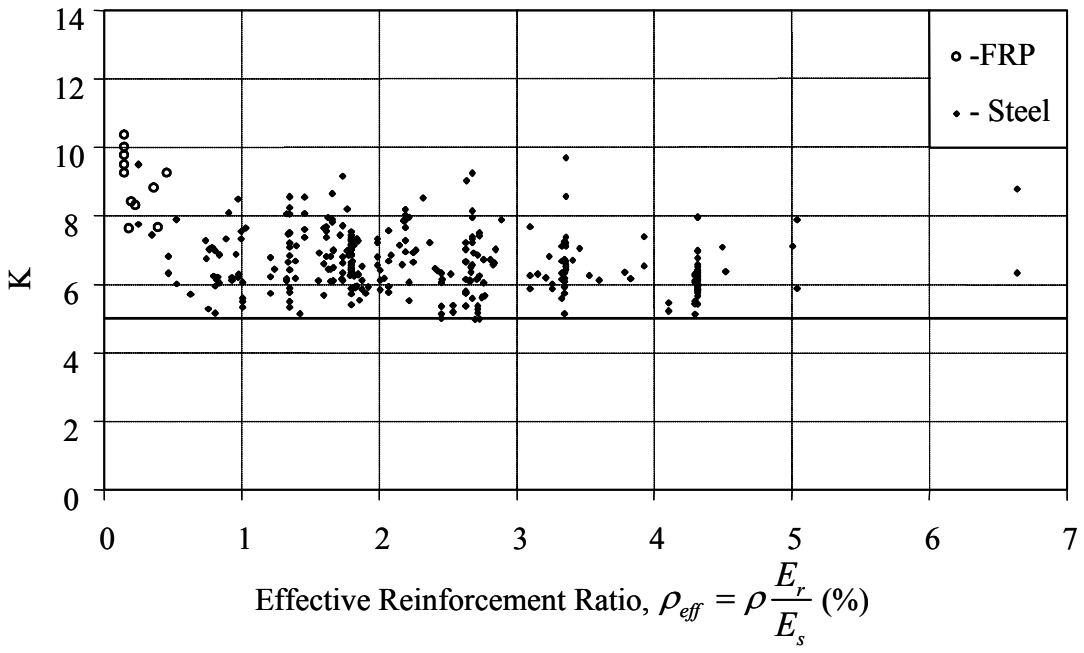

Figure 1.8: K Values (Tureyen 2000)

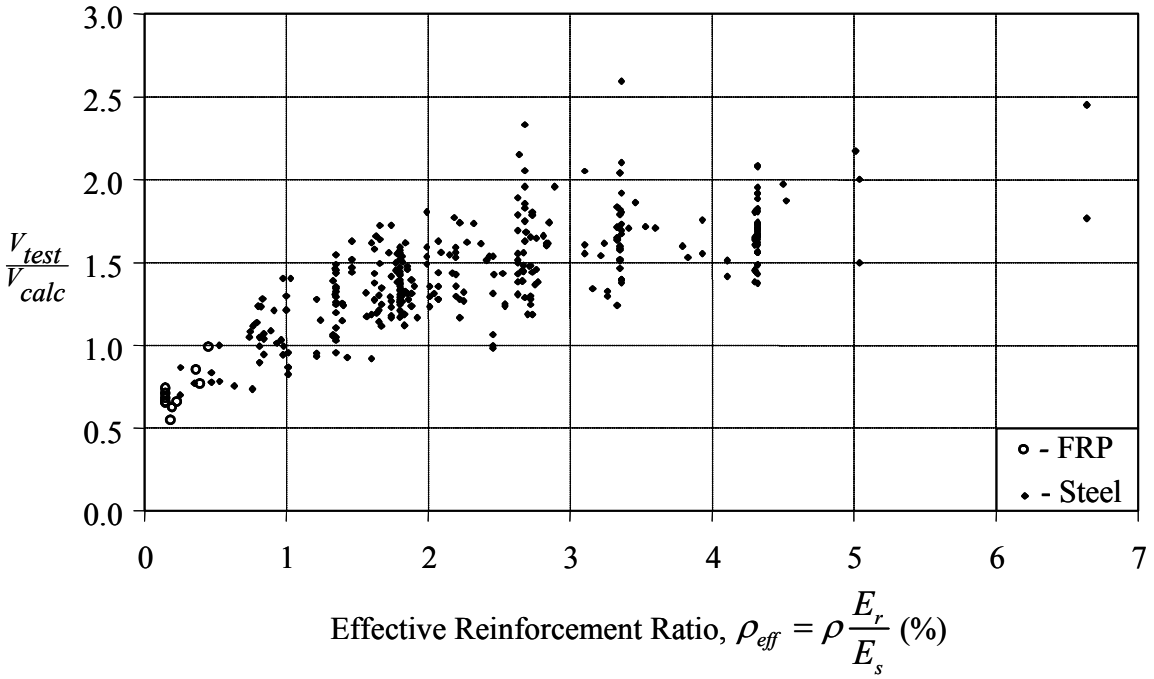

Figure 1.9(a): Performance of ACI 318 with Varying ρ_{eff} (Tureyen 2000)

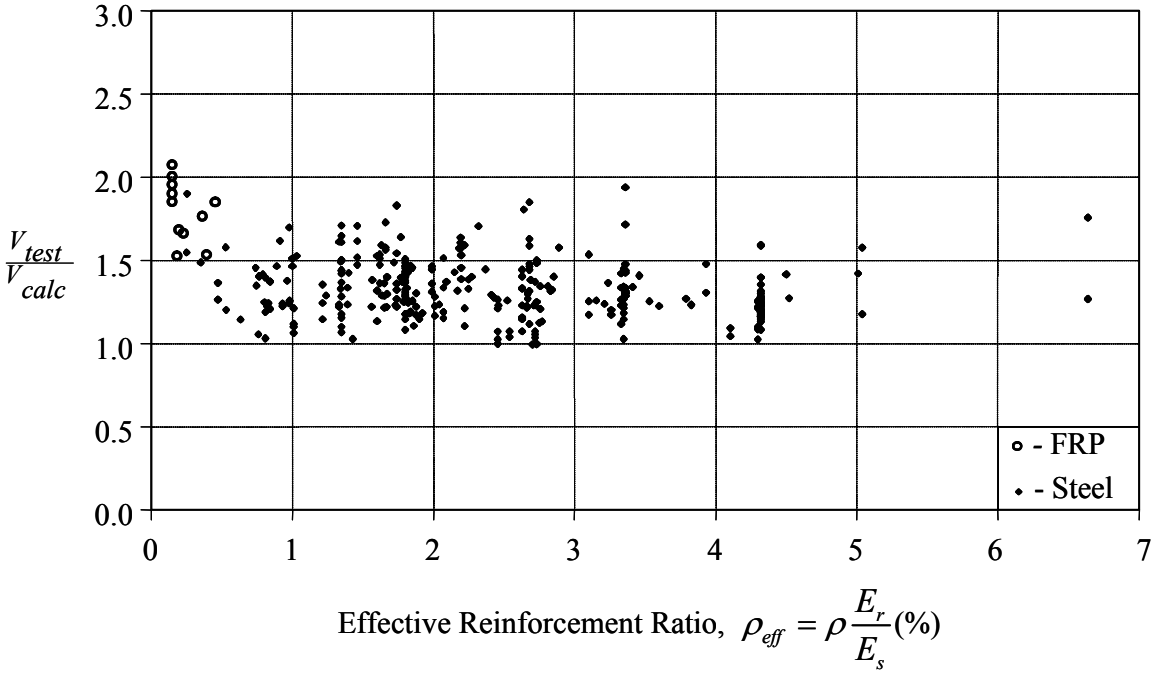

Figure 1.9(b): Performance of Equation 1.8 with Varying ρ_{eff} (Tureyen 2000)

1.8 Objective and Scope of Project

As shown in Figure 1.9(a), the method used by ACI to design reinforced concrete can be unconservative for members with low reinforcement ratios. Also, as recent research has indicated, it can also be unconservative for beams with large effective depths and high strength concrete. The shear model proposed by Tureyen is not influenced by changes in these parameters and yields consistently accurate shear strength calculations.

Although this model was derived for reinforced concrete, it is not specific to reinforced concrete. The fundamentals of this theory were derived using principal stresses and equilibrium, which are defined by basic mechanics. Therefore, it should be applicable to other types of material, other than reinforced concrete.

The objective of this research project is to investigate the applicability of the shear model and simplified design equation to prestressed concrete members. If the design equation can be extended for prestressed members, the shear design of structural concrete members (reinforced and prestressed) can be both unified and simplified.

CHAPTER 2
ANALYTICAL STUDY

2.1 Introduction

As presented in Chapter 1, the current methods for calculating shear strength of prestressed members are either empirically based, or time consuming and complicated. The current ACI 318 equations were based on experimental data that only encompassed a small percentage of the gamut of possible design combinations. The AASHTO LRFD Method, on the other hand, is a complicated and time consuming method. In this chapter, the shear strength model for evaluating reinforced concrete will be used to evaluate the shear strength of prestressed concrete sections. The validity of this design method will be determined using a database of prestressed rectangular and I-shaped sections.

2.2 Analytical Model

2.2.1 Equilibrium Analysis

In Chapter 1, two equations from ACI 318 were presented for the shear strength of prestressed sections; V_{ci} and V_{cw}. The proposed shear model provides a new method to calculate V_{ci}, the flexure-shear strength. With sufficient shear, cracks from flexural stresses turn into flexure-shear cracks. After the shear cracks form, the beam is still capable of supporting load. However, additional load can cause a sudden failure; therefore, the load which causes a flexure-shear crack is taken as V_{ci}.

When the external moment reaches the cracking moment of the section, flexural cracks begin to propagate through the section up to the neutral axis. Figure 2.1 shows a section of concrete cracked by flexural stresses. If shear is to be resisted by the uncracked concrete alone, the weakest section is inherently the portion of the concrete above a crack. This portion of the cross-section has the least area to resist the shear force which must transfer from the point of load application to the reaction. If the tensile stresses of the cracked concrete are ignored, the section would appear, mechanically, as the concrete portion in Figure 2.2(a).

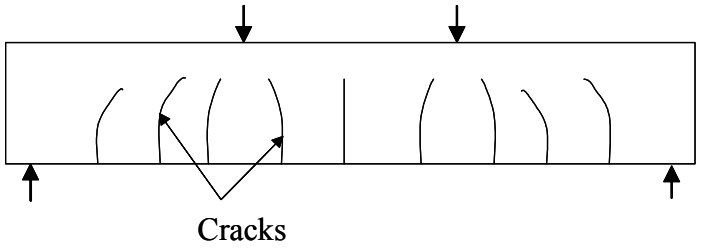

Figure 2.1: Cracked Beam

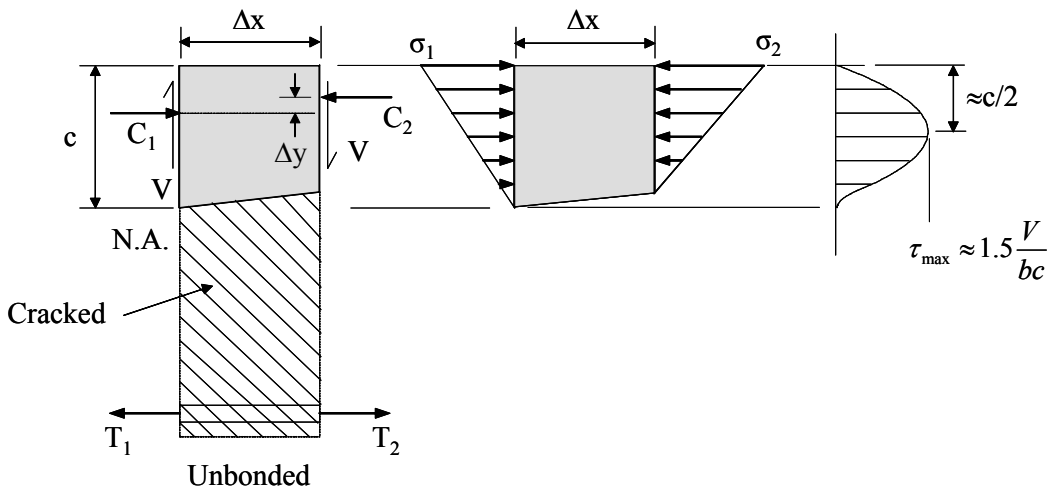

(a) Cracked Section (b) Flexural Stresses (c) Shear Stresses

Figure 2.2: Stresses on a Cracked Section

To resist the external moment caused by the loading, each side of the section has a compressive force located at the centroid of the compressive flexural stress distribution. Also, to keep the section in equilibrium, the compressive force is balanced by the tension force from the reinforcement. This is valid for both sides of the infinitesimal section Δx.

Analyzing the behavior of the tension reinforcement over the width Δx, the tension force must be constant. An increase in the reinforcement tensile force is caused by the concrete bonding to the tension reinforcement. The section shown is located at a flexure crack where the concrete cannot bond to the steel. Therefore, the tensile force on either side of the crack must remain constant. In order to maintain equilibrium, the compressive force must equal the tension force. Therefore, the compressive force must be constant across Δx.

C_1 and T_1 cause a clockwise moment on the section. Resisting this moment is the couple caused by C_2 and T_2. However, $V\Delta x$ also causes a clockwise moment. This additional moment could be resisted by increasing C_2 and T_2 to produce a larger moment. However, the compressive force in the concrete and the tensile force in the reinforcement must remain constant over Δx. Consequently, the additional moment must be resisted by another method than increasing the internal forces.

Internal moments are created by a tension and compression couple in the cross-section. With the forces remaining constant, the only alternative for the cross-section is to increase the moment arm of the forces. The tensile force must always act at the centroid of the tensile reinforcement. As a result, the compressive stress resultant must shift upwards.

This upward shift is caused by a shallower neutral axis depth. To keep the compressive forces equal, the strain at the top of the section must increase. The combination of the shift of the neutral axis upward and increase in the concrete strain increases the moment arm of the couple, keeping the section in equilibrium as shown in Figure 2.2 (b).

Horizontal slices of the section subjected to flexural stress are taken to determine the shear stress distribution, as shown in Figure 2.3. The difference between the integrated flexural stresses on each side of the section must be resisted by a horizontal shear force, V_{ih}. The shear stress, τ_i, on each section is found by Equation 2.1.

$$\tau_i = \frac{V_{ih}}{\Delta x \cdot b_i} \qquad \text{(Eq. 2.1)}$$

where:

b_i: width of cross-section at location of slice, in.

The shear stress distribution on the entire section is generated by taking an infinite number of horizontal slices across Δx. When an infinitesimally small section is taken at the top, there is zero shear stress because zero force exists on both sides of the section above the slice. A slice at the neutral axis also produces zero shear stress, because the compressive forces on both sides of Δx must be equal. The shear stress distribution is shown in Figure 2.2(c). It is important to note that below the neutral axis, there will be no shear stress. Therefore, all shear is transferred through the compression zone.

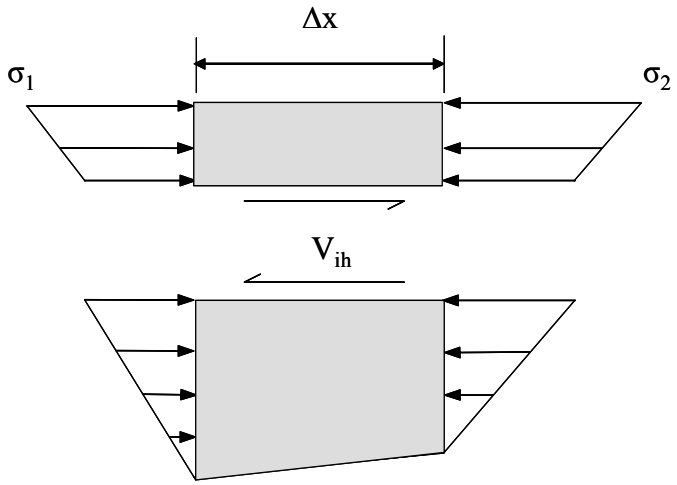

Figure 2.3: Determining Shear Stress

2.2.2 Principal Stress Analysis

The shear stress distribution can be used to determine when a flexure-shear failure will occur, using principal stresses. Considering the beam previously presented, a small element is isolated from above a crack. It is subjected to a flexural stress, σ, and a shear stress, τ, as shown in Figure 2.4. The stresses correspond to those determined in Section 2.2.1. These stresses are plotted on the Mohr's Circle shown in Figure 2.5. From the small element taken earlier, two points are plotted to define the circle; (σ, τ) and

$(0,-\tau)$. From this plot, the principal tensile stress can be determined from the following equation.

$$-f_t = \frac{\sigma}{2} - \sqrt{\left(\frac{\sigma}{2}\right)^2 + \tau^2} \qquad \text{(Eq. 2.2)}$$

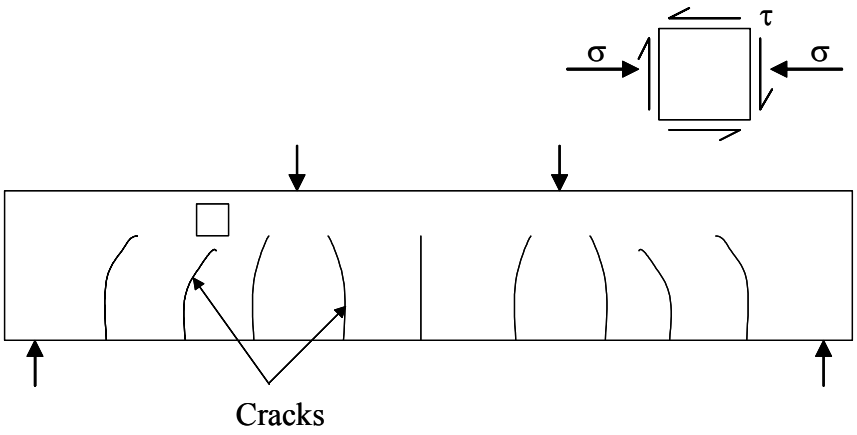

Figure 2.4: Element above a Crack

As the applied load increases, there is a corresponding increase in the bending moment and shear. This loading creates larger flexural stresses and higher shear stresses. The loading and magnitude of the principal tensile stress increase until the principal tensile stress exceeds the tension stress limit. This is considered the point of flexure-shear failure.

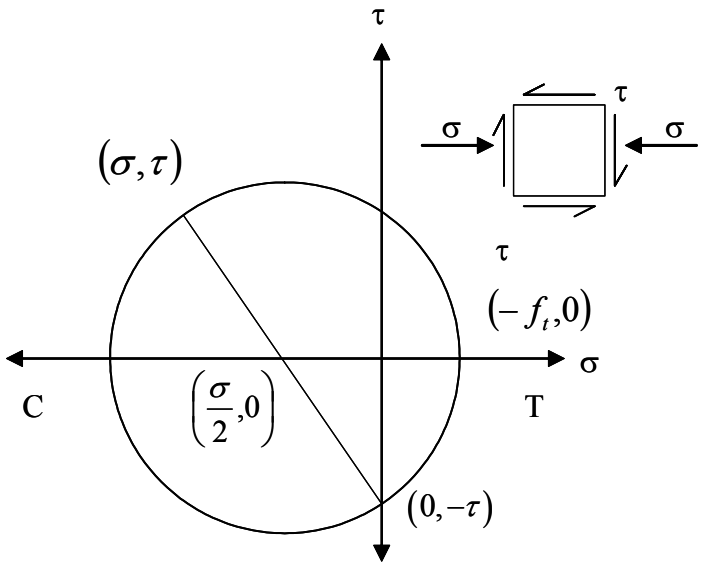

Figure 2.5: Mohr's Circle

2.2.3 Shear Strength

Using equilibrium and the principal stress analysis, the shear strength of a concrete section can be determined. The shear strength of a section is found by solving Equation 2.2 for the shear stress. The beam fails when τ_{cr}, calculated according to Equation 2.3, is exceeded by the shear stress at the section.

$$\tau_{cr} = \sqrt{\left(\frac{\sigma}{2} + f_t\right)^2 - \left(\frac{\sigma}{2}\right)^2} \qquad \text{(Eq. 2.3)}$$

Referring to Section 2.2.1, every horizontal slice has a corresponding flexural and shear stress, σ_i and τ_i. Figure 2.6 illustrates the relationship between flexural stresses and shear stresses for a typical beam. As an example, at a point 2.6 in. from the top of the section, the beam has a flexural stress, σ_n and shear stress, τ_n. Substituting σ_n into Equation 2.3 yields a τ_{cr}. If τ_n exceeds τ_{cr}, a flexure-shear crack forms in the compression zone and the beam is incapable of carry additional load safely. Therefore, V_{ci} is the load corresponding to the point when τ_n exceeds τ_{cr}.

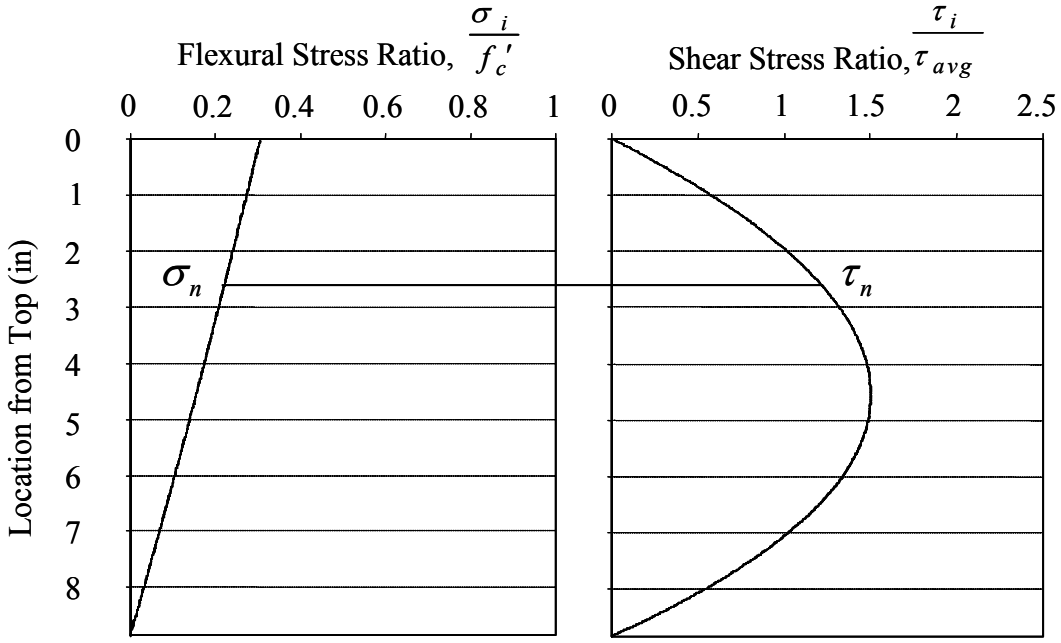

Figure 2.6: Flexural and Shear Stress Pair

2.3 Variation of the Neutral Axis with Prestress

The most important difference, for the shear model considered, between reinforced concrete and prestressed concrete is the behavior of the neutral axis. Reinforced concrete sections, with the concrete still in the elastic range, have a constant

neutral axis depth. If a section is prestressed, the neutral axis varies throughout the length of the beam.

Reinforced concrete sections have a constant neutral axis depth because of a simple stress-strain relation. The strain across the depth of the section must be linear considering plane sections remain plane. Using the modular ratio, n, the stress throughout the section is related to the linear strain distribution. The equation for tensile stress in the steel is given in Equation 2.4.

$$\sigma_s = n \cdot E_c \cdot \varepsilon_s \qquad \text{(Eq. 2.4)}$$

where:

n: ratio of $\frac{E_r}{E_c}$

To maintain equilibrium, the first moments of the compression and tension areas must be equal. Equation 2.5 shows this relationship for a rectangular section.

$$b \cdot c \cdot \frac{c}{2} = n \cdot A_s \cdot (d - c) \qquad \text{(Eq. 2.5)}$$

If this relationship is rearranged, Equation 2.6 is formed. Because of the proportional stress relationship, the neutral axis depth remains constant despite the loading.

$$c = \left[\sqrt{(\rho n)^2 + 2\rho n} - \rho n \right] d \qquad \text{(Eq. 2.6)}$$

Unlike reinforced concrete, the neutral axis in prestressed concrete varies with the level of applied moment. Using the modular ratio to transform the steel into concrete, a different stress relationship results with prestressed concrete as opposed to reinforced concrete. The steel has an initial tensile stress from the prestressing, as shown in Equation 2.7.

$$\sigma_s = n \cdot E_c \cdot \varepsilon_s + f_{se} \qquad \text{(Eq. 2.7)}$$

where:

f_{se}: effective prestress, psi

The effective prestress, f_{se}, causes the stress relationship between the concrete and the steel to become not solely dependant on the strain in the concrete. When a prestressed section cracks, the neutral axis depth is deeper than a similar reinforced concrete section. Unlike the reinforced concrete section, the neutral axis rises as the loading increases to resist the external moment. Therefore, throughout the length of a cracked beam, the neutral axis varies from point to point.

To explain the effects of prestressing on the neutral axis, three theoretical rectangular beams were selected. All specimen details are listed in Table 2.1.

Table 2.1: Details of Theoretical Beams

Specimen	Width, b_w (in.)	Effective Depth, d (in.)	Reinf. Ratio, ρ (%)	Effective Prestress, f_{se} (ksi)	Non P/S Neutral Axis, c (in.)	Cracking Moment, M_{cr} (k-ft)
0	6	10	1.00	0	3.12	6.4
60	6	10	1.00	60	3.12	24.4
120	6	10	1.00	120	3.12	42.4

Specimen 120 has the highest initial prestress and Specimen 0 has no prestress. If the sections were not prestressed, the nonprestressed neutral axis of all three of these sections would be identical, as shown in Table 2.1. The nonprestressed neutral axis depth was calculated as previously discussed.

A nonlinear analysis was performed for these three beams to determine the neutral axis depths at multiples of their cracking moment. The concrete stress was related to the concrete strain using the relationship derived by Hognestad (Lyn and Burns 1981), given in Equation 2.8.

$$\sigma = f_c' \left[\frac{2\varepsilon}{\varepsilon_0} - \left(\frac{\varepsilon}{\varepsilon_0} \right)^2 \right] \qquad \text{(Eq. 2.8)}$$

The neutral axis depth versus the multiple of the cracking moment is plotted in Figure 2.7.

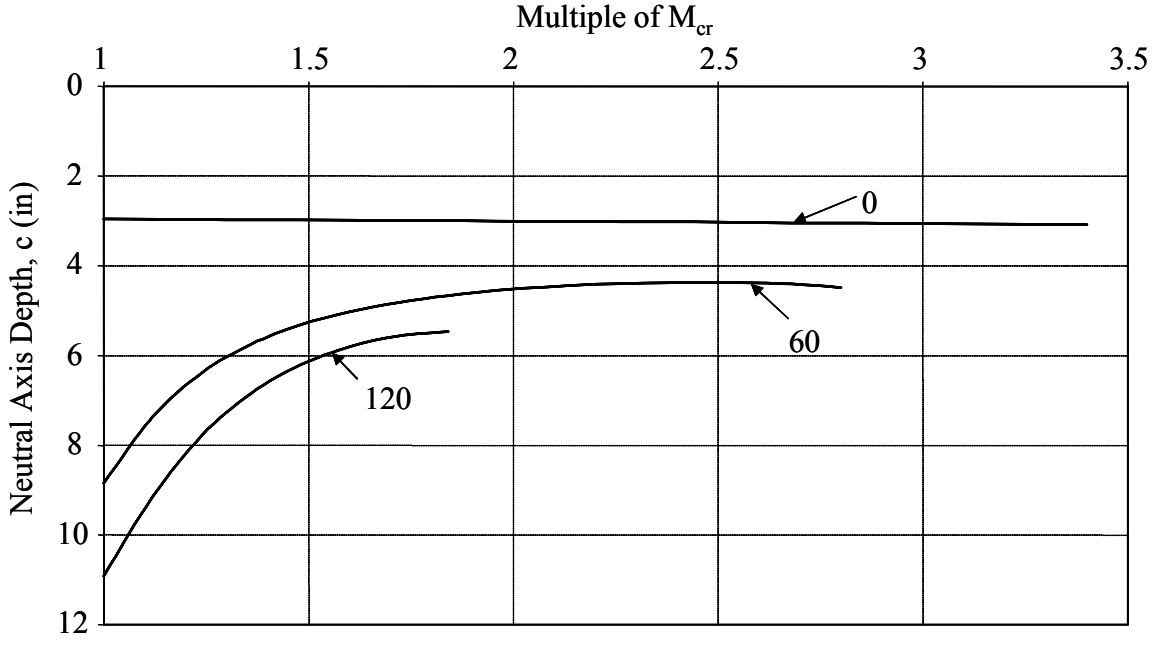

Figure 2.7: Variation of Neutral Axis Depth with Multiple of Cracking Moment

As shown in the graph, the highly prestressed section has the largest compression zone at the cracking moment. This is inherently true because the reinforcement has a larger tension force, needing a larger compression force to resist it. As the moment increases, the section with no prestress has an approximately constant neutral axis. It is not constant since a nonlinear stress-strain concrete model was used. However, the two prestressed sections have decreasing neutral axis depths that level off as the moment is increased.

Figure 2.8 presents a similar plot to Figure 2.7. The x-axis, however, is plotted showing the additional moment beyond the cracking moment. The data shows that the neutral axis decreases more rapidly in the section with a medium prestress level.

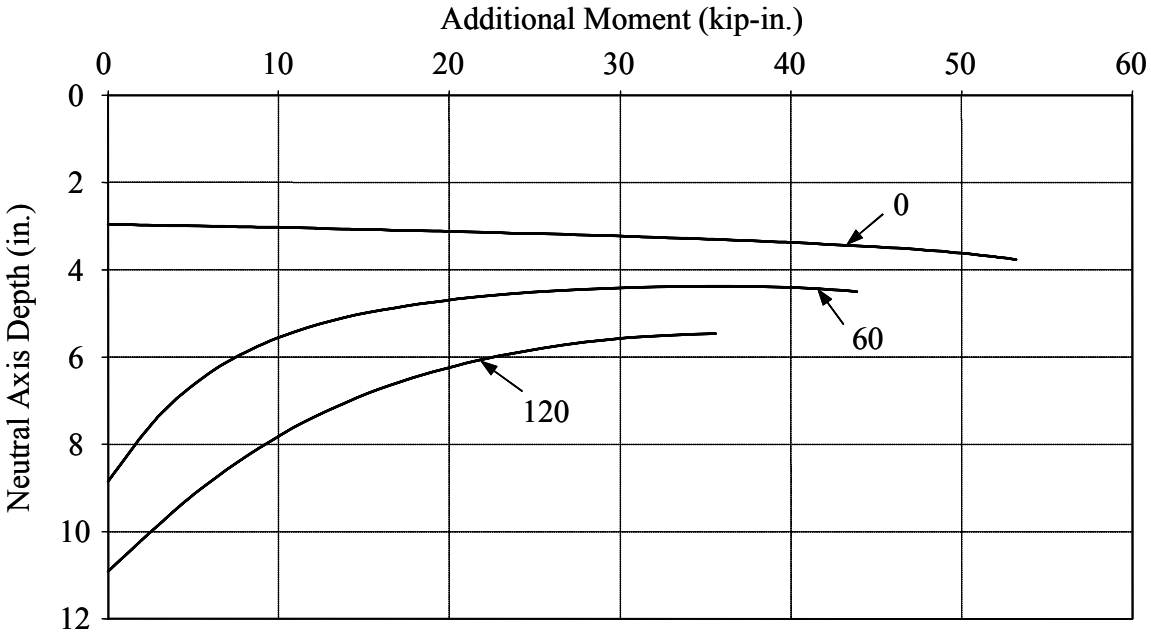

Figure 2.8: Variation of Neutral Axis with Additional Moment

At the y-intercept, the neutral axis positions represent the neutral axis at the cracking moment. Immediately above this moment, the neutral axis of the nonprestressed member drops slightly due to the nonlinear analysis. It continues to drift downwards throughout the loading. The neutral axis depth of Specimen 60 decreases the most rapidly initially, but slowly levels off towards the end of the section's capacity. The highly prestressed beam also starts with a rapidly decreasing compression zone which levels off before a flexural failure. Overall, by prestressing a concrete section, the neutral axis depth is deeper in the section than an identical nonprestressed beam. However, with increasing moments, the neutral axis depth decreases and levels off towards a shallower location.

2.4 Variation of K Value with Prestress

In Chapter 1, the formula for the shear strength of a reinforced concrete section was given as:

$$V_c = K\sqrt{f_c'}b_w c \qquad \text{(Eq. 2.9)}$$

The variable K was shown as a function of the flexural stress on the section. As the loading increases, the flexural stress increases on the section. Therefore, the section grows stronger with respect to shear as the beam is loaded.

However, prestressing also influences the flexural stress on the section. A highly prestressed section would need a large moment to crack the section. Consequently, the internal compressive stress and tensile force would be large in the section as it cracks. A large compressive stress increases the value of K, increasing shear strength. Inversely, a section with no prestress would have less flexural stress at cracking and lower shear strength.

To help explain this point, the same three rectangular beams are loaded again to determine the variability of the increase of K while loading. As shown in Figure 2.9, K increases with an increase in the bending moment. In addition, heavily prestressed beams have a higher initial value of K. Additional flexural stress enables the section to resist higher shear stresses. Therefore, prestressing a section allows it to have higher shear strength due to higher flexural stress at cracking.

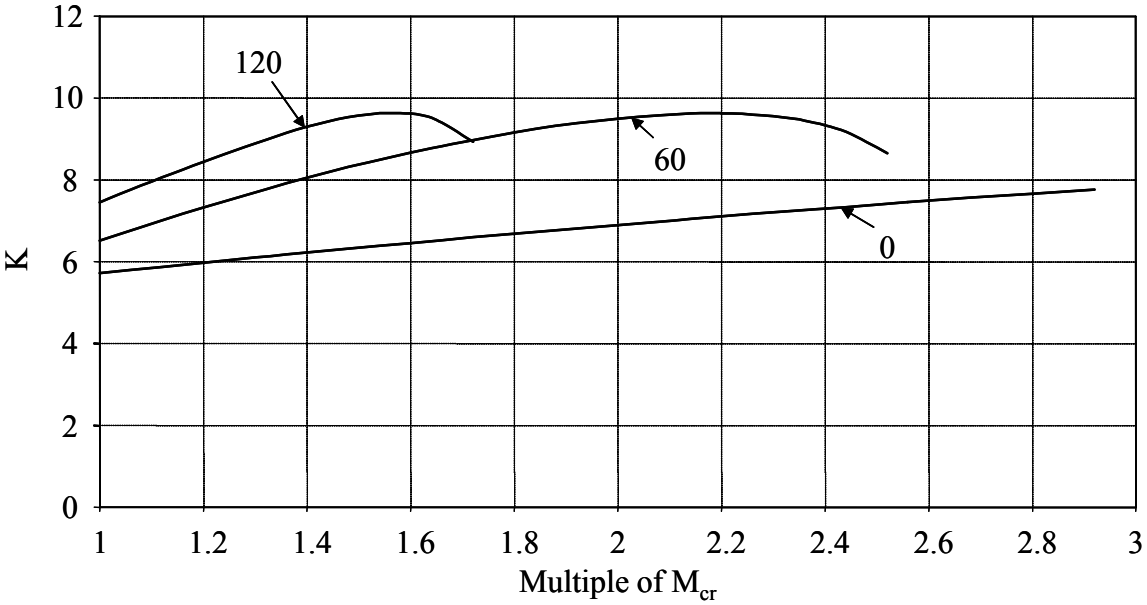

Figure 2.9: Variation of K

2.5 Variation of Kc with Prestress

K and c have both been shown to vary with additional applied moment. The neutral axis depth decreases, allowing for a reduced area to transfer shear. However, the

strength of the remaining uncracked concrete increases with higher applied moments. If Equation 2.9 is rearranged to link the variable parameters, Equation 2.10 remains.

$$V_c = (Kc)\sqrt{f_c'}b_w \qquad \text{(Eq. 2.10)}$$

The values for $\sqrt{f_c'}$ and b_w are not dependent on the load applied. However, K and c are shown to vary as the section is loaded. Therefore, the strength of the section relies on the interaction of these two variables. As shown in Section 2.3, the neutral axis begins deep in a prestressed beam and drifts shallower as the moment increases. At high moments, the neutral axis depth does not change significantly. Inversely, the value of K begins at a low value and increases linearly with the increased loading, until K is influenced by the nonlinear stress distribution. Therefore, the product of K and c produce a minimum value based on the slope of K and c at a given moment. Figure 2.10 displays the variation of Kc at varying moments.

The interaction between K and c is a function of many variables, such as prestress level and amount of reinforcement. Specimens 60 and 120 both have minimum shear strength values at moments equal to their flexural capacity. However, Specimen 0 has a minimum shear strength at its cracking load. Analyses of past experiments (Sozen, Zwoyer and Siess 1959) show that there is no discernable pattern to determine the absolute minimum point for a general beam, without extensive analysis. Beams with no prestress have a constant neutral axis (due to the nonlinear analysis, the neutral axis in Figures 2.7 and 2.8 are not constant); therefore their minimum shear strength would always be at the cracking moment. Some specimens observed had minimum shear strengths between the cracking moment and flexural capacity moment. Others, such as Specimens 60 and 120 have the absolute minimum at the flexural failure moment.

The absolute minimum values for shear strength, however, can be less than the shear that caused a beam to fail. In order to reach the absolute minimum shear strength, the corresponding bending moments must also be reached. For beams with low a/d ratios, the levels of moment causing the absolute minimum shear strength may not be reached. Failure can occur due to high shear occurring at a lower level of applied moment. Therefore, using the absolute minimum shear strength for V_{ci} can be overly conservative for sections with low a/d ratios.

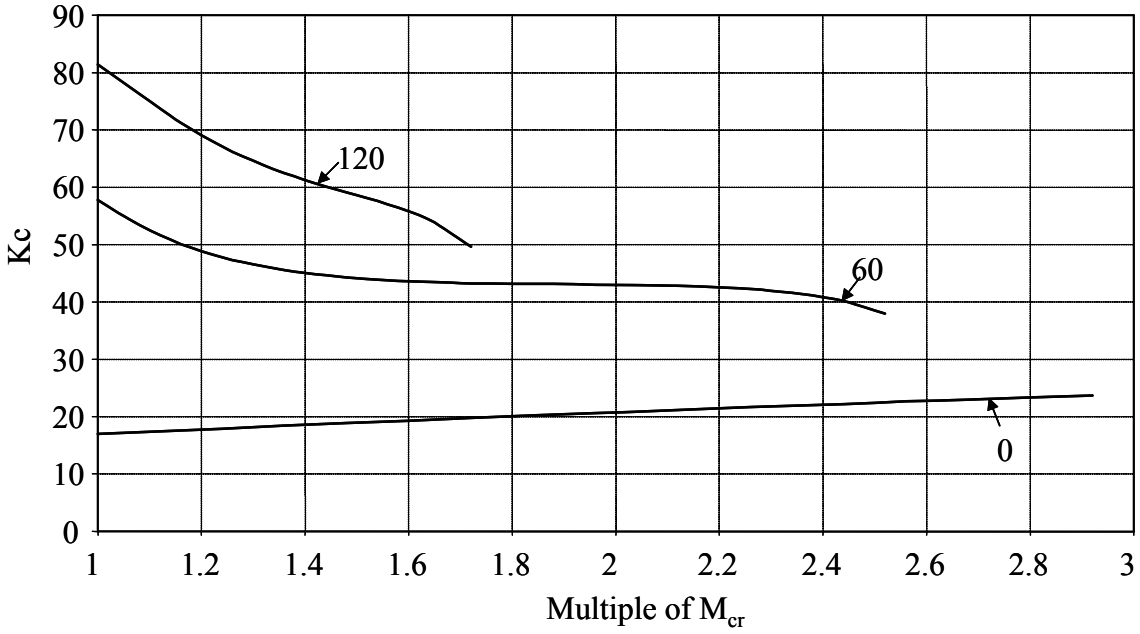

Figure 2.10: Variation of Kc with Multiple of Cracking Moment

2.6 Analytical Study

2.6.1 Prestressed Concrete Database

In order to test the shear model, a database of prestressed concrete beams which failed in shear was generated from past experiments (Sozen, Zwoyer and Siess 1959). The original test data included 99 beams, comprised of 43 rectangular beams and 56 I-beams. Failure modes were identified in the references as flexural and shear.

2.6.1.1 Flexural Failures

Nine test specimens were identified as having failed in flexure. These specimens, listed in Table 2.2, were removed from the database because the focus of this investigation was to determine the effectiveness of this model for calculating shear strength.

2.6.2.2 Web-shear Failures

Four test specimens were identified as exhibiting characteristics of web-shear cracking during testing. These specimens, listed in Table 2.3, were removed from the database because secondary inclined cracking of the web formed in a section of the web that was previously uncracked by flexure. Flexure-shear failure, which is the subject of this investigation, occurs when sufficient shear stress turns a flexural crack into a flexure-shear crack. After eliminating the sections which were not applicable to this investigation, the remaining sections were used as the prestressed beam database. The details of the specimens in the prestressed beam database are shown in Appendix A.

Table 2.2: Flexural Failures

Specimen I.D
A.12.48
A.12.60
A.22.26
A.32.08
A.32.11
A.32.17
B.11.07
B.12.07
B.13.07

Table 2.3: Web-shear Failures

Specimen I.D
C.22.62
C.22.73
C.12.50
C.12.57

2.6.2 Database Analysis

A complete analysis was performed on the remaining specimens in the database using the process detailed in this section. Also, the data was analyzed used ACI 318, Equation 11-10 (also presented here as Equation 1.3). Figure 2.11(a) presents V_{test}/V_{calc} versus the initial axial precompression stress, P/A, caused by prestressing. Figure 2.11(b) presents V_{test}/V_{calc} plotted against the a/d ratio. Figure 2.12(a) and 2.12(b) presents the same data using ACI 318, respectively. Statistical results are listed in Table 2.4.

2.6.3 Database Analysis Discussion

The shear model provided uniform results for both varying initial axial precompression and a/d ratio. Examining the statistical results, the proposed shear model is consistent when dealing with I-sections and rectangular sections. The majority of data points fall in a band of V_{test}/V_{calc} equal to 0.8 and 2.0. The current method for shear design in ACI 318 is overly conservative for sections with small amounts of effective prestress. There is also variation of the performance of ACI 318 between rectangular and I-sections. The majority of the data for this set fall between 0.8 and 3.0, with some points near 3.5. The inability of ACI to adapt to varying levels of prestress produce considerable variation in the results.

Along with the calculation of the flexure-shear strength, the flexural capacity of each section was also calculated. Of the 86 specimens remaining in the database, 13 of these specimens failed at loads greater than the load calculated which would fail the beam in flexure. These beams are listed in Table 2.5, along with the test failure shear and the shear which would cause a flexural failure, V_{flex}. Generally, the shear that failed the beam is within 10% of the shear that would cause flexural failure. Also, the flexural

capacity is based on an assumption of a limiting compressive strain of 0.003. Therefore, it is possible that the sections could withstand a higher moment, which is supported by the reinforcement stress calculated at the flexural limit. Examining the tensile stress of the reinforcement at the flexural capacity of the section, the majority of the reinforcement could resist more tension, which could increase the moment capacity of the section. The tensile stress limit of the reinforcement was 250 ksi. Because these sections were not reported to have failed in flexure, these sections were included in the database.

Lastly, the web-shear strength of the sections was determined using a principal stress analysis. To be consistent, the analysis was based upon a tensile strength of $6\sqrt{f_c'}$. Again, one section failed at a load above the calculated web-shear capacity. The failure shear, at a distance d away from the support, along with the calculated web-shear strength is listed in Table 2.6. Once more, because this specimen was not identified as exhibiting characteristics of a web-shear failure and because the web-shear is based on an assumed tensile strength ($6\sqrt{f_c'}$), this specimen was included in the database.

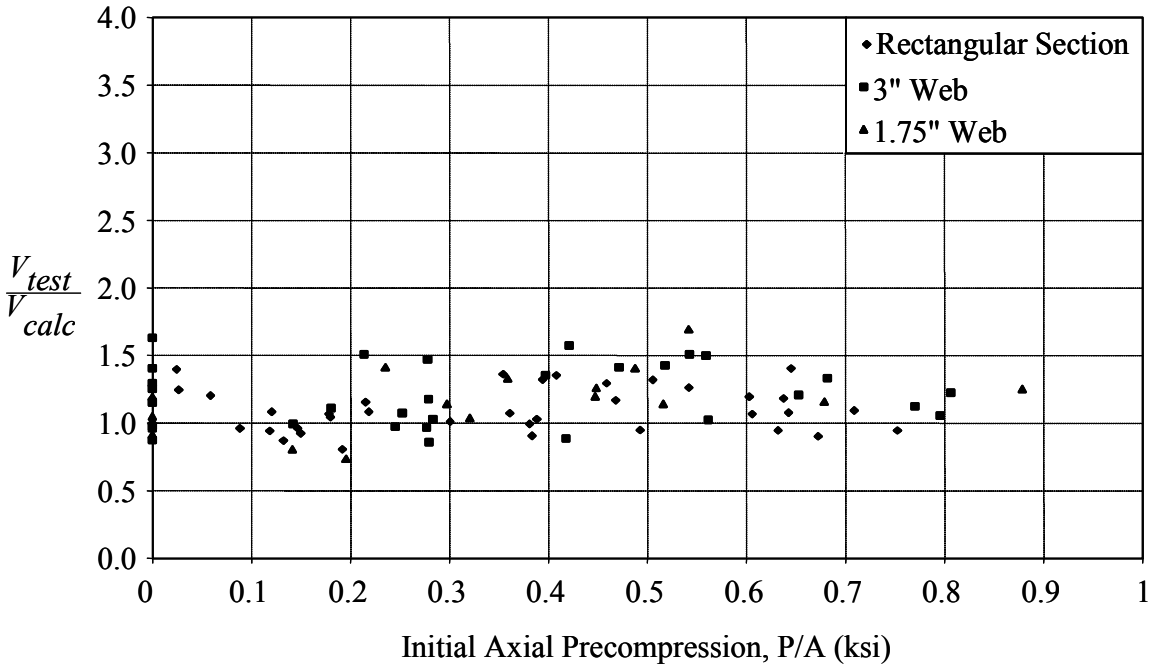

Figure 2.11(a): Analysis Results versus the Initial Axial Precompression

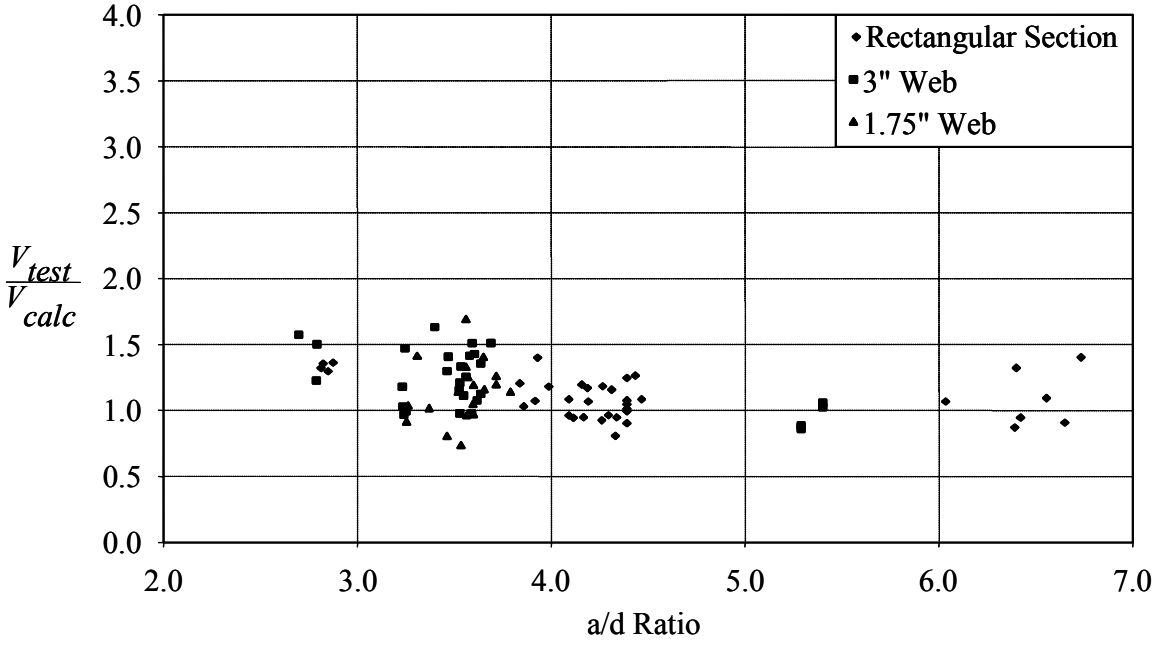

Figure 2.11(b): Analysis Results versus a/d Ratio

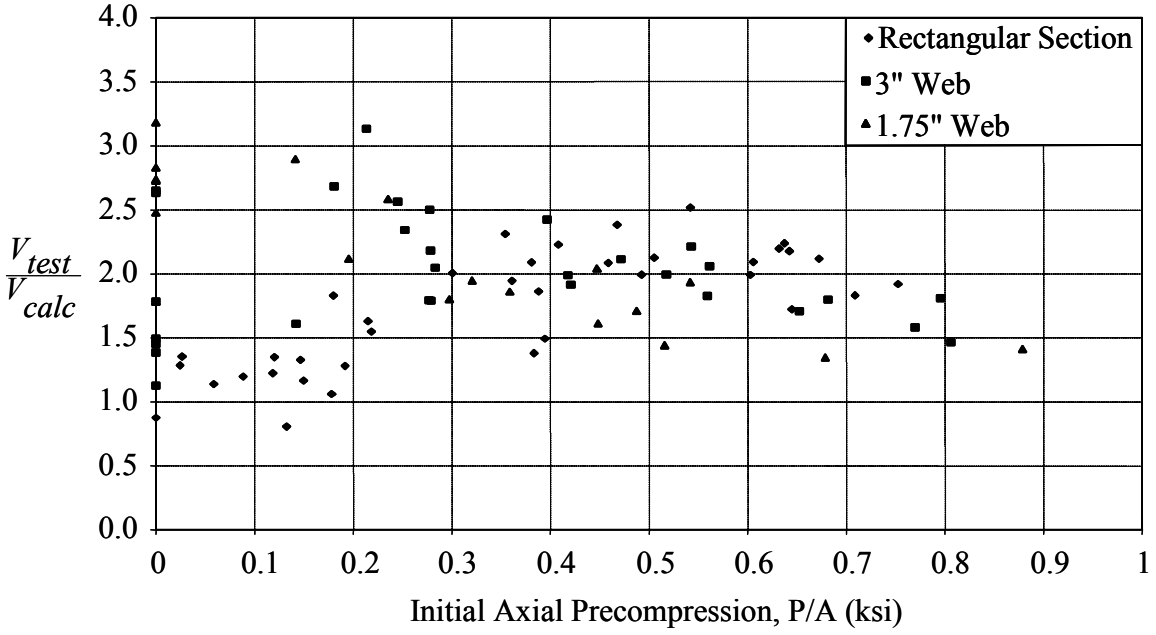

Figure 2.12(a): ACI 318 Results versus Initial Axial Precompression

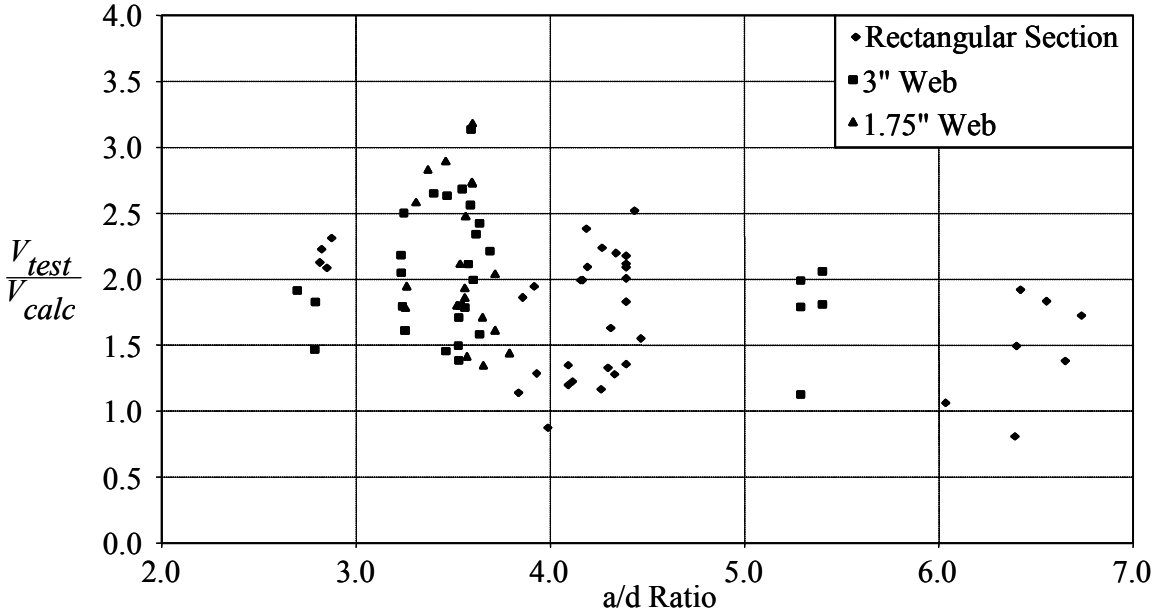

Figure 2.12(b): ACI 318 Results versus the a/d Ratio

Table 2.4: Statistical Results of Analysis

	Statistic	ACI	Analysis
All	**All Sections**		
	Average	1.91	1.15
	ST DEV	0.508	0.203
	Correl	0.802	0.897
Section Shape	**Rectangular Sections**		
	Average	1.72	1.11
	ST DEV	0.461	0.160
	Correl	0.751	0.913
	I-Sections		
	Average	2.05	1.19
	ST DEV	0.500	0.226
	Correl	0.895	0.874
Prestress Level	**Prestressed Sections**		
	Average	1.75	1.11
	ST DEV	0.444	0.162
	Correl	0.783	0.875
	Nonprestressed Sections		
	Average	2.08	1.14
	ST DEV	0.743	0.209
	Correl	0.179	0.424

Table 2.5: Potential Flexural Failures

Specimen I.D	V_{test} (kips)	V_{flex} (kips)	f_{ps} (ksi)	$\frac{V_{test}}{V_{flex}}$
A.11.43	12.15	11.61	213.9	1.05
A.11.51	6.93	6.28	209.5	1.10
A.11.53	9.31	8.89	209.5	1.05
A.11.96	9.40	8.02	161.5	1.17
A.12.53	12.19	11.62	202.6	1.05
A.12.69	12.42	10.30	183.0	1.21
A.12.73	14.13	13.17	173.5	1.07
A.12.81	11.64	10.82	175.9	1.08
A.14.39	14.59	14.44	235.9	1.01
A.14.44	16.10	15.88	226.5	1.01
A.14.55	18.24	17.41	204.5	1.05
A.14.68	15.05	13.52	186.5	1.11
B.12.19	8.67	8.21	248.1	1.06

Table 2.6: Potential Web-shear Failure

Specimen I.D	V_{test} (kips)	V_{cw} (kips)	$\frac{V_{test}}{V_{cw}}$
C32.80	5.47	5.23	1.05

CHAPTER 3
ANALYSIS SIMPLIFICATIONS

3.1 Introduction

As shown in the previous chapter, the shear model performs well when used to analyze prestressed concrete sections. The flexural stresses that occur when a beam is loaded causes cracks in the tension side of the section. With sufficient shear, the concrete can exceed its tension limit locally in the compression zone, and a flexure-shear failure can occur. The analysis to determine these local stresses, however, can be time consuming and complicated. Therefore, there is a need to simplify the analysis method.

3.2 Shear Stress

As shown earlier, prestressed sections have a shear stress distribution acting on the entire compression zone of the section. The combination of each shear stress and corresponding flexural stress are used to determine if a flexure-shear failure will occur. However, examining each point is time consuming. Therefore, it would be useful if a critical average shear stress over the compression zone could be obtained.

This critical average stress is represented by $K\sqrt{f_c'}$ which acts over the compression zone. Unlike reinforced concrete, the value of K cannot be readily determined. With a varying neutral axis depth, K cannot be found by dividing the test failure load by $\sqrt{f_c'}bc$. Two methods were used to determine a simplified K value. Method 1 used the shear model described earlier to determine a lower bound value of K. Method 2 was an empirical method using the prestressed beam database to determine the value of K that would produce conservative results.

3.3 Method One

The first method to determine a simplified value for K involved using the prestressed beam database to calculate a lower bound value for K. Using the shear model, K at failure was determined by dividing the calculated failure shear by $\sqrt{f_c'}bc$, where c is the neutral axis depth at the failure moment. A complication occurs with sections which fail in shear at high flexural moments, where nonlinear flexural stresses are present. As shown in Section 2.4, K increases with the compressive stress on the section. However, nonlinear effects near the flexural capacity of the section can cause K to decrease rapidly. For sections behaving linearly, K increases with increasing moment. When nonlinearity is present, due to moments near the flexural capacity, K decreases rapidly. Therefore, sections in the linear region at failure will have similar values, while sections in the nonlinear region will have significantly lower values.

Specimen 60 is examined again to explain how nonlinearity influences shear strength. Figure 3.1(a) presents the flexural stress ratio, σ_i / f_c', plotted on the x-axis versus the depth of the compression zone at the cracking moment. At the cracking

moment, the flexural stress distribution is, for practical purposes, linear. Figure 3.1(b) presents the shear stress ratio, τ_i / τ_{avg} , plotted on the x-axis versus the depth of the compression zone at the cracking moment. The peak shear stress ratio is approximately 1.5, which is typical for rectangular sections in the linear stress range. Also, Figure 3.1(c) shows the shear strength of the section plotted versus the depth of the compression zone at the cracking moment. Due to the lack of significant shear stress, the shear strength of the section is very large near the top and bottom of the compression zone.

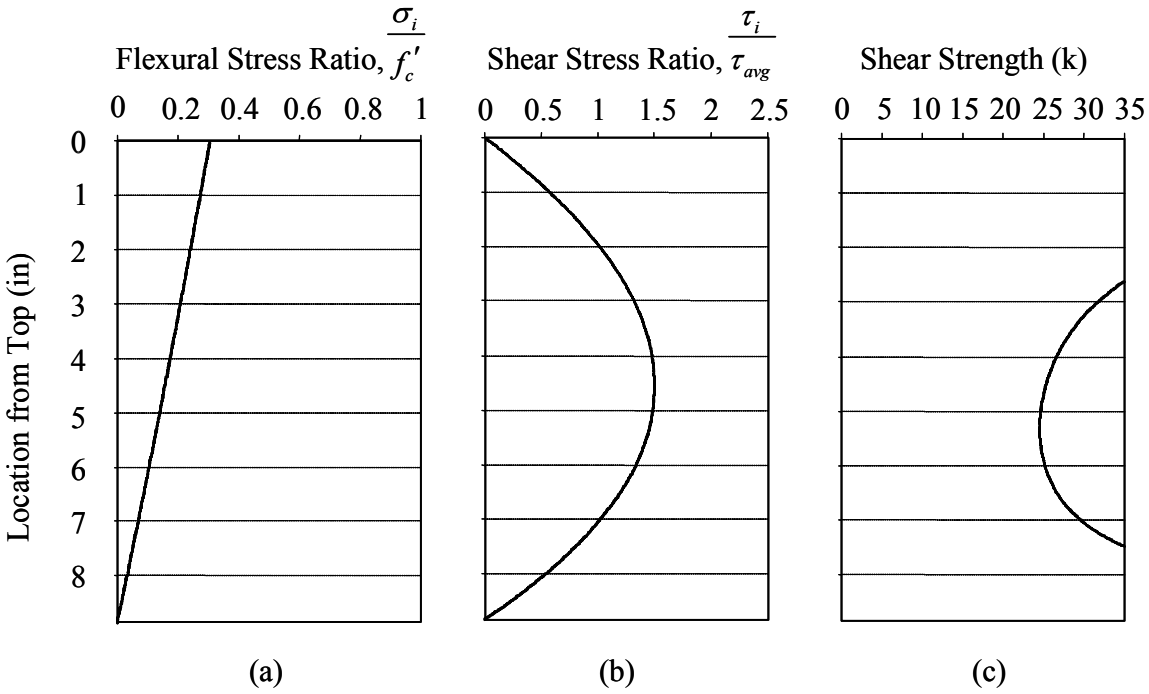

Figure 3.1: Variation of the Stress Ratios and Shear Strength throughout the Compression Zone at M_{cr}

Specimen 60 was then analytically loaded to 1.42 times the cracking moment. In Figure 3.2, the stress ratios are plotted against the same axes as before. The flexural stress ratio distribution has become slightly nonlinear and the shear stress ratio has compressed into a smaller compression zone, but has maintained approximately the same shape. At the cracking moment, the maximum shear stress ratio was 1.5 at a relative location of $0.51 \cdot c$, at $1.42M_{cr}$ it is 1.51 at $0.53 \cdot c$. Similarly, the relative location of the minimum shear strength of the section has shifted downwards in the compression zone as well. The reduction of the compression zone and increased maximum shear stress ratio results in a lower shear strength. The minimum shear strength at the cracking moment was 24.5 kips at a location of $0.60 \cdot c$, where now it is 19.0 kips at $0.64 \cdot c$.

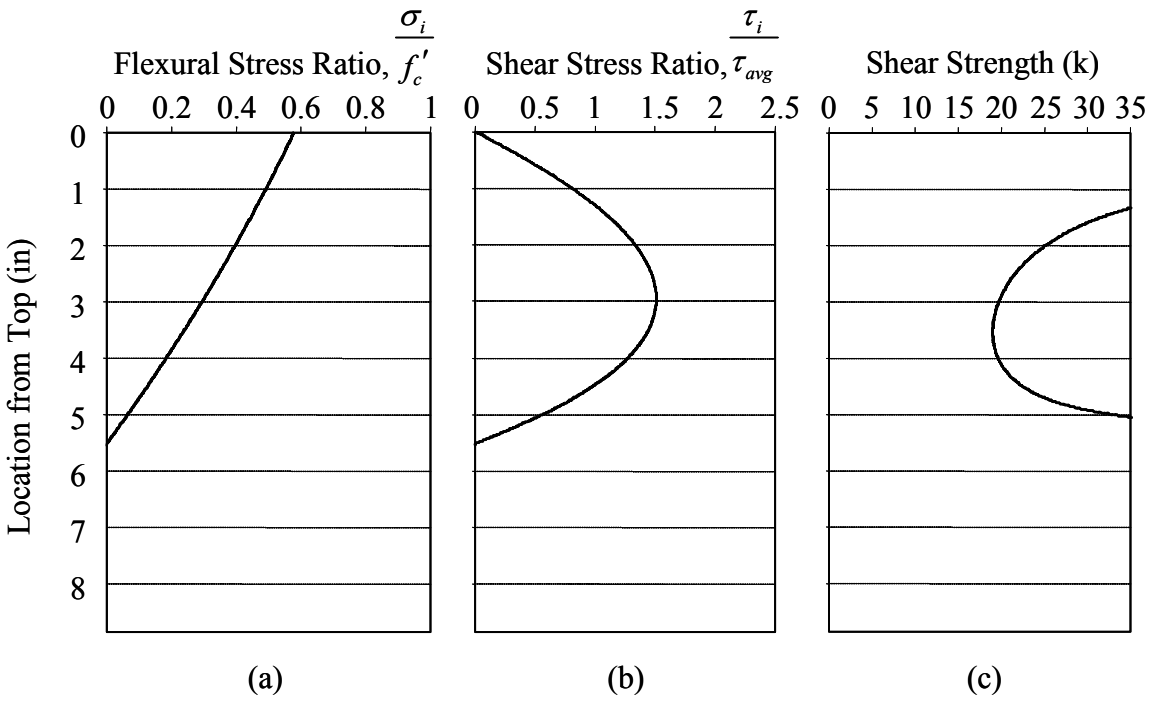

Figure 3.2: Variation of the Stress Ratios and Shear Strength throughout the Compression Zone at 1.42 M_{cr}

Lastly, Specimen 60 was analytically loaded to its nonlinear flexural failure moment, located at 2.84 times the cracking moment. Again, the same attributes are plotted on the identical axes in Figure 3.3. Clearly, the flexural stress ratio distribution is nonlinear. This extreme nonlinearity causes the maximum shear stress ratio to shift upwards in the compression zone to a maximum of 2.24 at $0.28 \cdot c$. Also, the shear strength is minimum at $0.28 \cdot c$ for a strength of 18.4 kips.

Therefore, although increasing the flexural stress can increase the shear strength of a section while it is behaving linearly, nonlinearities and decreasing neutral axis depth can cause the strength of the section to have a lower shear strength. As shown, nonlinearity of the flexural stress distribution can increase the magnitude of the maximum shear stress ratio significantly.

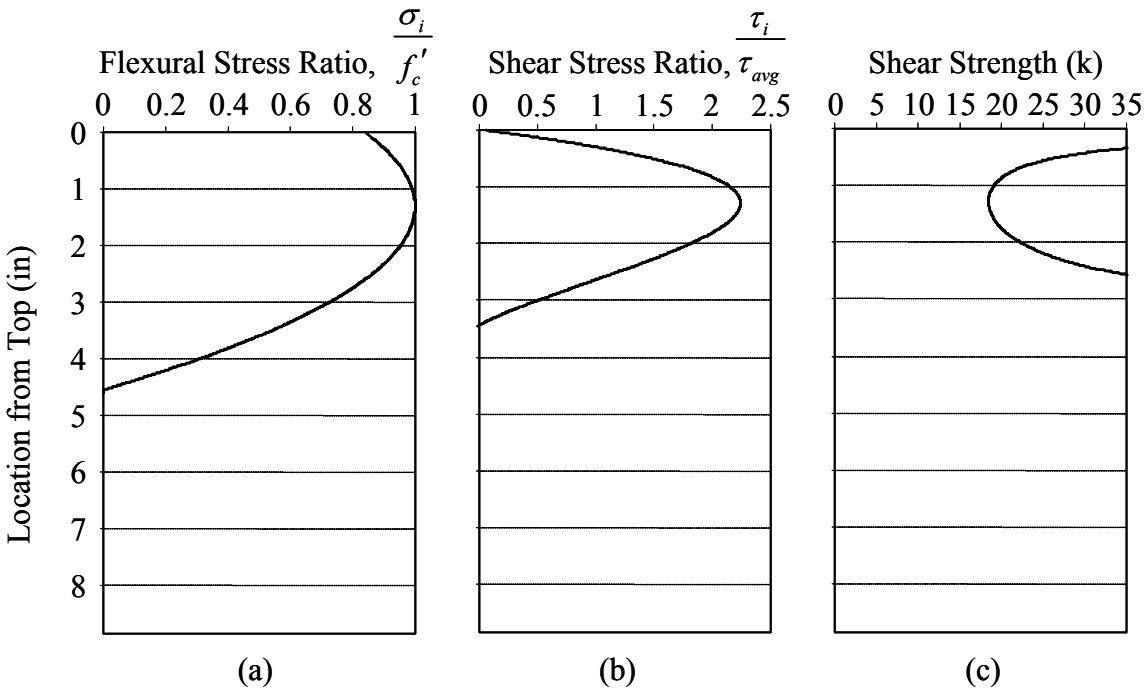

Figure 3.3: Variation of the Stress Ratios and Shear Strength throughout the Compression Zone at 2.84 M_{cr}

After an analysis of Sozen's rectangular test specimens was performed, data was recorded regarding the load, neutral axis depth and value of K at failure. K was found by dividing the calculated failure load by $\sqrt{f_c'}bc$, where c is the neutral axis depth at the failure moment. The values of K were plotted versus the initial axial precompression, P/A, in Figure 3.4 and versus the multiple of cracking moment in Figure 3.5.

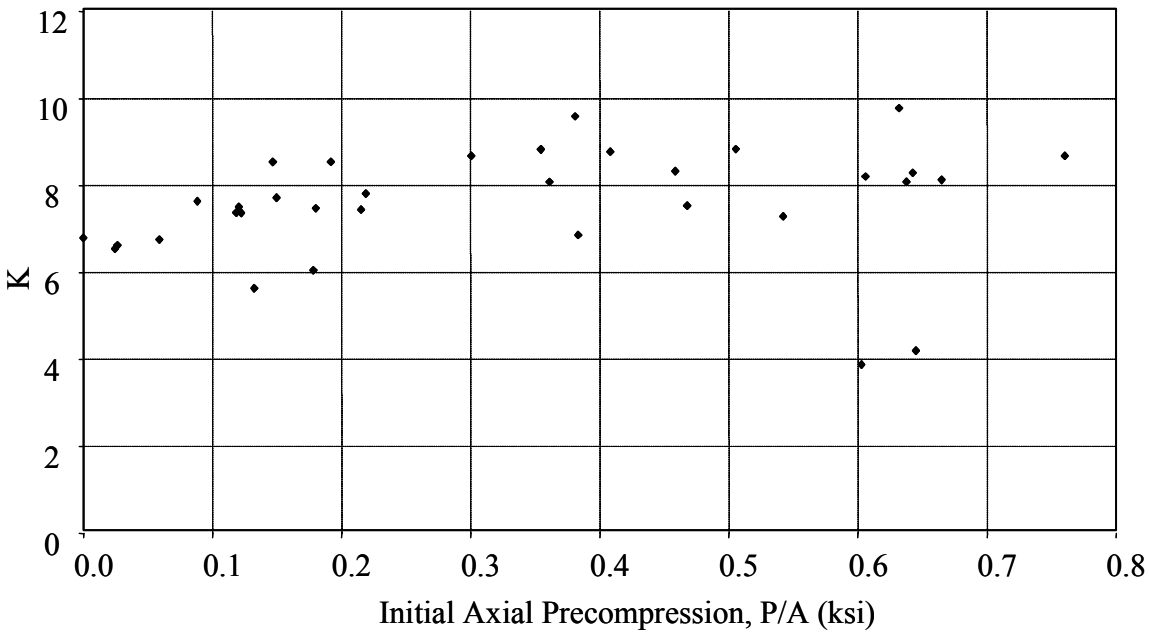

Figure 3.4: K at Failure Varying with Initial Axial Precompression (Method 1)

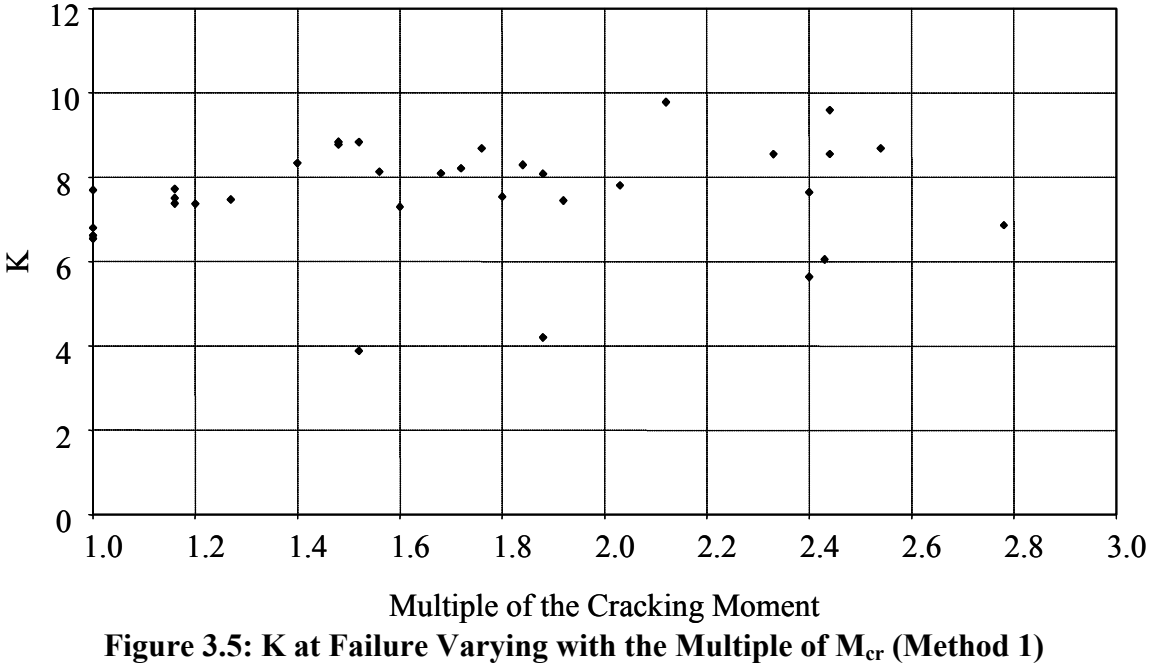

Figure 3.5: K at Failure Varying with the Multiple of M_{cr} (Method 1)

Although most values lie above 5 on the graph, there is no consistent trend of the data in either graph. The two points that lie below the value 5 are products of nonlinear effects. Both of these specimens were close to flexural failure at the failure of the test specimen in shear. As the flexural stress becomes more nonlinear, the shear stress has

more of a prominent peak value in the compression zone. As shown earlier, a higher shear stress creates a weaker section. Because K is determined by dividing the strength of the section by its physical properties, a weak section will have a lower value for K. Therefore, nonlinearities in the flexural stress distribution can cause the shear strength of a section to become weaker, regardless of high flexural stress.

3.4 Method Two

The second method to determine K utilized the experimental data to determine a conservative value of K. As in Method One, Sozen's rectangular data was used to determine a value of K to be a lower bound. $K\sqrt{f_c'}$ is a value that represents the average shear stress which causes a local shear failure. It was shown in Chapter 2 that K is based upon the flexural stress on the section. Therefore, K was evaluated considering the multiple of the cracking moment.

The general form of this equation for K is given by Equation 3.1.

$$K = 5 + \alpha(\nu - 1) \qquad \text{(Eq. 3.1)}$$

where:

ν : multiple of the cracking moment

α : integer to modify the influence of the applied moment

Method One indicated that for sections behaving linearly, a value of K equal to 5 provides a reasonable lower bound. A value of 5 was selected as the value for K at the cracking moment $(\nu = 1.0)$ to match the equation proposed by Tureyen for nonprestressed sections. For nonprestressed sections, which have a constant neutral axis depth, the location of the cracking moment $(\nu = 1.0)$ is the weakest section along the length of the beam.

Listed in Table 3.1 are the statistical results for the variation of α. Only one nonprestressed rectangular section was reported to have failed as a result of flexure-shear; therefore, the standard deviation and coefficient of correlation values were not applicable for the nonprestressed sections. In addition, Figure 3.6 shows the variation of the accuracy of the different α values. As shown in Figures 3.6 (a) and 3.6(b), using an α equal to 2 and 1 returns unconservative results. It is conservatively recommended to use a value of α equal to 0. Therefore, Equation 3.1 simplifies to 5, regardless of the level of applied moment and is represented by Equation 3.2.

$$V_{ci} = 5\sqrt{f_c'}bc \qquad \text{(Eq. 3.2)}$$

Table 3.1: Performance of α Values

	α =	2	1	0
All	**All Rectangular Sections**			
	Average	1.34	1.40	1.49
	StDev	0.238	0.228	0.215
	Correl	0.881	0.899	0.924
Prestress Level	**P/S Rectangular Sections**			
	Average	1.33	1.40	1.48
	StDev	0.237	0.228	0.217
	Correl	0.876	0.895	0.921
	Non-P/S Rectangular Sections			
	Average	1.61	1.61	1.61
	StDev	N/A	N/A	N/A
	Correl	N/A	N/A	N/A

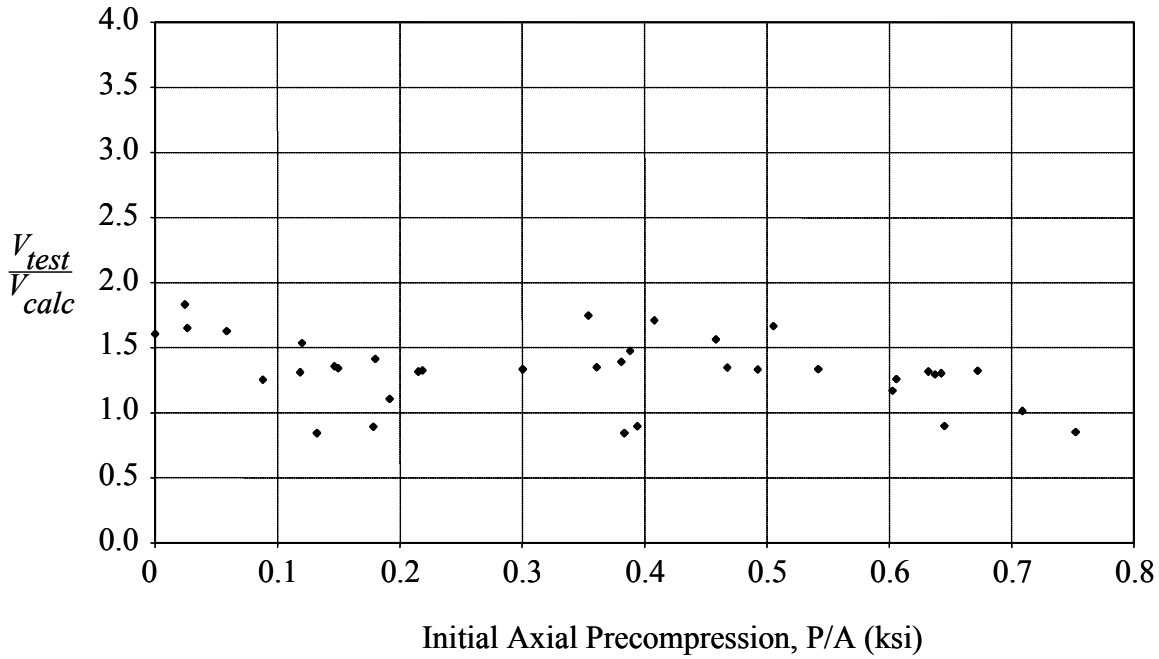

Figure 3.6(a): Performance of a = 2

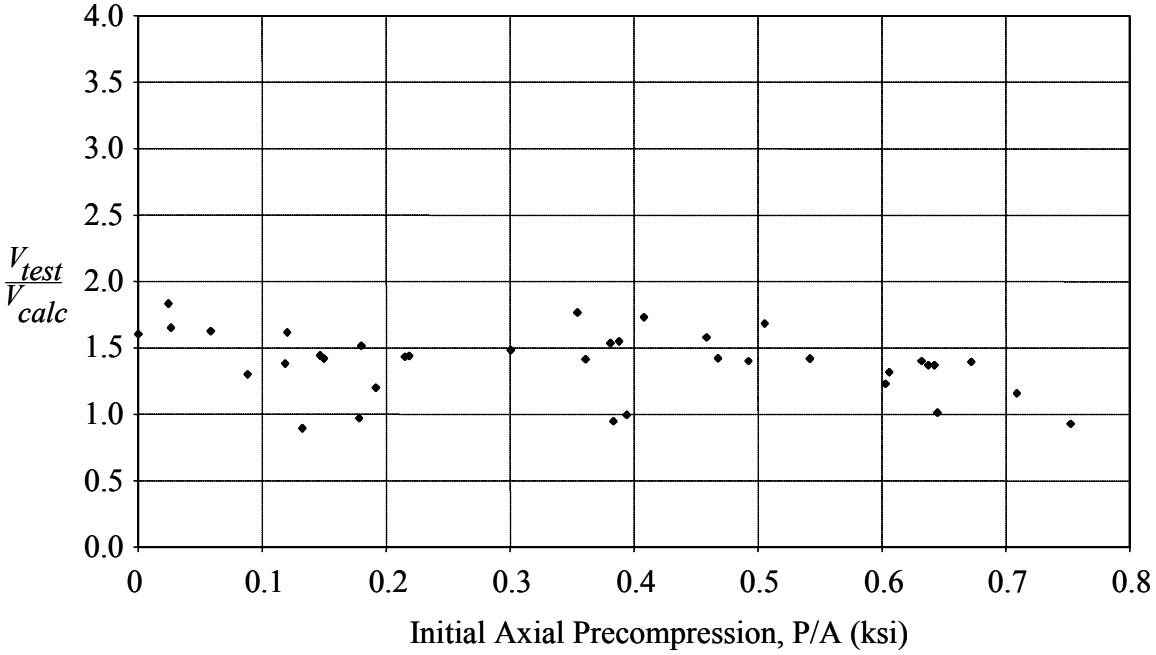

Figure 3.6(b): Performance of a = 1

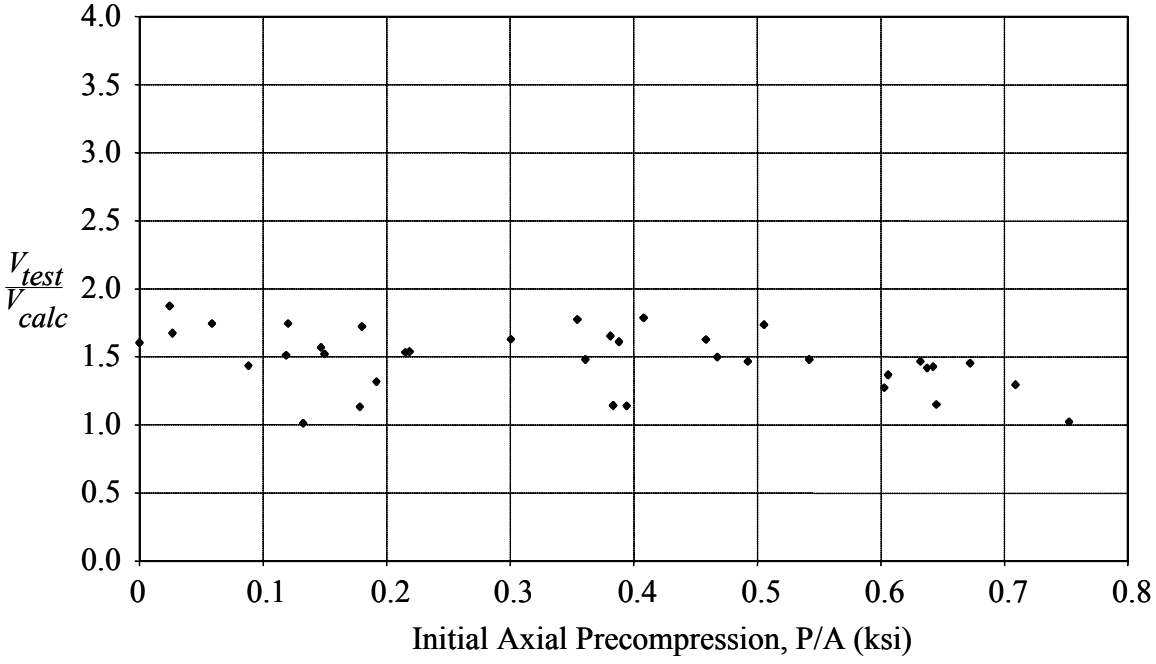

Figure 3.6(c): Performance of a = 0

Method One and Method Two attempted to simplify the calculations for shear strength by determining a lower bound value for K. Method One used the analytical

model to determine K, however, complications from nonlinearity during the analysis prevented a general value from being determined. Method Two used empirical data to find a conservative value for K. Equation 3.1 was reduced to a constant value of 5 due to its consistent and conservative results. Given that Method Two is accurate with the prestressed database and consistent with the proposed approach to nonprestressed beams, Method Two was selected to simplify K.

3.5 Irregular Compression Zones

K was determined from an analysis of rectangular sections subjected to combined flexure and shear. However, this computation method does not directly apply to irregular shapes such as I and T-sections. K represents an average shear stress on the entire compression zone which causes a flexure-shear shear failure. The irregular compression zones of I and T-sections provide a complication. Equation 3.2 considers the entire compression zone to act equally in shear resistance. If b is taken to be b_w, the equation does not account for any of the flanges to resist shear. In order to obtain a more accurate shear strength calculation for sections with irregular compression zones, the contribution of the flanges needed to be determined.

To determine this method, a database of 150 reinforced concrete T-beams was analyzed (Kani 1979; Placas and Regan 1971; Farmer and Ferguson 1967; Laupa, Siess and Newmark 1953). Reinforced concrete sections were considered for this analysis, as the neutral axis depth does not change throughout loading causing the weakest point for shear to be located at the cracking moment. When a reasonably accurate method was developed for reinforced concrete, it was tested to determine its applicability to prestressed T-sections.

3.5.1 Reinforced Concrete Beams

Initially, the T-beams were analyzed using Equation 3.3.

$$V_c = 5\sqrt{f_c'}A_{eff} \qquad \text{(Eq. 3.3)}$$

In Equation 3.3, two areas were used for A_{eff}. The first area involved the entire compression zone. Figure 3.7(a) presents the cross-section of Specimen 4858 from a test series by Kani (Kani 1979), along with its neutral axis location at flexure-shear failure. The hatched area represents the effective shear resistance area of the T beam, which was found using an elastic analysis of a reinforced concrete section. At failure, this method calculated a shear capacity of 19.28 kips. However, the actual failure of this specimen resulted was 17.20 kips.

The next method computed the shear strength using an effective shear area equal to $b_w c$. The hatched area in Figure 3.7(b) illustrates the effective area for this method. The neutral axis depth is identical to the last method, but the flanges are ignored when determining the effective shear area. At failure, this method gives a shear capacity of 7.52 kips. As stated earlier, the failure load was 17.20 kips.

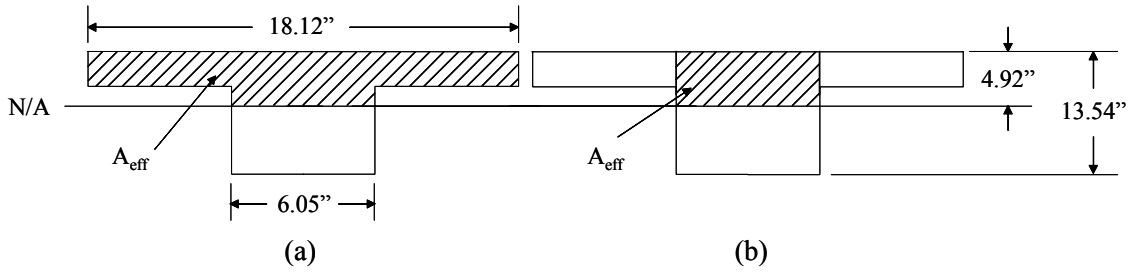

Figure 3.7: T-Beam Shear Resistance Areas

All of the database specimens were analyzed using the entire compression zone to resist shear and the results are shown in Figure 3.8. Also, the same specimens were analyzed using $b_w c$ as the effective shear area and the results are shown in Figure 3.9. Ultimately, using the entire compression zone accounts for too much area to resist shear and using $b_w c$ accounts for too little. Portions of the flanges of a T-section, therefore, contribute to the shear resistance and an equivalent area involving the flanges was determined.

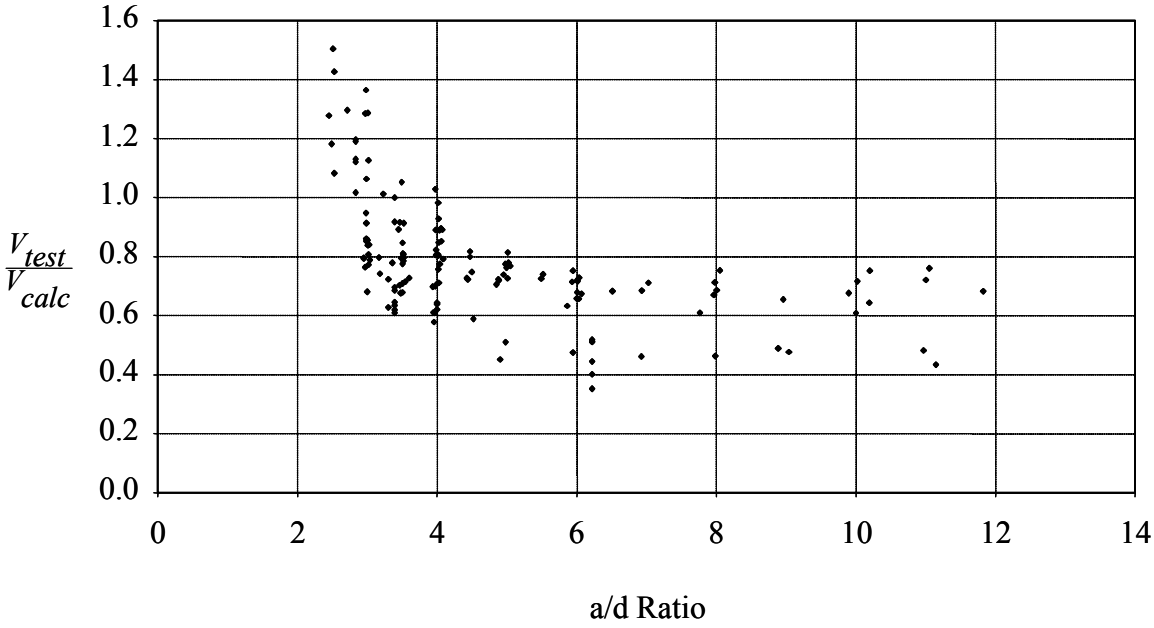

Figure 3.8: Performance of Entire Compression Zone Resisting Shear

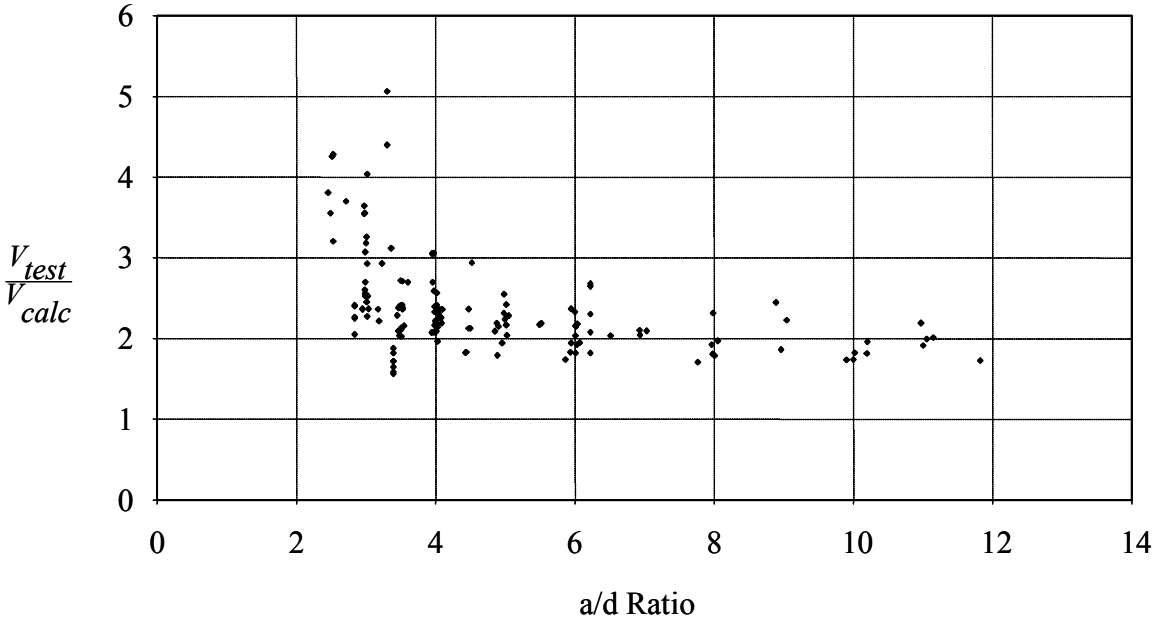

Figure 3.9: Performance of $b_w c$ Resisting Shear

To determine the effective shear area, two methods were used to ascertain the amount that the flanges contributed to the shear strength. First, an effective flange width was used to limit the contribution of the flanges in wide flanged members. In the second method, the shear area was determined considering an angled area from the web.

3.5.1.1 Method One

Method One involves using an effective flange width, similar to the method currently used by ACI to evaluate T-beams for flexural strength. Sections with narrow flanges are not influenceed by this limitation while wide flanged sections are limited to a flange width which is a function of either the web width or the flange thickness.

Analyses were performed on the database to determine the effective flange width. The generalized equation for shear strength was as shown in Equation 3.3, where A_{eff} is defined in Equation 3.4.

$$A_{eff} = b_w c + (b_{eff,v} - b_w) t_f \quad \text{if } c \geq t_f \qquad \text{(Eq. 3.4)}$$

$$A_{eff} = b_{eff,v} c \quad \text{if } c \leq t_f$$

The only unknown in Equations 3.3 and 3.4 is $b_{eff,v}$. The required A_{eff} was computed from the measured failure shear. From $A_{eff,}$, $b_{eff,v}$ was determined and represented as the web width plus an additional effective overhang, as shown in Figure 3.10. The total effective overhang was expressed as a constant times either the flange thickness or the web width, as shown in Equations 3.5 and 3.6, respectively. These two methods will be referred to as the t_f and b_w methods, respectively. The results for the ideal coefficients for t_f are shown in Figure 3.11, while the results for b_w are shown in Figure 3.12.

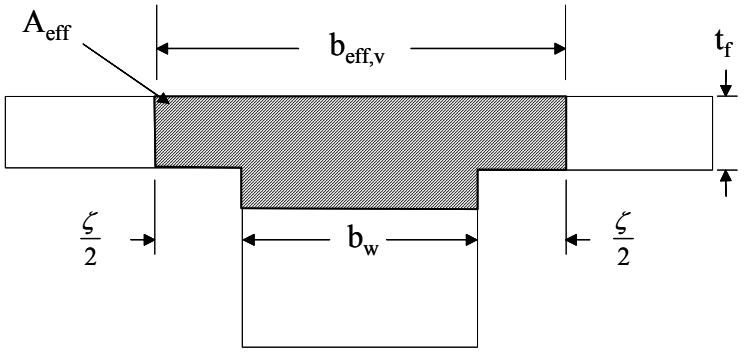

Figure 3.10: Definition of $b_{eff,v}$

$$\zeta = \beta \cdot t_f \qquad \text{(Eq. 3.5)}$$

where:

ζ : total effective overhang, in.

β : constant to modify t_f

$$\zeta = \gamma \cdot b_w \qquad \text{(Eq. 3.6)}$$

where:

γ : constant to modify b_w

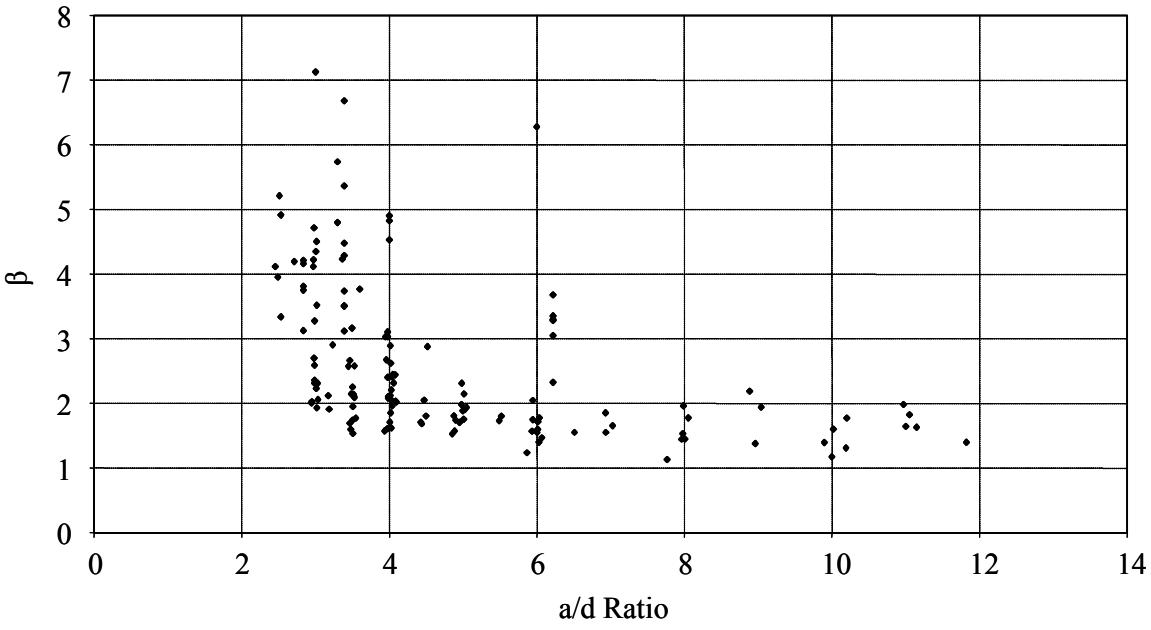

Figure 3.11: Ideal Coefficients for t_f Method

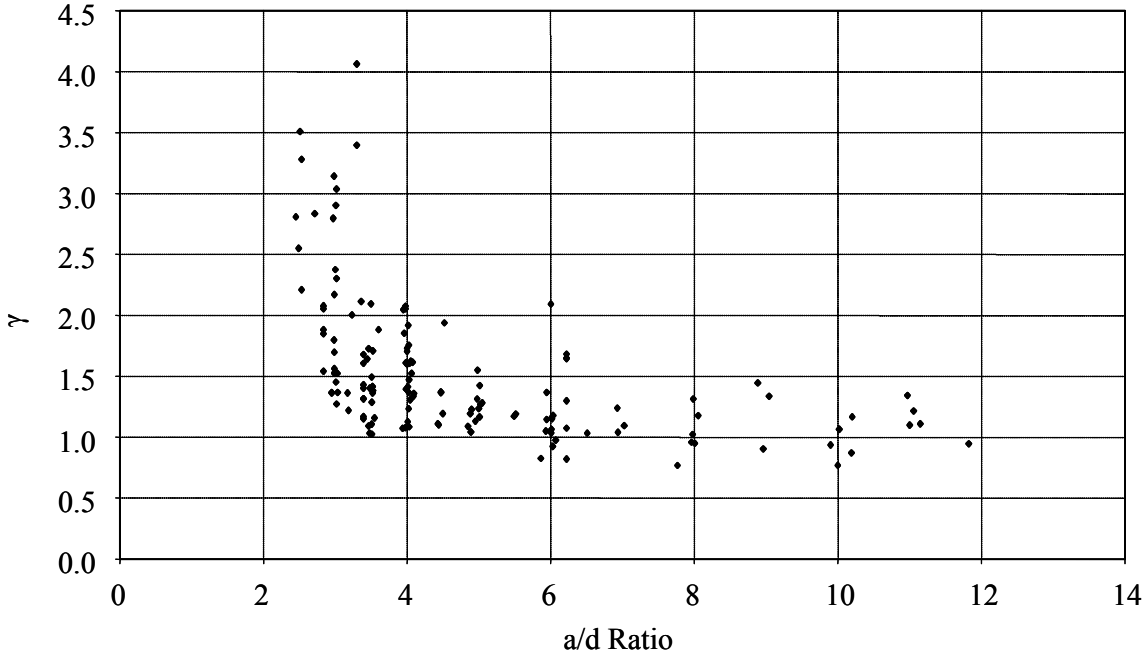

Figure 3.12: Ideal Coefficients for b_w Method

Examining the results for β, the coefficients of t_f are scattered from 1 to 8, where most lie between 1 and 6. Examining γ yields better results. The coefficients of b_w are in a band from 0.75 to 4.0 with the majority lying between 0.75 and 2.0. However, in both analyses, 20 of the 150 specimens required an effective flange that exceeded the actual width of the section.

Considering these results, each specimen was evaluated using lower bound values of $b_{eff,v}$ which were calculated using β equal to 1.0 and γ equal to 0.75. The results for the t_f method are shown in Figure 3.13 and the results of the b_w method are shown in Figure 3.14.

For most data points, both methods performed similarly. At high a/d ratios, both methods accurately calculated the strength of the specimens. At low a/d ratios, both methods are increasingly conservative as the a/d ratio approaches 2.0. However, the t_f method is slightly more conservative at low a/d ratios. Even so, for a/d ratios greater than 3, both methods calculated shear strength values consistent with the test failure shears.

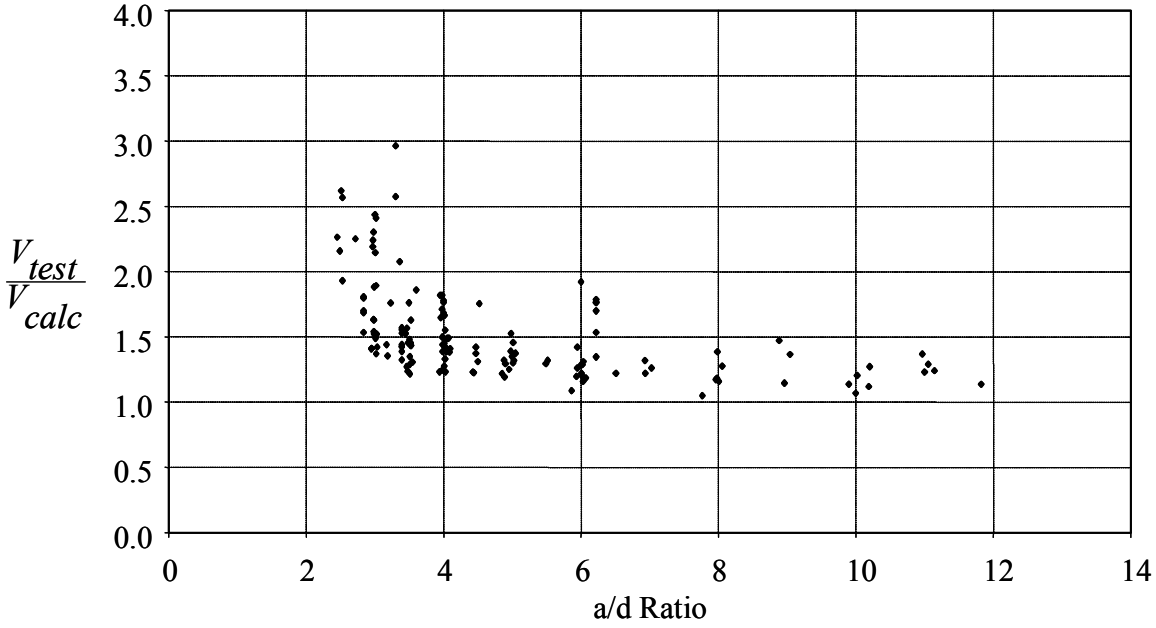

Figure 3.13: Results Using Total Effective Overhang Equal to $1.0t_f$

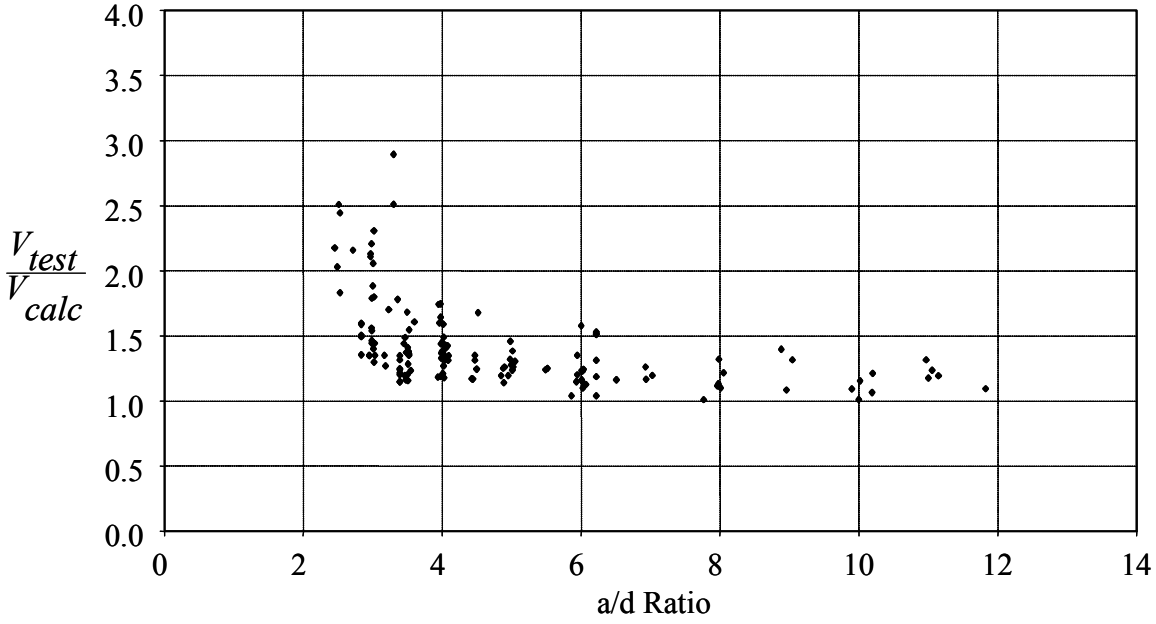

Figure 3.14: Results Using Total Effective Overhang Equal to $0.75b_w$

3.5.1.2 Method Two

Method Two involved first determining the neutral axis depth of the nonprestressed section and then defining the shear area. Again, the shear strength was taken as Equation 3.3. However, A_{eff} was taken equal to $b_w c$ plus an area formed by inclined slices of the portion above the flange-web junction, as shown in Figure 3.15.

The required A_{eff} was calculated from the experimental results and the angle required was determined. Figure 3.16 shows the ideal angles of each beam in the database needed to calculate the shear strength exactly. A lower-bound and simple value of 45^0 was used to determine A_{eff}. Again, several of the members with compact flanges had less physical area than the 45^0 angle required. An example is shown in Figure 3.17. Therefore, the widths of those sections were limited to their actual physical flange widths. The database was then evaluated using the 45^0 angle effective area and the results are shown in Figure 3.18.

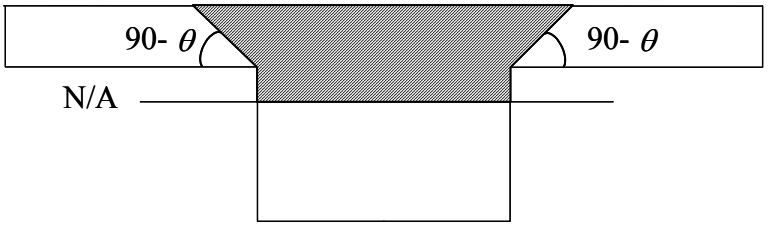

Figure 3.15: Application of Angled Effective Shear Area

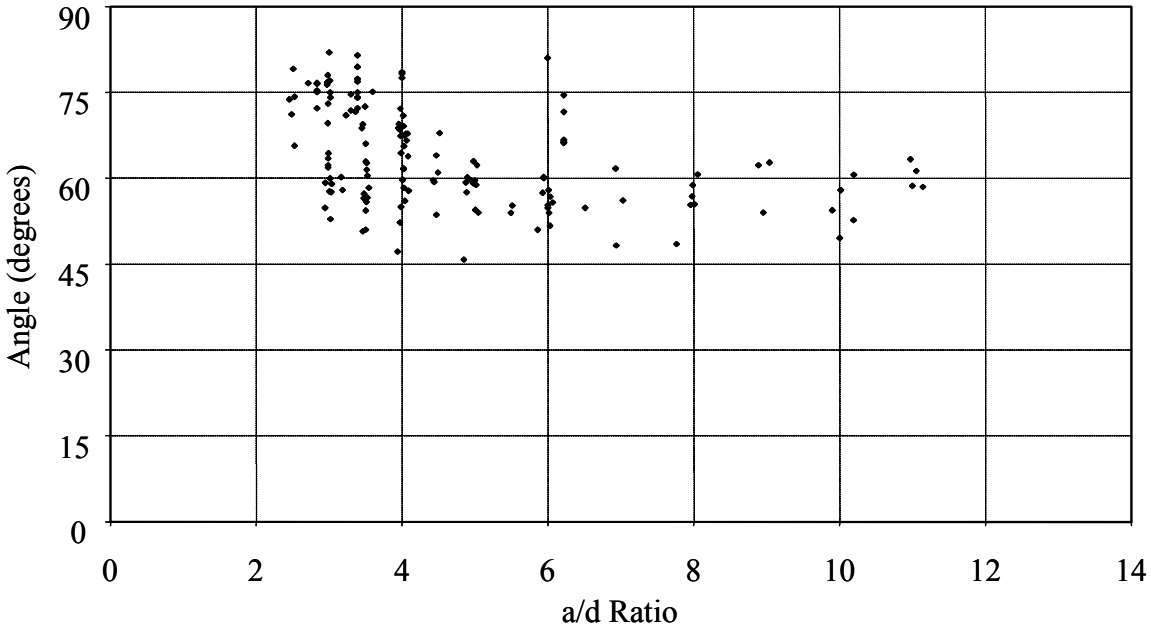

Figure 3.16: Ideal Angle for Angled Effective Shear Area

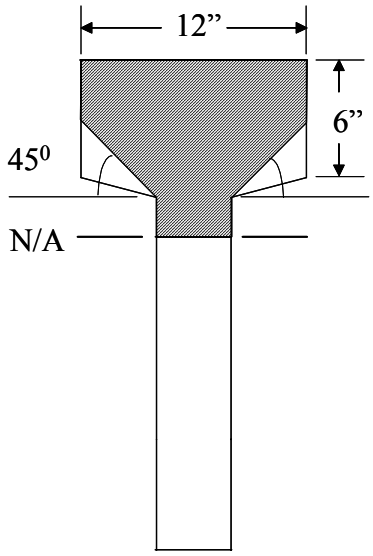

Figure 3.17: T-Section with Compact Flanges

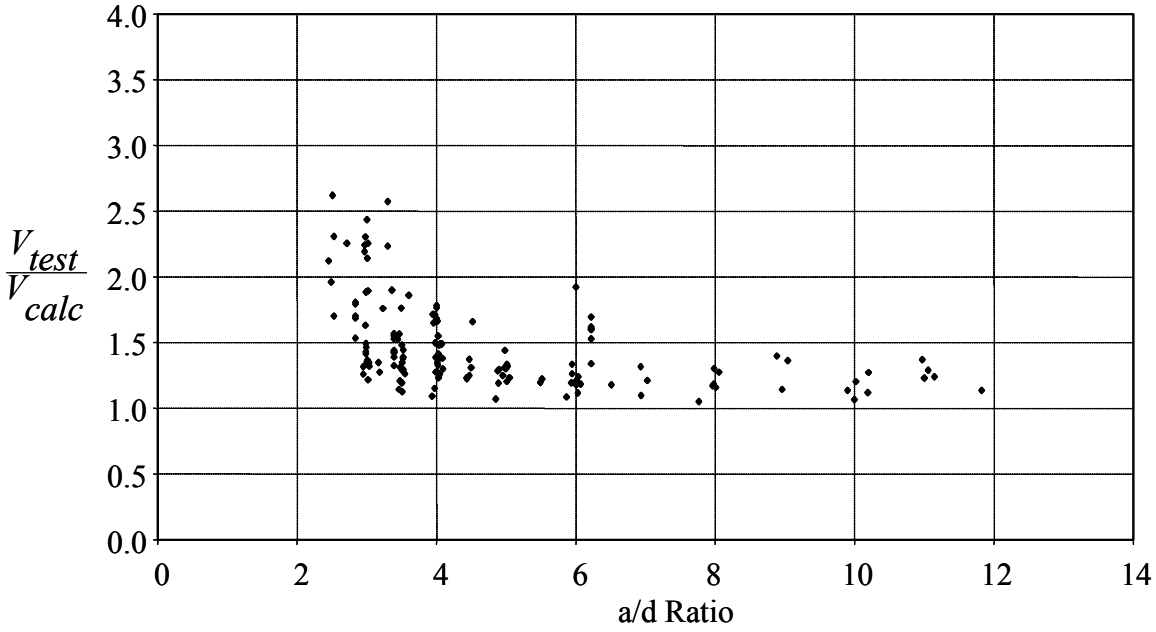

Figure 3.18: Results using an Angle of 45^0 to Determine the Effective Shear Area

3.5.2 Reinforced Concrete Conclusion

Because of their empirical derivations, all three methods to determine an A_{eff} performed well with the reinforced concrete database. The statistical results of all three methods are listed in Table 3.2. Each method limits the area which can be used to resist shear. Sections with wide flanges are limited to more compact flanges, while compact

sections are not affected. Each method worked well with reinforced concrete and was applied to the prestressed database to determine their applicability to these sections.

Table 3.2: Results of T-Beam Analysis Using Effective Area Methods

	$0.75b_w$ Method	$1.0t_f$ Method	45^0 Angle Method
Average	1.41	1.52	1.46
StDev	0.322	0.345	0.326
Correl	0.815	0.813	0.810

3.6 Application of Effective Overhang to Prestressed Beam Database

The three effective shear areas were used to calculate the shear strength of the sections in the prestressed beam database to determine their applicability to prestressed sections. Two basic shapes were used in the database; a set with a nominal 3" web and a set with a nominal 1.75" web. Typical beams from each set are shown in Figure 3.19. For clarity, the prescribed shear area for each method is shown on each cross-section. For the t_f method, t_f was taken as the thickness of the flange, not including the chamfer.

After the analyses were performed on the sections using the three methods, it was clear that the use of the 45^0 angle and t_f method provide better results than the b_w method. The b_w method is more conservative for both sets of I sections, especially the thin webbed sections (1.75"). The results of the b_w method are shown in Figure 3.20. The main difficulty with this method is that it does not adjust to sections with thick flanges. It maintains the same width throughout the depth of the flange. Sections with wide flanges and thin webs have little effective area to resist shear. This is compounded by wide flanged sections tending to have shallow neutral axes, reducing the effective shear area. For these reasons, this method can be very conservative.

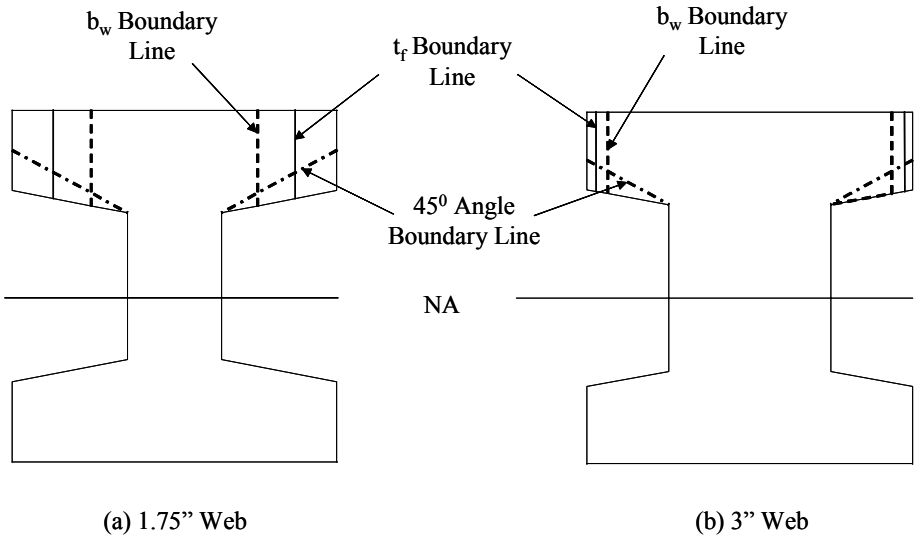

Figure 3.19: I-Sections from the Prestressed Beam Database with Effective Shear Areas

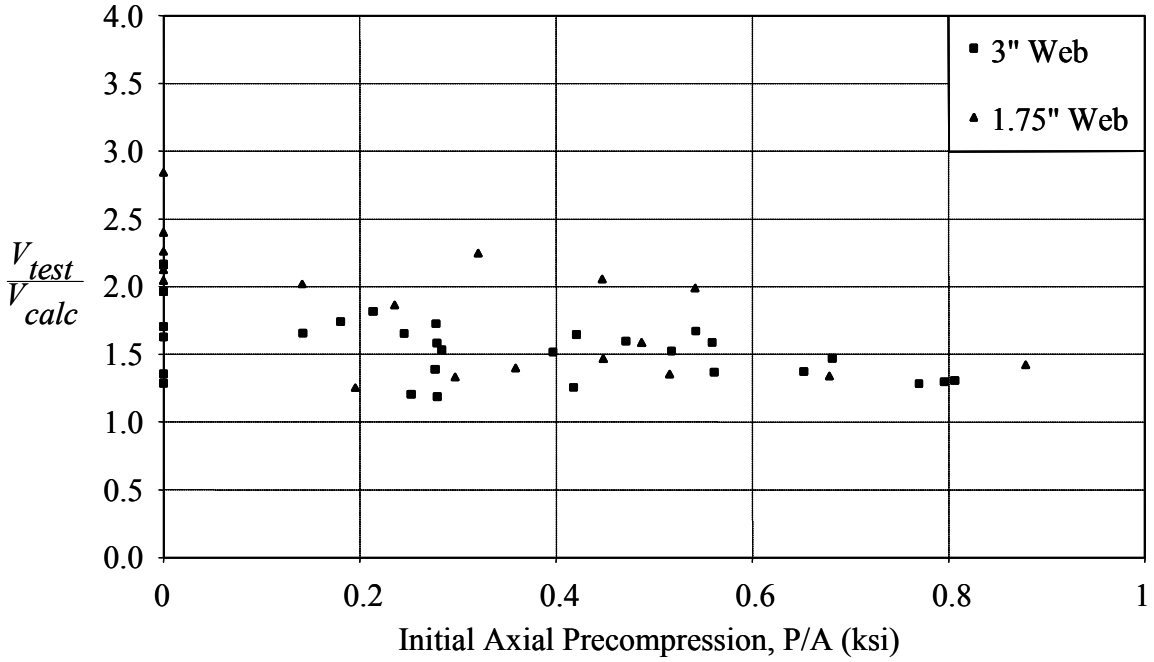

Figure 3.20: Application of b_w Method to Prestressed I-Beams

The 45^0 and t_f methods are not only dependant on the width of the web, but also the thickness of the flange. Therefore, these methods do not encounter the same problems as the b_w method. The results of the t_f method are shown in Figure 3.21 and the results for the 45^0 method are shown in Figure 3.22. The 45^0 method models itself as a "shear funnel", which represents the shear flowing towards the web of the section. If the flanges are thick, portions of the flange away from the web contribute to the strength due to a direct path to the web.

The adaptability of the t_f and 45^0 methods allow for the use of a simple area to apply a uniform shear stress. These methods work relatively well with both prestressed and reinforced sections. The statistical results of all three methods are presented in Table 3.3, for the prestressed database. Statistically, the 45^0 angle method performs the best, but the t_f method is both accurate and simple. Therefore, the t_f method was selected to determine the effective shear area of sections with irregular compression zones. The results of the entire prestressed database, including both rectangular and I-sections, are shown in Figure 3.23 using a shear strength of $5\sqrt{f_c'}A_{eff}$.

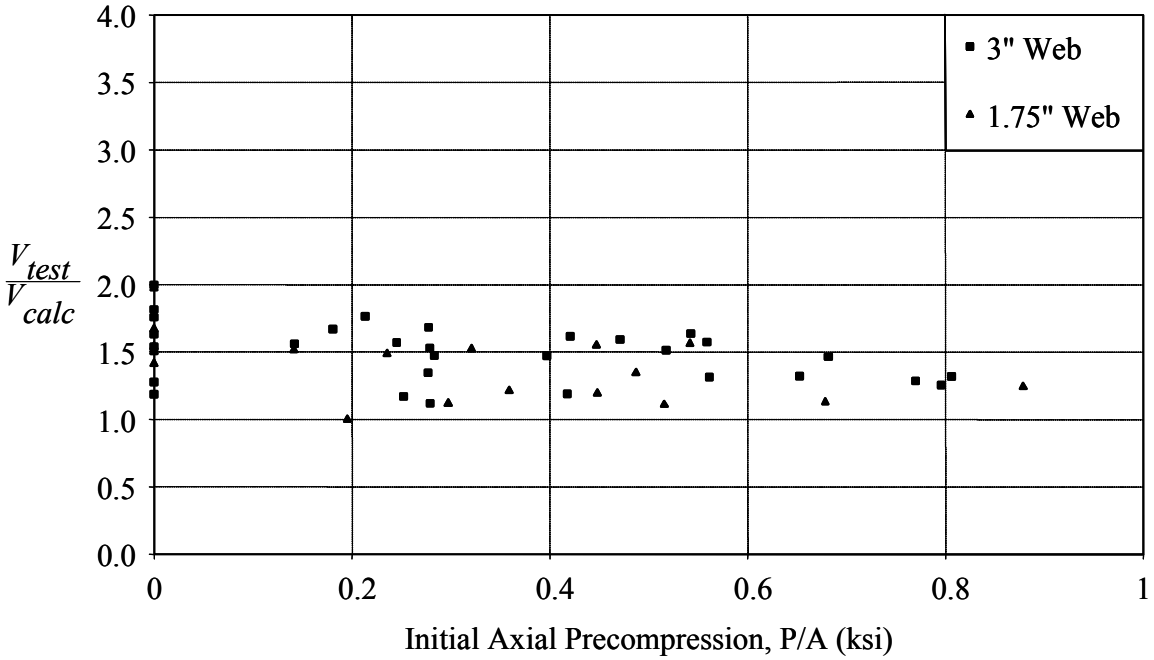

Figure 3.21: Application of t_r Method to Prestressed I-Beams

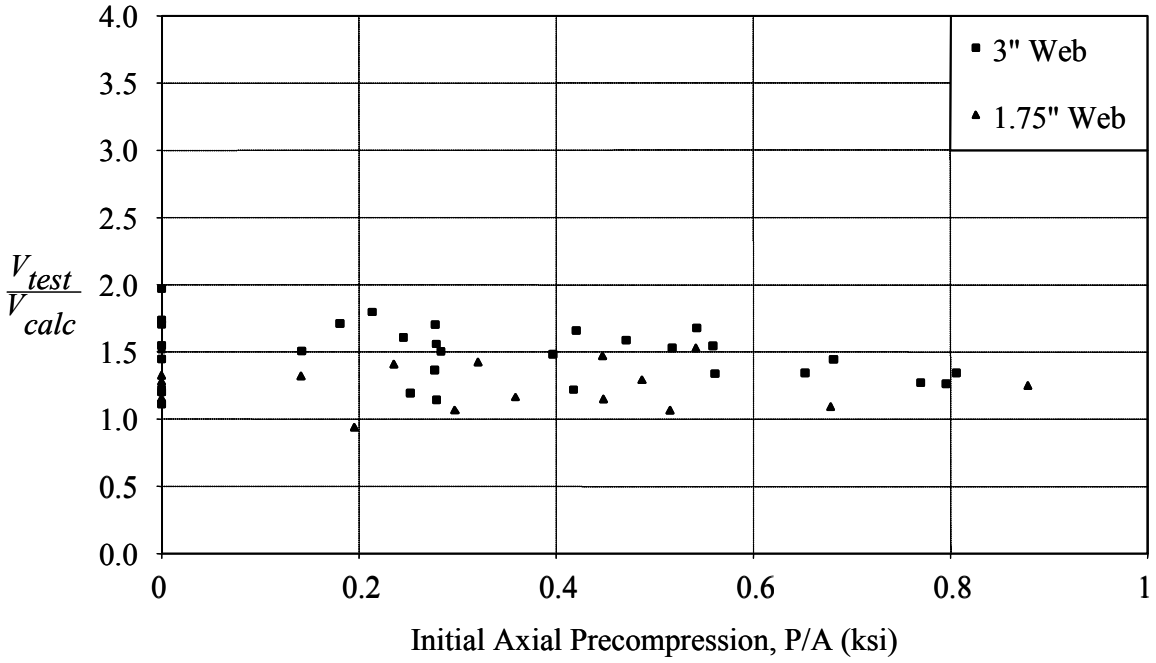

Figure 3.22: Application of 45^0 Angle Method to Prestressed I-Beams

3.7 Recommendations

In this chapter, the simplification of a critical average shear stress was made to limit the number of calculations needed to determine the shear capacity of prestressed concrete sections. Using this simplification, the design equation for flexure-shear strength is as shown in Equation 3.7. For rectangular sections, A_{eff} is equal to the area of the compression zone. However, special provisions are needed for sections with irregular compression zones. Introducing an effective overhang distance for I and T-Sections allows the critical average shear stress simplification to be applied to irregular shapes.

The shear design equation provides a simple method to calculate the flexure-shear strength of prestressed sections. To give perspective, the results for the shear model are shown again in Figure 3.24 and the statistical results of both methods are shown in Table 3.4. Although the data is not as compact using the design equation when compared to the shear model, it is consistently conservative and practical for use in design.

$$V_{ci} = 5\sqrt{f_c'}A_{eff} \qquad \text{(Eq. 3.7)}$$

where:

f_c' : compressive strength of concrete, psi

A_{eff} : effective shear resistance area, in^2

Table 3.3: Statistical Analysis of Methods

	Statistic	ACI 318	45^0 Method	t_w Method	t_f Method
All	**All Sections**				
	Average	1.91	1.44	1.59	1.47
	ST DEV	0.508	0.223	0.320	0.221
	Correl	0.802	0.928	0.932	0.933
Section Shape	**Rectangular Sections**				
	Average	1.72	1.49	1.49	1.49
	ST DEV	0.461	0.215	0.215	0.215
	Correl	0.751	0.924	0.924	0.924
	I-Sections				
	Average	2.05	1.40	1.67	1.46
	ST DEV	0.500	0.223	0.364	0.227
	Correl	0.895	0.923	0.932	0.933
Prestress Level	**Prestressed Sections**				
	Average	1.75	1.48	1.48	1.48
	ST DEV	0.444	0.217	0.217	0.217
	Correl	0.783	0.914	0.921	0.919
	Nonprestressed Sections				
	Average	2.08	1.44	1.96	1.61
	ST DEV	0.743	0.256	0.420	0.234
	Correl	0.179	0.463	0.589	0.699

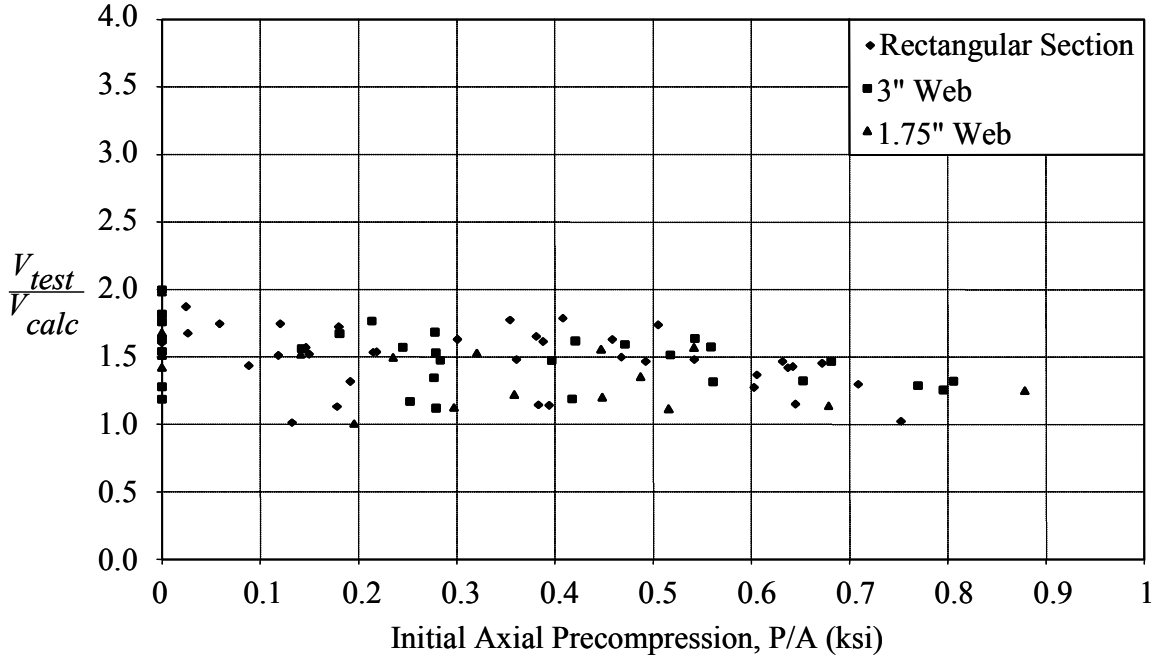

Figure 3.23: Results using $5\sqrt{f_c'}A_{eff}$

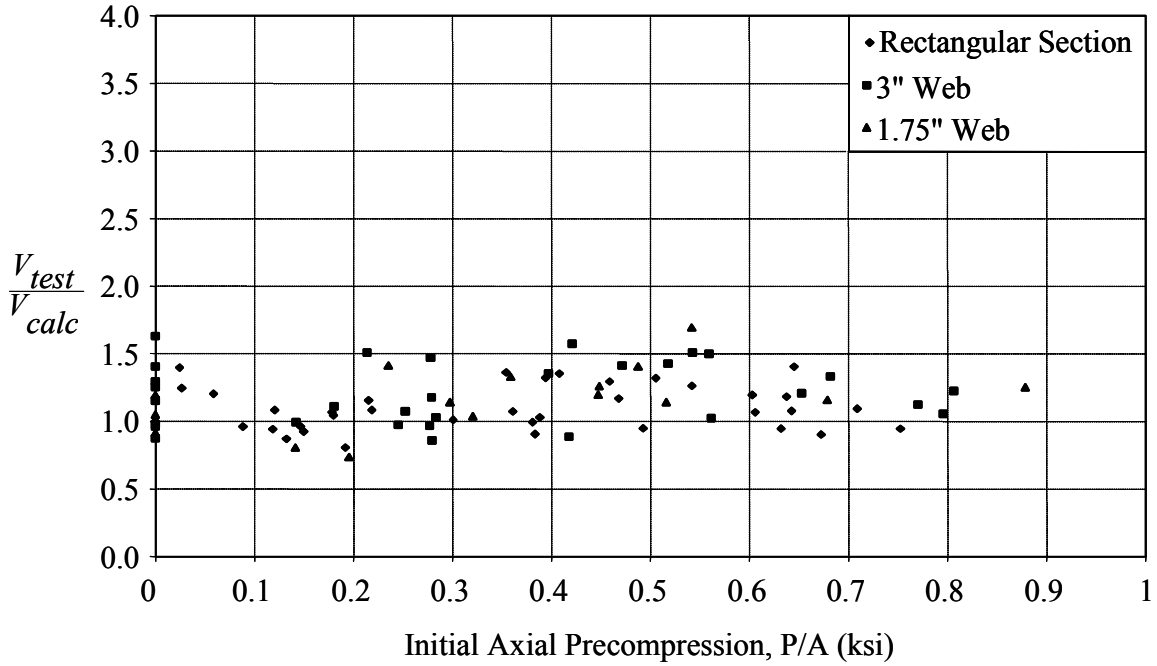

Figure 3.24: Performance of Shear Model

Table 3.4: Results of Analyses

	Statistic	Shear Model	Simplified Method
All	**All Sections**		
	Average	1.15	1.47
	ST DEV	0.203	0.221
	Correl	0.897	0.933
Section Shape	**Rectangular Sections**		
	Average	1.11	1.49
	ST DEV	0.160	0.215
	Correl	0.913	0.924
	I-Sections		
	Average	1.19	1.46
	ST DEV	0.226	0.227
	Correl	0.874	0.933
Prestress Level	**Prestressed Sections**		
	Average	1.11	1.48
	ST DEV	0.162	0.217
	Correl	0.875	0.919
	Nonprestressed Sections		
	Average	1.14	1.61
	ST DEV	0.209	0.234
	Correl	0.424	0.699

CHAPTER 4
DESIGN CONSIDERATIONS

4.1 Introduction

In the previous chapter, a design equation was proposed to calculate the flexure-shear strength of prestressed concrete. The equation was derived by simplifying the shear model in order to generate an equation which could be easily implemented in design. In this chapter, an example is used to demonstrate the design procedure using the proposed design equation.

4.2 Example Beam Design: Uniform Load

An example beam was chosen to illustrate the design process using the proposed design equation. The example beam is simply supported and subjected to a live load of 1.5 kip/ft over its entire 70 foot span. Using ACI 318-02 load and resistance factors, the moment at midspan corresponds to the maximum allowable moment of the section, which is 1815 k-ft. The moment and shear diagrams for the loading are shown in Figure 4.1. The maximum design shear, which is located at a distance d away from the support, is 95.1 kips. Because the load is uniformly distributed along the beam, the applied shear is linearly sloped and equal to zero at midspan.

To determine the cross-section, the example beam was designed based on the maximum applied moment. Any applied shear which cannot be resisted by the section will be resisted by stirrups. The material properties and dimensions, as well as the effective overhang, are shown in Figure 4.2. Because the effective overhang is a function of only the geometry of the section, the effective shear area is only a function of the neutral axis depth.

As stated in Section 2.3, the neutral axis depth varies with the applied moment. Therefore, the neutral axis depth, and subsequently the shear strength, is dependant on the applied moment. For each point along the length of the beam, the neutral axis depth was determined based upon the factored moment corresponding to that point. The neutral axis depths are plotted on the half span in Figure 4.3.

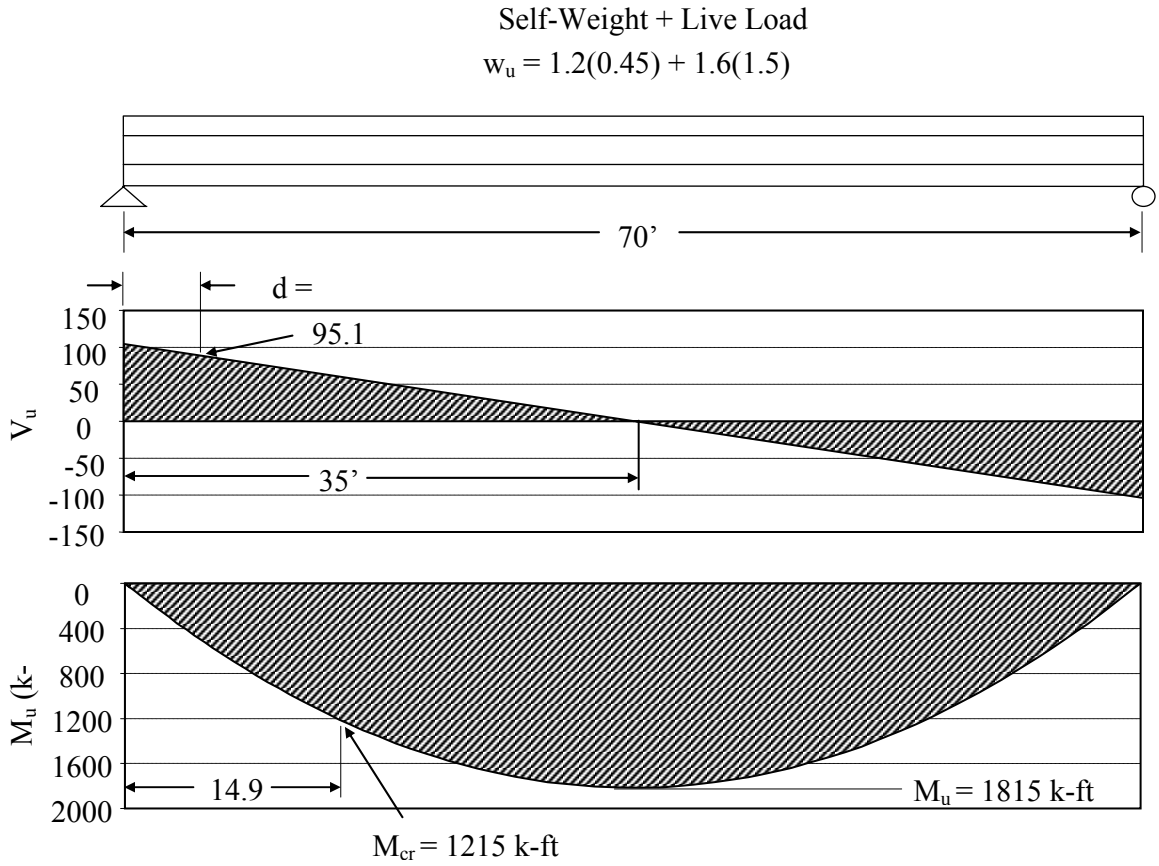

Figure 4.1: Shear and Moment Diagrams for Example Beam

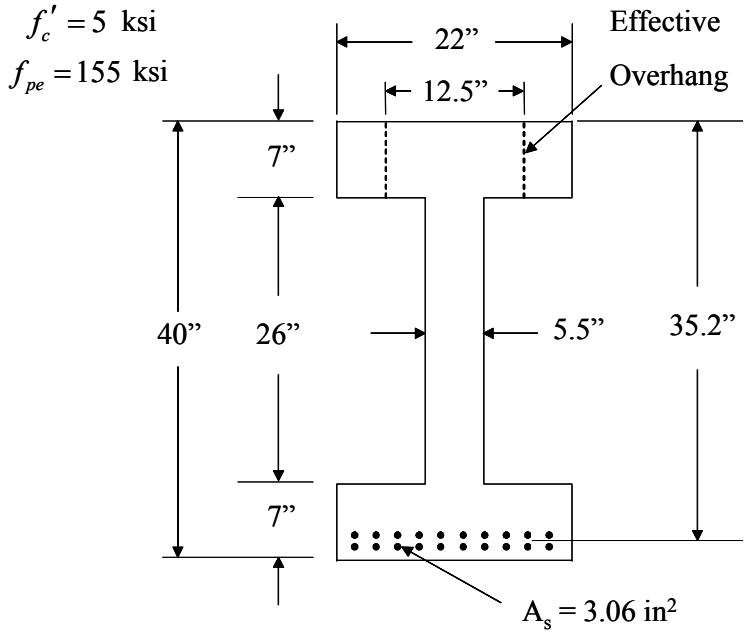

Figure 4.2: Details of Example Beam

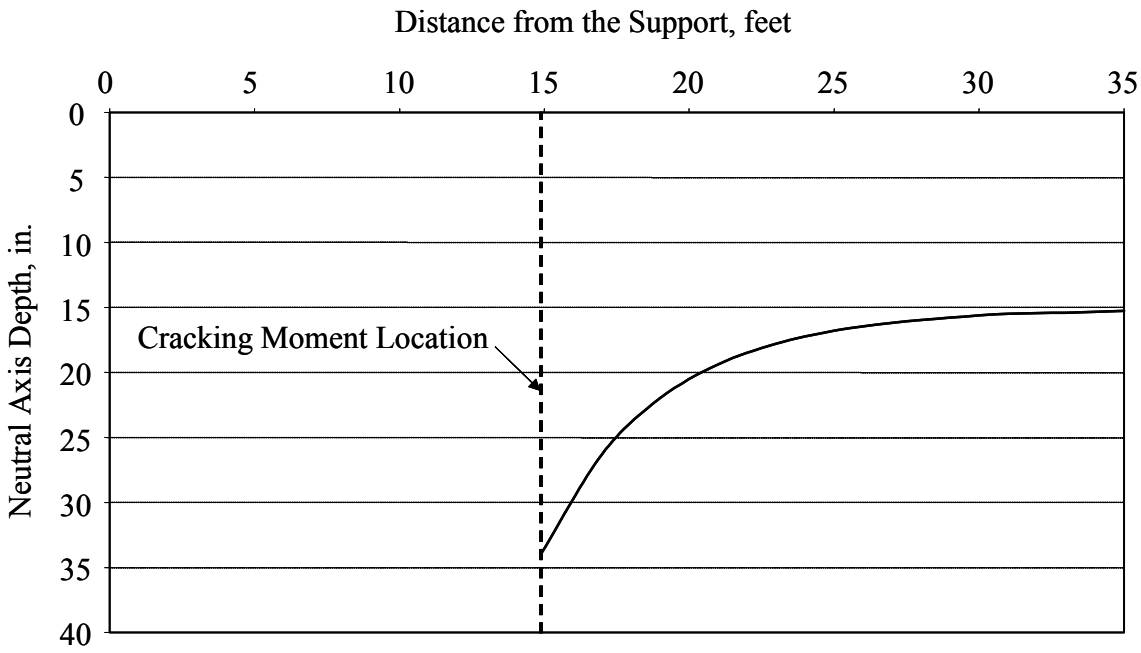

Figure 4.3: Variation of the Neutral Axis Depth

4.2.1 Design Method

The shear strength provided by the concrete is given in Equation 4.1.

$$V_{ci} = 5\sqrt{f_c'}A_{eff} \qquad \text{(Eq. 4.1)}$$

It should be noted that the shear resistance at sections that have an applied moment which does not exceed the cracking moment is provided by the web-shear strength of the section. The web-shear strength will be discussed later.

Twelve points were chosen to determine the shear strength curve for the beam. One point was located at the cracking moment, another at the support and ten spaced 2 ft apart between the midspan and the location of the cracking moment. The location, applied loading and neutral axis depth are tabulated in Table 4.1, along with the shear strength. The nominal shear, V_n, was found by dividing the factored shear by the current resistance factor for shear ($\phi = 0.75$), using ACI 318-02. If the AASHTO 16th Edition Specifications were used, the process would be identical; however, the load and resistance factors would change. AASHTO uses higher load factors (1.3D+2.17L) than ACI (1.2D+1.6L); but the higher load factors are offset due to the differing phi factors (0.85 for AASHTO and 0.75 for ACI). While differences depend on the dead load to live load ratio, similar results can be expected.

V_{ci} was calculated using A_{eff}, which is a product of the neutral axis depth and the effective overhang. V_{ci} is graphed on half the span in Figure 4.4, along with the applied shear.

Figure 4.4 shows that the concrete alone is not capable of carrying the applied shear. The hatched portions on Figure 4.4 represent applied shear which cannot be resisted by the concrete alone. At these locations, vertical reinforcement would need to be provided to prevent a shear failure. The spacing and amount of the vertical reinforcement would then be determined using existing ACI 318 provisions.

Table 4.1: V_c Calculation for Example Beam with Design Equation

Location from Left End (ft)	Nominal Shear, V_u (k)	Moment M_u (k-ft)	Neutral Axis Depth, c (in.)	Flexure-Shear Strength, V_{ci} (k)	Web-shear Strength, V_{cw} (k)
0.00	138.3	0	N/A	N/A	105.0
14.9	79.5	1215	33.9	83.3	105.0
17.0	71.1	1335	26.3	68.6	105.0
19.0	63.2	1436	22.0	60.0	105.0
21.0	55.3	1525	19.4	55.0	105.0
23.0	47.4	1602	17.8	52.0	105.0
25.0	39.5	1667	16.8	50.0	105.0
27.0	31.6	1720	16.2	48.9	105.0
29.0	23.7	1762	15.8	48.0	105.0
31.0	15.8	1792	15.5	47.5	105.0
33.0	7.9	1809	15.4	47.2	105.0
35.0	0.0	1815	15.3	47.1	105.0

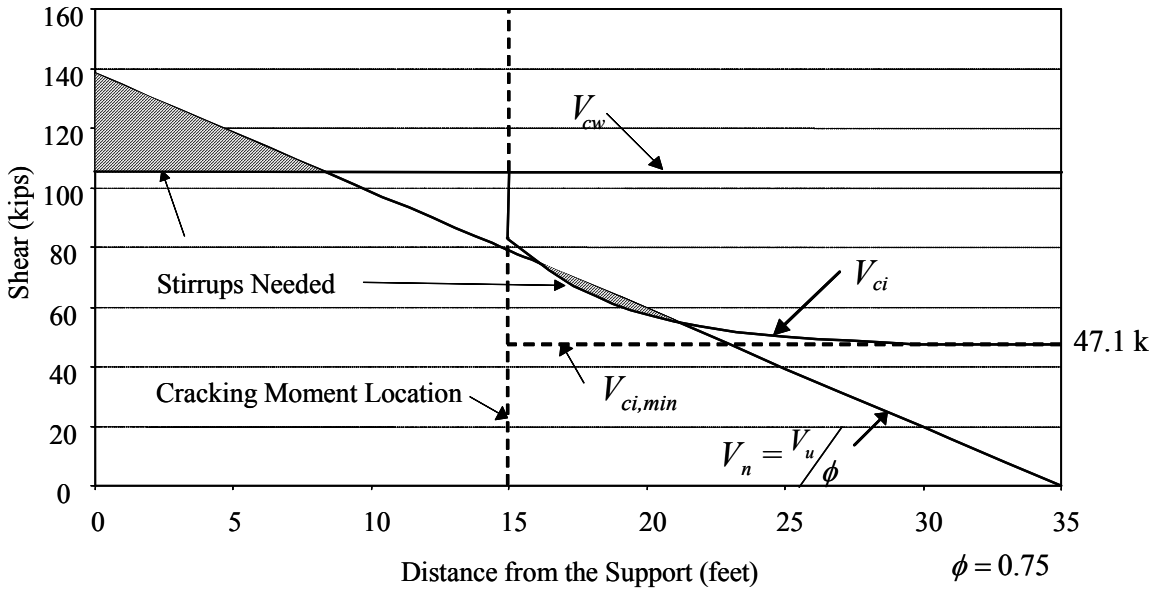

Figure 4.4: Design Equation Shear Strength for Example Beam

4.2.2 Minimum Shear Strength

An alternative flexure-shear strength is plotted on Figure 4.4 as $V_{ci,min}$. $V_{ci,min}$ represents the minimum V_{ci}, which is calculated at the maximum applied moment. This value can be taken as a lower bound shear strength for each point subjected to a moment greater than the cracking moment. Although using this method results in a lower shear strength than if the shear strength was calculated at multiple points, it provides a simple method to calculate shear strength.

4.2.3 Calculation of V_{cw}

As stated in Section 1.5.1, ACI 318 provides two methods to calculate the web-shear strength of prestressed concrete sections. The alternative approach discussed in ACI 318 Section 11.4.2.2 recommends using a principal stress analysis of an uncracked section. Using a tensile strength of $4\sqrt{f_c'}$, the web-shear strength of the section can be determined. The other method listed in ACI 318 Section 11.4.2.2 is provided by Equation 4.2 (ACI 318, Equation 11-12). This equation provides a simple approximation of the principal stress analysis (Lyn and Burns 1981).

$$V_{cw} = \left(3.5\sqrt{f_c'} + 0.3 f_{pc}\right) b_w d + V_p \qquad \text{(Eq. 4.2)}$$

To be consistent, the web-shear strength was calculated using the alternative approach recommended by ACI 318. This approach is identical to the theory which derived V_{ci} for the proposed shear model. The only discrepancy is that ACI 318 recommends using a tensile strength of $4\sqrt{f_c'}$, where the shear model was developed using a tensile strength of $6\sqrt{f_c'}$. Using the alternative approach, the web-shear strength was calculated as 105.0 kips. If Equation 4.2 were used, the corresponding web-shear strength would be 109.1 kips.

4.2.4 ACI 318 Shear Strength Design

To illustrate the differences between the design equation and the current approach used by ACI 318, the same beam was designed for shear using ACI 318. The shear strength was determined using ACI 318, Equation 11-10 (shown here as Equation 4.3) For Equation 4.3, M_{cr} must be determined using ACI 318, Equation 11-11 (shown here as Equation 4.4) at each point where the shear strength is to be calculated. Unlike the definition of M_{cr} for the proposed shear model, M_{cr} represents the moment which causes flexural cracking from externally applied loads alone.

$$V_{ci} = 0.6\sqrt{f_c'} b_w d + V_d + \frac{V_i M_{cr}}{M_{\max}} \geq 1.7\sqrt{f_c'} b_w d \qquad \text{(Eq. 4.3)}$$

$$M_{cr} = \frac{I}{y_t}\left(6\sqrt{f'_c} + f_{pe} - f_d\right) \qquad \text{(Eq. 4.4)}$$

The same twelve points used earlier were evaluated using ACI 318. Also, two additional points were used to evaluate the shear strength between the support and the cracking moment. The results are tabulated in Table 4.2. In Figure 4.5, the shear strength and applied shear are plotted to illustrate the results of Table 4.2. To be consistent, the alternative method discussed in ACI 318 was used to calculate the web-shear strength of the example beam.

Table 4.2: V_c Calculation for Example Beam with ACI 318

Location from Left End (ft)	Nominal Shear, V_u (k)	Moment M_u (k-ft)	Flexure-Shear Strength, V_{ci} (k)	Web-shear Strength, V_{cw} (k)
0.0	138.3	0	N/A	105.0
5.0	118.5	482	225.2	105.0
10.0	98.8	889	106.1	105.0
14.9	79.5	1215	66.8	105.0
17.0	71.1	1335	55.2	105.0
19.0	63.2	1436	47.0	105.0
21.0	55.3	1525	40.2	105.0
23.0	47.4	1602	34.3	105.0
25.0	39.5	1667	29.1	105.0
27.0	31.6	1720	24.4	105.0
29.0	23.7	1762	23.3	105.0
31.0	15.8	1792	23.3	105.0
33.0	7.9	1809	23.3	105.0
35.0	0.0	1815	23.3	105.0

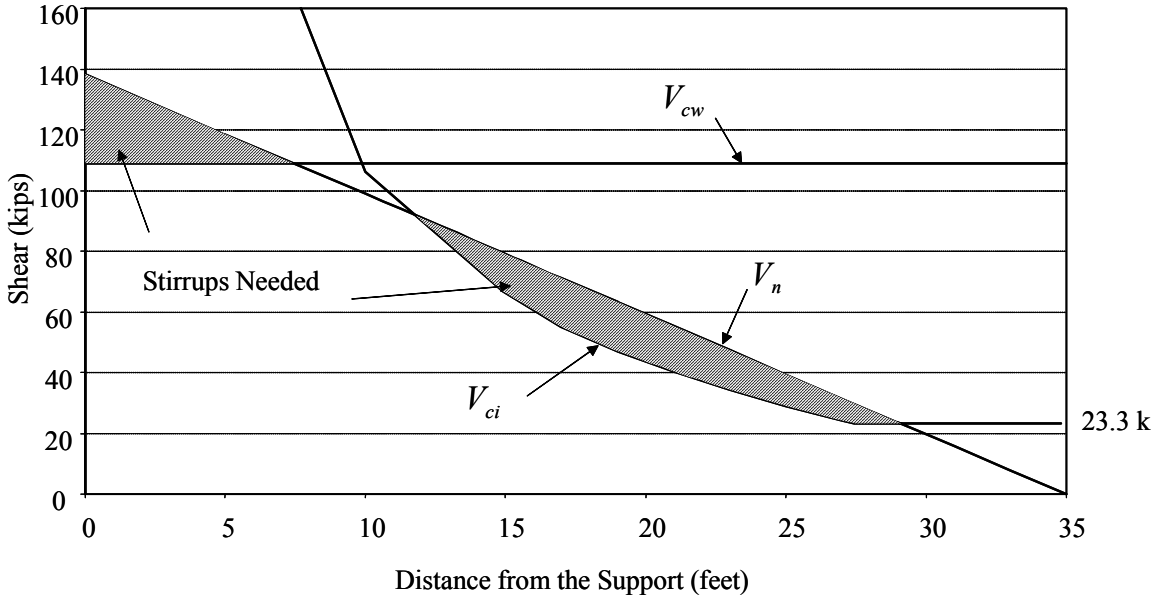

Figure 4.5: ACI 318 Shear Strength for Example Beam

4.2.5 Comparison of Design Methods

For either method, in order for the example beam to resist the design shear loads, stirrups must be provided. As V_{ci} begins to control the shear strength, the strength calculations of the two methods begin to differ. The design equation consistently calculates higher shear strength than the method used by ACI 318. Therefore, calculating the shear strength using the design equation would require less stirrups to resist the design shear loads.

A key difference between the two methods is at the transition where flexure-shear strength begins to control the shear strength design. When calculating shear strength using ACI 318, both V_{ci} and V_{cw} are calculated throughout the length of the beam, where the lesser of the two controls. The proposed design equation calculates shear strength differently. This equation considers that flexure-shear cracks begin as flexure cracks. With sufficient shear, these flexural cracks turn into flexure-shear cracks (MacGregor 1997; Lyn and Burns 1981; ACI 318-02). Flexure-shear failure is a direct result of flexure-shear cracks. Therefore, flexure-shear failure cannot occur where flexural cracks are not present, such as where the applied moment is less than the cracking moment. Consequently, the web-shear strength of the section is the controlling shear strength for locations where the applied moment is less than the cracking moment. At higher moments, the lesser of the flexure-shear and web-shear strength controls.

4.3 Prestressed Beam Database: Another Perspective

In the previous section, the design equation calculated consistently higher shear strengths for the example beam. In order to determine if the design equation would be conservative for design, the prestressed beam database was revisited.

In Chapter 3, to determine the performance of the design equation, each beam was treated as a test specimen, not as a beam used in design. Analytically, the beam was loaded to determine the load which would cause a flexure-shear failure. Beginning with the load which causes flexural cracks, for each load increment, the shear strength along the beam was determined. When the applied shear on the beam exceeded the shear strength at any point, the beam was considered to have failed due to flexure-shear. The corresponding shear was taken as the shear strength, V_{ci}.

In this section, the flexure-shear strength was determined based on the concentrated loads which ultimately failed the test specimen. A specimen from the database was chosen to illustrate this procedure.

Specimen A.11.43, shown in Figure 4.6, was a simply supported beam with a length of 9 feet. The beam was subjected to a single point load at midspan equal to its failure load, 24.3 kips. Along with the point load, the beam was also subjected to its self weight. The corresponding shear and moment diagrams are shown in Figure 4.7.

Figure 4.6: Example Beam A.11.43

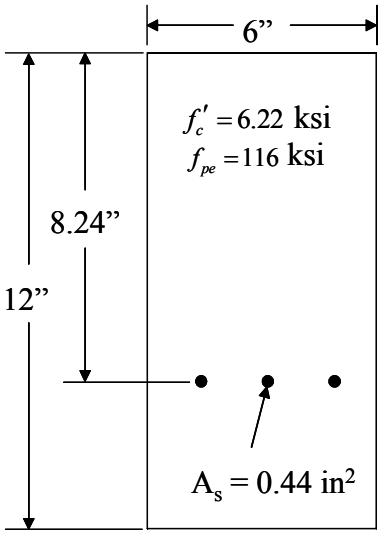

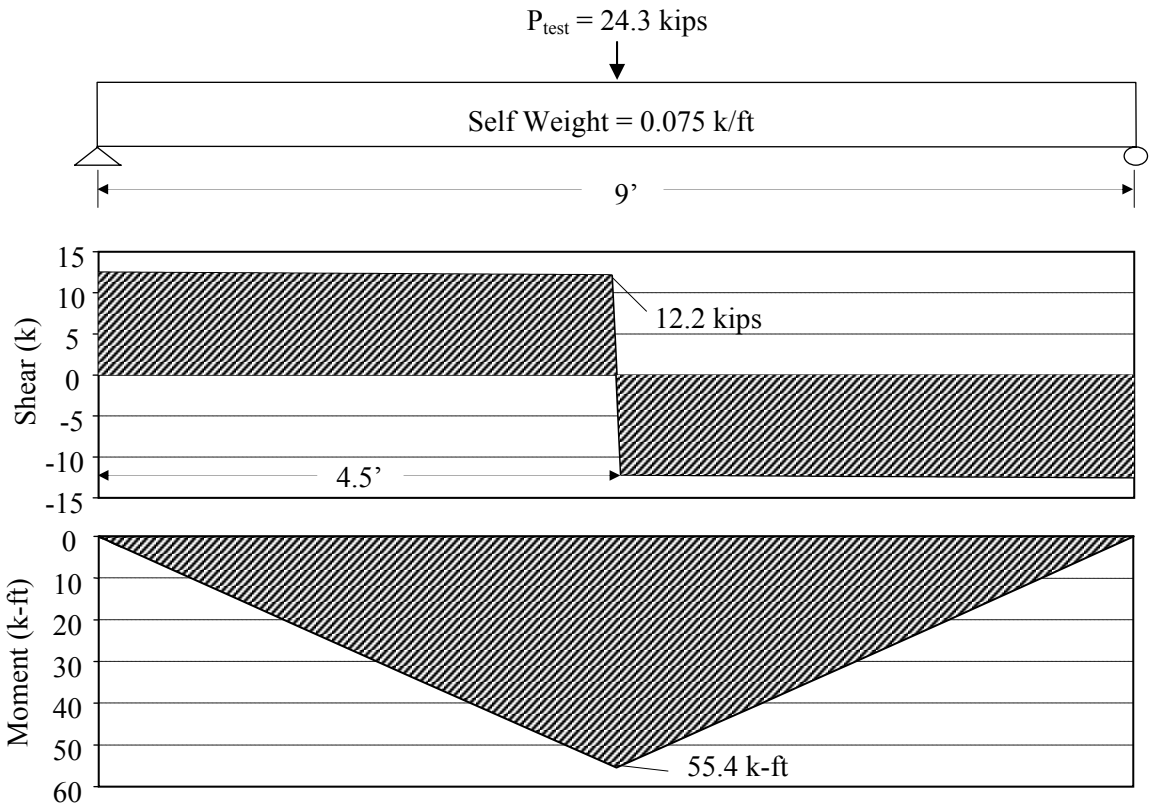

Figure 4.7: Shear and Moment Diagrams for Beam A.11.43 at Failure

4.3.1 Analysis Method

With the section properties and factored moments along the length of the beam known, the shear strength was calculated at 7 points along the beam. The locations of the points, along with other pertinent information, are provided in Table 4.3. Again, the shear strength is plotted on the half span along with the applied shear, in Figure 4.8.

As shown in Figure 4.8, the design equation would have calculated that the concrete could not support the load that ultimately caused the beam to fail. In design situations, ACI 318 would require that stirrups be provided if A.11.53 was designed for that loading.

On Figure 4.8, V_{ci} and $V_{ci,min}$ are again plotted to illustrate the difference between calculating the shear strength at multiple points along the beam and calculating one single minimum V_{ci} value. Examining the two shear strength curves, while not as accurate, the minimum shear strength provides a conservative, simple method to determine shear strength.

Table 4.3: V_c Calculation for A.11.43 with Design Equation

Location from Left End (ft)	Shear, V_{test} (k)	Moment M_{test} (k-ft)	Neutral Axis Depth, c (in.)	Flexure-Shear Strength, V_{ci} (k)	Web-shear Strength, V_{cw} (k)
0	12.5	0.0	N/A	N/A	27.3
2.0	12.3	24.8	7.88	18.6	27.3
2.5	12.3	31.0	5.52	13.1	27.3
3.0	12.3	37.1	4.41	10.4	27.3
3.5	12.2	43.3	3.93	9.3	27.3
4.0	12.2	49.4	3.72	8.8	27.3
4.5	12.2	55.4	3.67	8.7	27.3

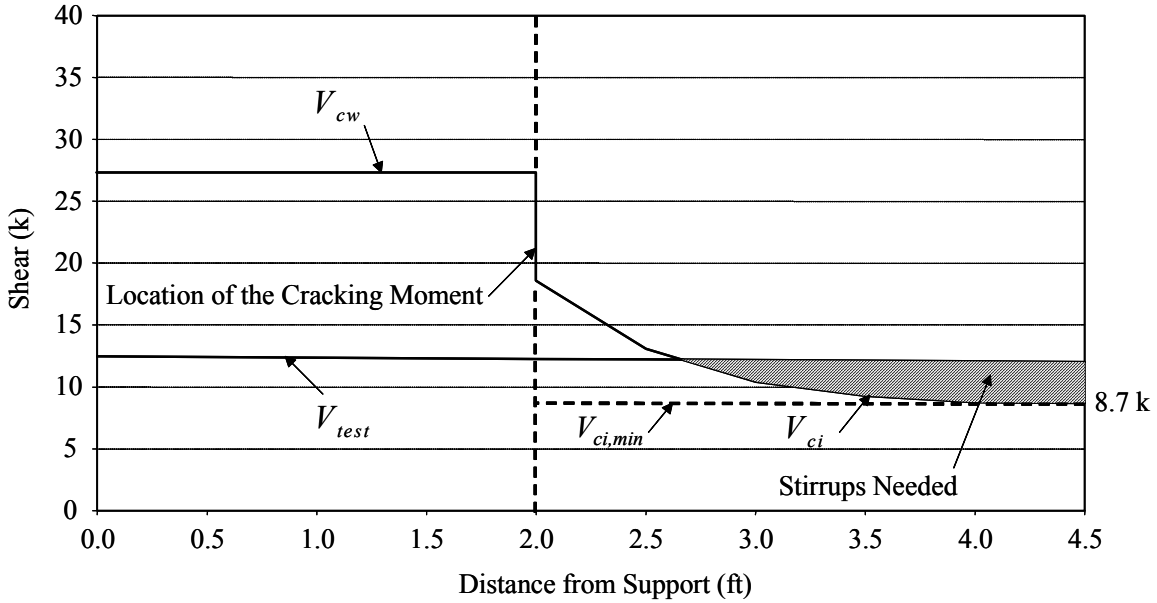

Figure 4.8: Design Equation Shear Strength for A.11.43 at Failure

4.3.2 Calculation of V_{cw}

Similar to Section 4.2 the web-shear was calculated using the alternative approach discussed in ACI 318.

4.3.3 ACI 318 Design

To determine the shear strength of A.11.43 using ACI 318, ten points along the half span were used. The pertinent data for the determination of the ACI 318 shear strength curve is given in Table 4.4. The method currently used by ACI 318 also conservatively calculates a flexure-shear failure for Specimen A.11.43, as shown in Figure 4.9.

4.3.4 Analysis of Prestressed Beam Database

Each specimen in the prestressed beam database was analyzed using the method described in this section to determine if both methods would have calculated flexure-shear failures. Figures 4.10 and 4.11 represent the effectiveness of each method, using the analyses performed in Section 4.3 on the prestressed database.

Table 4.4: V_c Calculation for A.11.43 with ACI 318

Location from Left End (ft)	Shear, V_{test} (k)	Moment M_{test} (k-ft)	Flexure-Shear Strength, V_{ci} (k)	Web-shear Strength, V_{cw} (k)
0.0	12.5	0.0	N/A	27.3
0.5	12.5	6.2	47.0	27.3
1.0	12.4	12.5	23.1	27.3
1.5	12.4	18.7	15.0	27.3
2.0	12.3	24.8	10.8	27.3
2.5	12.3	31.0	8.2	27.3
3.0	12.3	37.1	6.6	27.3
3.5	12.2	43.3	6.6	27.3
4.0	12.2	49.3	6.6	27.3
4.5	12.2	55.2	6.6	27.3

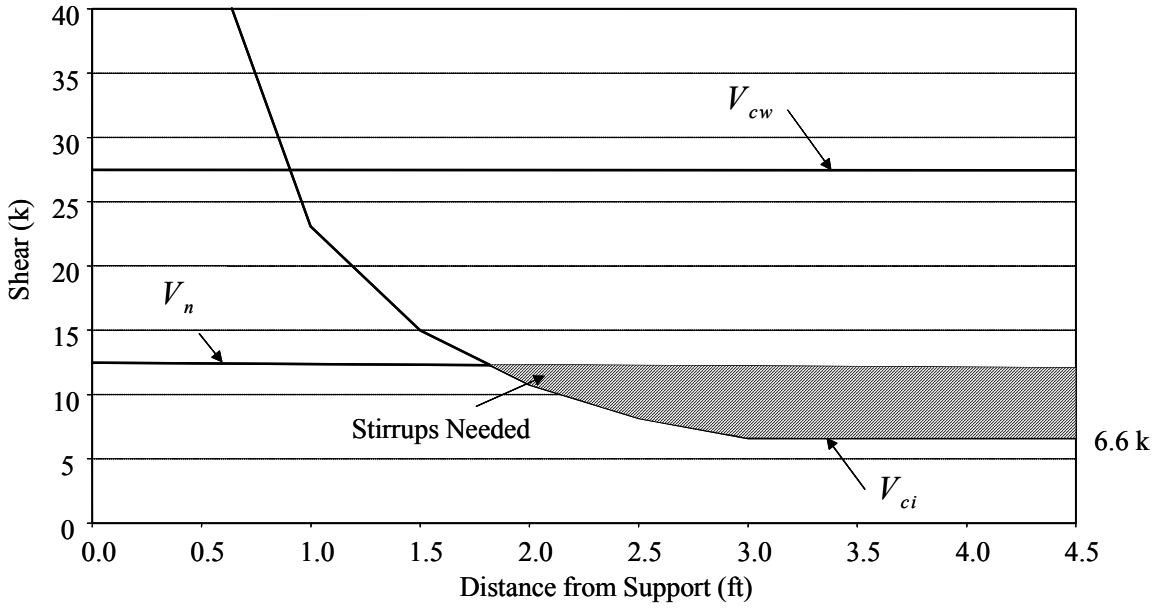

Figure 4.9: ACI 318 Shear Strength for A.11.43 at Failure

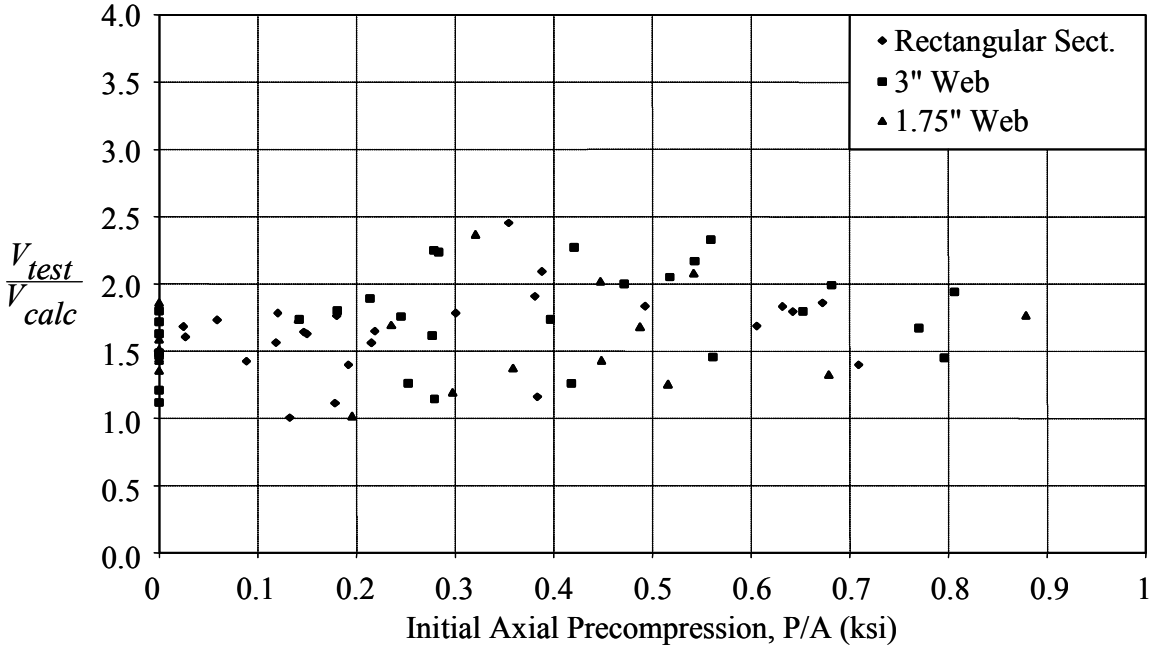

Figure 4.10: Performance of Design Equation at Failure

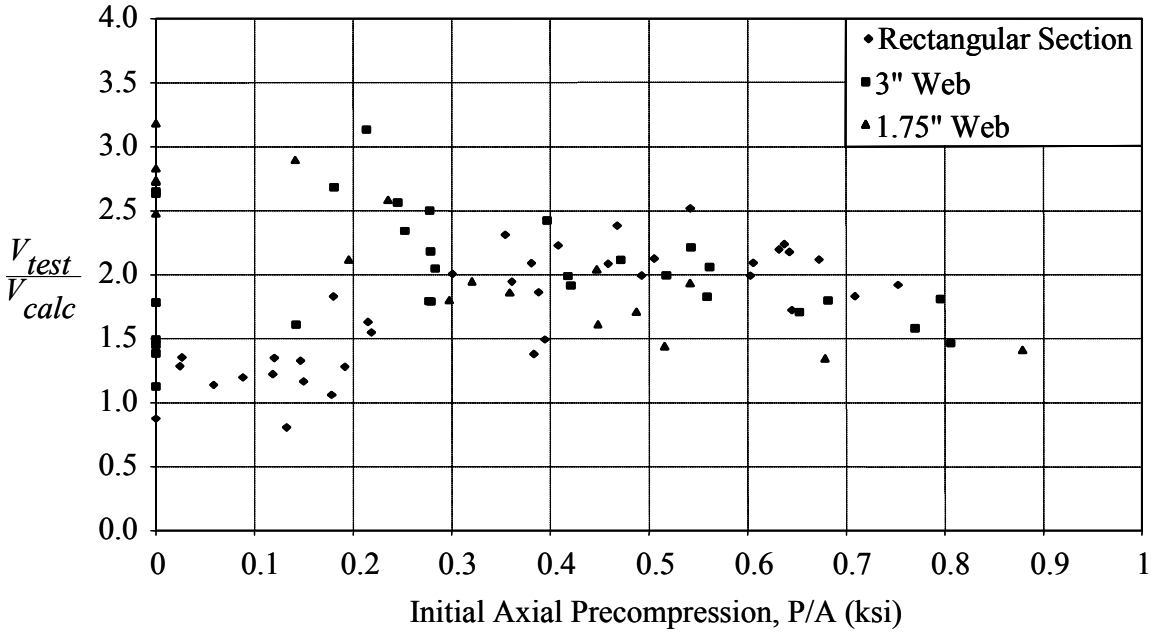

Figure 4.11: Performance of ACI 318 at Failure

4.4.5 Comparison of Design Methods

Both methods primarily yield conservative results for the calculation of shear strength for prestressed concrete members. However, ACI 318 does not calculate the shear strength of all the points conservatively. Also, the ACI 318 graph (Figure 4.11) has

a considerable amount of scatter within its results. Conversely, the design equation calculates the flexure-shear strength of the sections in the database consistently.

4.4 Conclusions

In this chapter, two analyses were used to illustrate the design process using both the current method provided in ACI 318 and the proposed design equation. Calculating shear strength using either method requires the calculation of approximately the same number of variables. However, the shear strengths calculated using the two methods can vary significantly, as shown in the design example.

In the second analysis, it was shown that design equation calculated the shear strength more accurately for the prestressed beam database. With increased accuracy, fewer stirrups would be required to resist the applied design shear.

CHAPTER 5
NEUTRAL AXIS DEPTH

5.1 Introduction

In the previous chapter, two beams were analyzed to illustrate the current ACI 318 and simplified shear model equations. In order to calculate the shear strength using the simplified shear model, the neutral axis depth must be calculated at points along the length of the beam. While the neutral axis depth can be readily computed by a strain-compatibility analysis, it is impractical to calculate this depth by hand for prestressed sections. To make the simplified method easier for design office use, a simple method to determine the neutral axis depth would prove useful. This chapter investigates a method to conservatively approximate the neutral axis depth at various moments for a given section.

5.2 Parametric Study of Neutral Axis Depths

A parametric study of neutral axis depths for various cross-sections was performed to determine a conservative approach to calculate the neutral axis depth. The main goal of this study was to determine an equation which can be used to estimate the neutral axis depth of a beam, regardless of its shape, size and material properties. The neutral axis depth is a function of many different variables; therefore, it was necessary to incorporate several variables into the parametric study. The variables in the study were the shape, concrete strength, effective depth, area of steel and effective prestress level.

a) *Cross-Section Shape:* A total of nine shapes were evaluated in the parametric study. Three rectangular cross-sections, all with widths of 6 in., had heights of 12 in., 18 in. and 24 in.. Along with the rectangular sections, the six standard AASHTO shapes were used.

b) *Concrete Strength:* The concrete strength for all shapes was varied. Concrete strengths of 3000, 5000 and 7000 psi were considered.

c) *Effective Depth:* The effective depth of each shape varied according to the overall height of the shape. Two effective depths were used for each rectangular section and three effective depths were used for each standard AASHTO sections. The largest effective depth was located 2 in. from the bottom of the beam. The remaining effective depths for each shape were spaced according to the centroid of the shape. An example of the effective depths of a typical rectangular section and AASHTO section are shown in Figure 5.1.

d) *Area of Steel Reinforcement:* The area of steel reinforcement for each shape was varied. Six different values related to the cross-sectional area of each shape were considered. The area of steel was considered as 0.125%, 0.25%, 0.5%, 1.0%, 1.5% and 2.0% of the entire cross-sectional area of each section.

e) *Effective Prestress Level:* Ten different values were used for the effective prestress level, f_{se}, for the various shapes. The f_{se} values used included: 0, 30, 45, 60, 80, 100, 115, 130, 145 and 160 ksi.

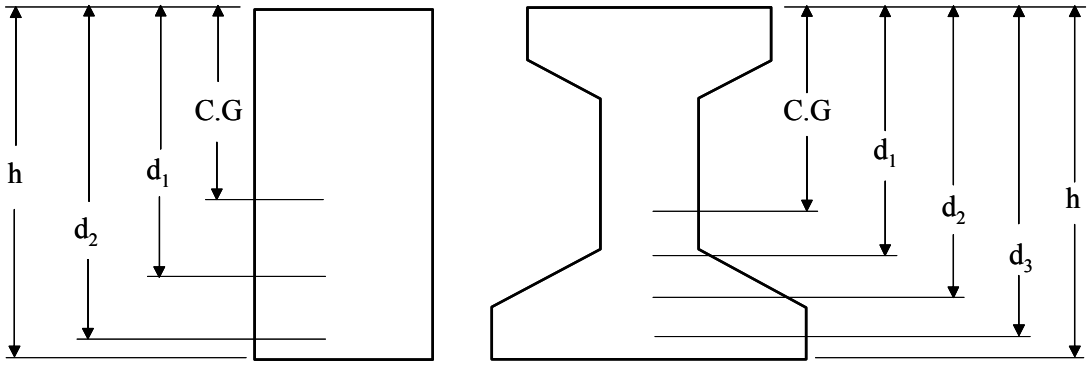

6x18 Rectangular Section

C.G = 9" d_1 = 12"

d_2 = 16" h = 18"

AASHTO Type III Section

C.G = 24.7" d_1 = 27" d_2 = 36"

d_3 = 43" h = 45"

Figure 5.1: Variation of Effective Depth

A total of 2,907 theoretical beams were analyzed to determine the neutral axis depths at various multiples of their cracking moment. The calculated neutral axes were normalized as a multiple of the nonprestressed, cracked section neutral axis. Of the 2,907 beams, only 2,182 beams were used to determine a simplified equation for the neutral axis depth. The criterion for the database was that each beam must have a flexural capacity greater than 1.2 times the cracking moment, or $1.2M_{cr}$. ACI 318 specifies that the flexural capacity of a beam must be at least 1.2 times the cracking moment, therefore, any specimen that did not comply was eliminated.

To determine the influence of each parameter, one parameter was varied while the other parameters were held constant. One value for each parameter was chosen as the control value. The control values for each parameter are shown in Table 5.1. Therefore, as one parameter was varied, the other parameters would be equal to their corresponding control values.

Table 5.1: Control Parameter Values

Parameter	Control Value
Concrete Strength	5000 psi
Effective Depth	2 in. from bottom of section
Area of Steel	0.25% A_g
Effective Prestress Level	80 ksi

5.2.1 Influence of Cross-Section Shape

For rectangular shapes, because the cross-sectional width is constant, the shape of the section does not influence the neutral axis depth significantly. However, for the AASHTO shapes, the varying widths along the depth of the cross-section influenced the neutral axis depth significantly. If the neutral axis is located in the upper flange at the cracking moment, the neutral axis depth will not decrease significantly, due to the large flange width, for increasing applied moment. However, if the neutral axis is located in the web at the cracking moment, the neutral axis depth may decrease at a substantial rate until it reaches the top flange, where the rate of change of the neutral axis depth decreases drastically.

5.2.2 Influence of Concrete Strength

While the flexural stress distribution on the section is linear, the concrete strength does not influence the neutral axis depth substantially. The primary influence of a higher concrete strength is an increased modulus of elasticity. The relationship between the concrete strength and modulus of elasticity, for normal weight concrete, is shown in Equation 5.1.

$$E_c = 57,000\sqrt{f_c'} \qquad \text{(Eq. 5.1)}$$

where:

E_c: Modulus of elasticity of concrete, psi

f_c': Concrete compressive strength, psi

For identical strain profiles, increasing the modulus of elasticity increases the compressive stress and subsequently the compressive force on the compression zone. Therefore, with more compressive force available, the neutral axis is not required to be as deep in a section with a higher compressive strength.

In Figure 5.2, the results of changing the concrete strength are illustrated. The top graph represents the normalized neutral axis depths at the cracking moment. The subsequent graphs represent moments equal to 1.25 and 1.5 times the cracking moment, respectively. As stated previously, while the concrete strength was varied, the other parameters were held constant at their control values. For clarity, only the "6x18" rectangular section, AASHTO Type II and Type IV girders are shown. Examining Figure 5.2, clearly there is a relationship between the neutral axis depth and concrete strength. As expected, for higher concrete strengths, the neutral axis depth decreases. Also, as the applied moment increases, the influence of the concrete strength on the neutral axis depth is less significant.

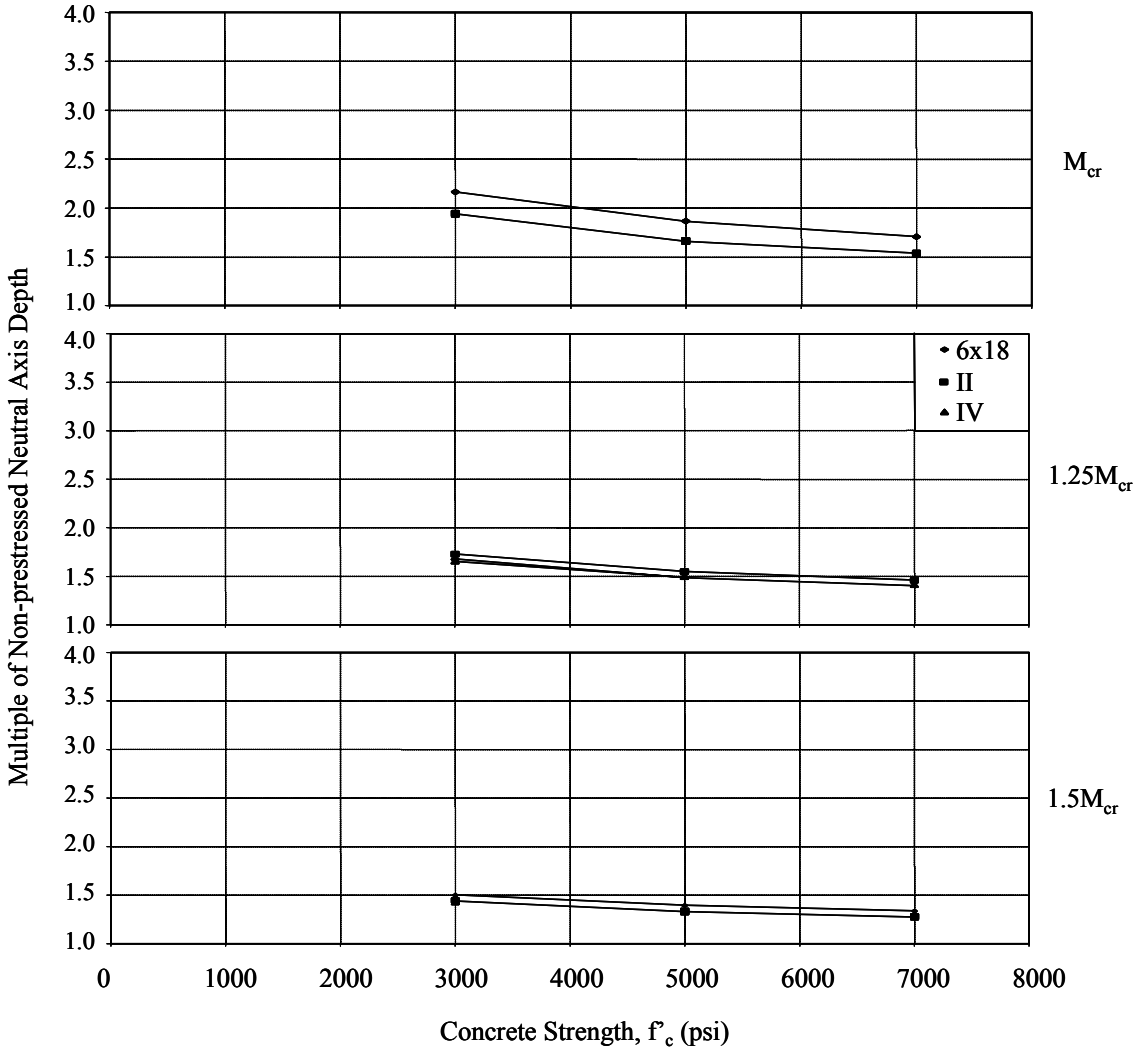

Figure 5.2: Influence of Concrete Strength

5.2.3 Influence of Effective Depth

The effective depth, along with the area of steel, was varied to represent possible strand patterns that could be implemented in beam design. The effective depth represents the location of the centroid of the tension reinforcement, which relates to the eccentricity of the longitudinal reinforcement. When the reinforcement is prestressed, it changes the moment which cracks the section by providing an initial compressive force on the bottom of the section. This compressive force prevents cracks from forming on the tension side of the beam.

The effective depth also defines the strain profile along the depth of the beam. The geometric relationship of the concrete strain at the top of the section and the longitudinal reinforcement stress at the effective depth determines the neutral axis depth. Figure 5.3 presents the influence of the variation of the effective depth, while other parameters are held constant. Once again, there are definite trends between the effective depth and the neutral axis depth, which level off with increased moments.

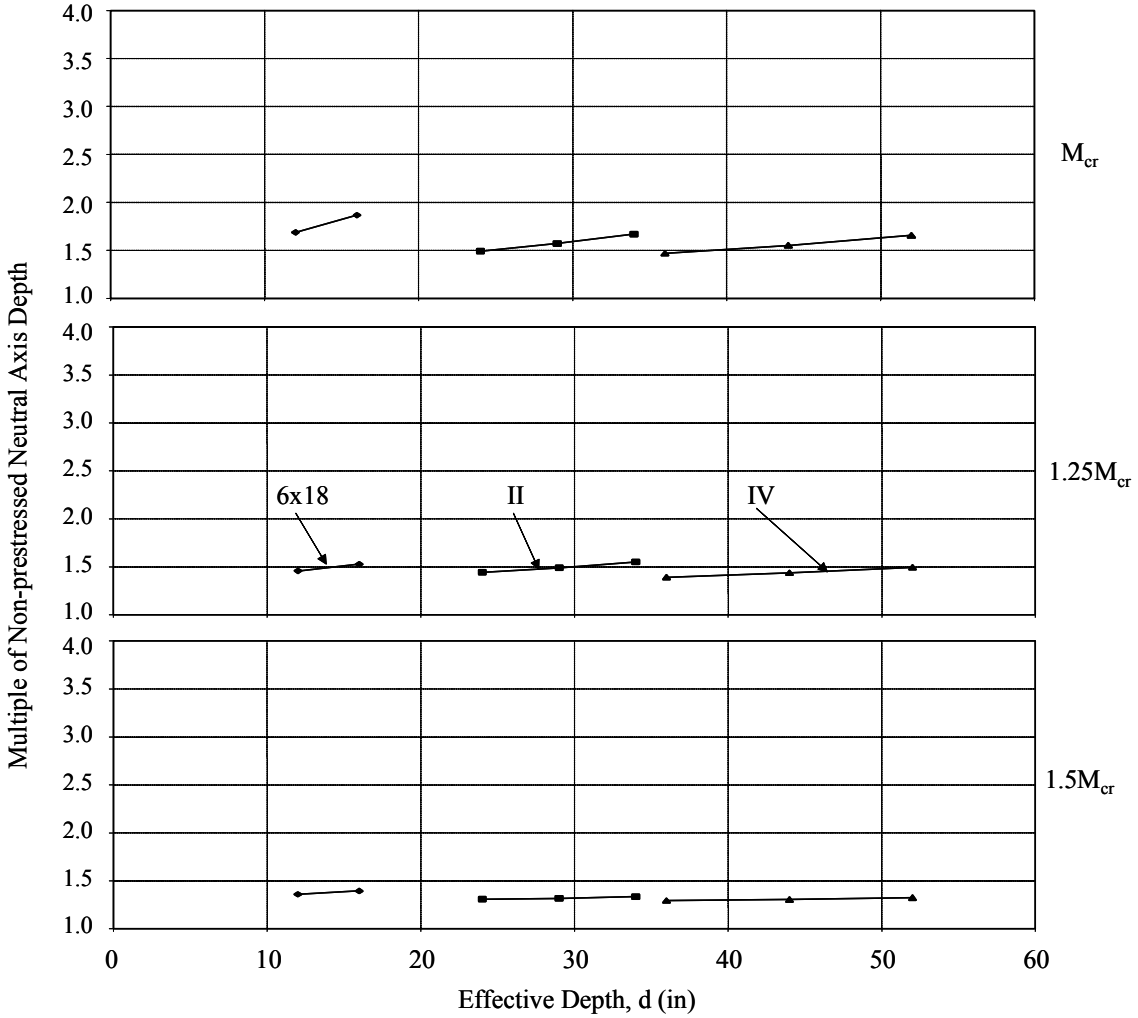

Figure 5.3: Influence of Effective Depth

5.2.4 Influence of Area of Steel Reinforcement

As stated earlier, the purpose of altering the area of steel and effective depth was to simulate the spectrum of possible strand patterns. This variation of the steel area influences the neutral axis significantly. An increase in the area of steel makes it possible to provide more tensile force at the bottom of the section, which in turn requires more compressive force to maintain equilibrium. To obtain an increased compressive force, a deeper neutral axis depth would be required.

The results of varying the area of steel are shown graphically in Figure 5.4. After examining the graphs, two points, one from the AASHTO Type II set and one from the AASHTO Type IV set, are not present on the $1.5M_{cr}$ graph. Between $1.25M_{cr}$ and $1.5M_{cr}$, these beams reached their flexural capacity.

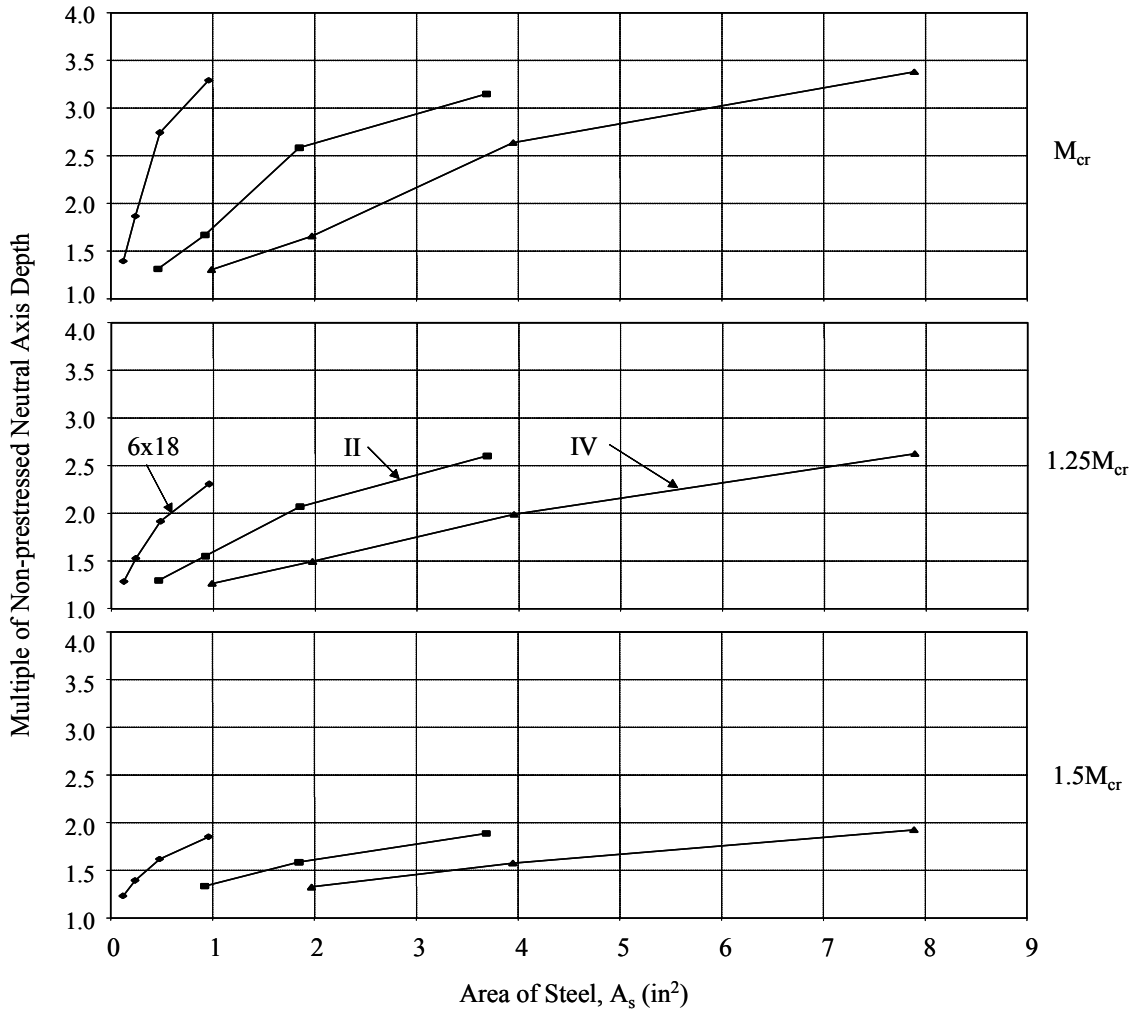

Figure 5.4: Influence of Area of Steel

5.2.5 Influence of Effective Prestress Level

Initially, only three values of effective prestress were used in the parametric study, but analyzing the data showed that the effective prestress level was a significant cause of variation for the neutral axis depth. Therefore, the study was expanded to include seven other effective prestress values. The effective prestress level, along with the area of steel, provides the initial tension in the section at the cracking moment which must be resisted by the compression zone to maintain equilibrium. Also, the initial prestressing causes the relationship between the concrete and steel stress to become complicated. When the section is not prestressed, the neutral axis can be calculated with a simple, closed-form equation. As shown in Chapter 2, prestressing the section creates a non-proportional relationship between concrete and steel stresses.

In Figure 5.5, the influence of varying the effective prestress level is shown. As expected, with a higher prestress level, and thus a higher tension force, the compression zone must be larger. At the cracking moment, the prestress level influences the neutral axis significantly, however, at higher moments, the influence of prestress level diminishes.

Once again, between $1.25M_{cr}$ and $1.5M_{cr}$, two test specimens from the AASHTO Type II and Type IV sets failed in flexure and a neutral axis depth could not be calculated at $1.5\ M_{cr}$. Another problem arises at high prestress levels and large applied moments. Yielding of the tension reinforcement causes the neutral axis depth to drop drastically to approximately the nonprestressed neutral axis depth. After the steel has yielded, the concrete strain must increase dramatically to produce a small increment of tensile stress increase. With the tensile stress incapable of increasing significantly, in order to produce a higher moment, the distance between the centroid of the tensile and compressive force must increase. This increase in moment arm is accomplished by shifting the neutral axis upward. This phenomenon predominantly occurred in sections with small amounts of steel and high prestress levels. In these sections, the tensile stress in the reinforcement is high, but with low areas of steel, the provided tensile force is small.

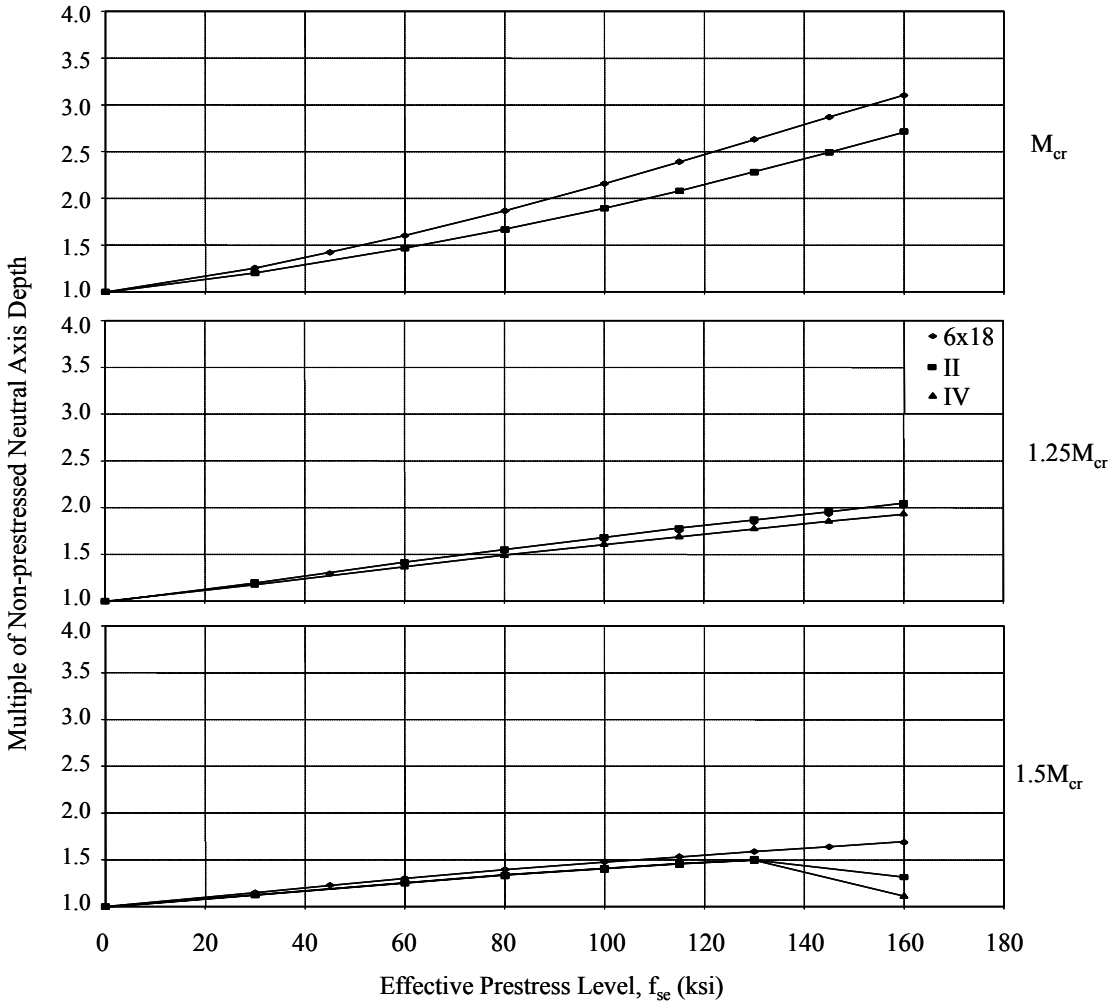

Figure 5.5: Influence of Effective Prestress Level

5.2.6 Conclusions of Parametric Study

As expected, each variable in the parametric study had an impact on the neutral axis depth. However, these effects diminished as the applied moment increased. At high

moments, the neutral axis depth of each section approaches the nonprestressed neutral axis of the cross-section. However, unless there is substantial nonlinearity in the concrete or steel stress, the neutral axis depth of prestressed sections cannot equal the nonprestressed neutral axis depth. The initial tension in the steel requires additional compression, thus a larger compression zone.

To determine a simple equation, which encompasses the shapes and properties of each beam, all the sections were plotted versus a variable that accounts for each parameter. The bottom fiber stress, f_{pe}, after the application of the effective prestressing force, which is shown in Equation 5.2, accounts for every parameter except for the concrete strength. In order to take the concrete strength into account, f_{pe} was divided by the concrete strength, as shown in Equation 5.3. This variable, the bottom fiber stress ratio (f_{per}), represents how near the bottom fiber stress is to the concrete compressive strength after the effective prestressing force is applied. The normalized neutral axis depths of all the sections are plotted versus this variable in Figures 5.6(a) and 5.6(b).

$$f_{pe} = \frac{f_{se}A_s}{A_c} + \frac{f_{se}A_s e}{S_b} \qquad \text{(Eq. 5.2)}$$

$$f_{per} = \frac{f_{se}A_s}{A_c f_c'} + \frac{f_{se}A_s e}{S_b f_c'} \qquad \text{(Eq. 5.3)}$$

At the cracking moment, although there is a trend in the data with increasing f_{per}, there is a significant amount of scatter at a value of f_{per} equal to approximately 0.2. Most of the erroneous points are members of the AASHTO Type V and Type VI sets. Due to the large upper flanges of these sections, the nonprestressed neutral axis is generally located in the upper flange. At the cracking moment, the neutral axis generally lies significantly below the upper flange, due to the thin web. However, increasing the moment to 1.25 times the cracking moment consolidates the data significantly. The neutral axis depth decreases rapidly until the neutral axis meets the upper flange. When the neutral axis is in the upper flange, it will not decrease significantly with additional moment. Examining subsequent moments, the data points continue to consolidate until a compact band forms. Therefore, at the cracking moment, it is difficult to estimate the neutral axis depth accurately, but with increasing moments, the accuracy increases.

Along with the data points, two lines are plotted in Figures 5.6(a) and 5.6(b). These lines represent approximate lower-bound estimates of the neutral axis depth, given as Equation 5.4. Using Equation 5.4, along with a critical shear stress of $5\sqrt{f_c'}$ and the effective overhang, provides a simple method to calculate shear strength. This simplification provides that only the applied moment influences the shear strength. Equation 5.4 provides a conservative, simple equation to calculate the neutral axis depth at various moments, regardless of the cross-section or properties of the beam.

$$c = \lambda c_{npt} \qquad \text{(Eq. 5.4)}$$

where:

$$\lambda = 1 + \frac{4}{v^2} f_{per} \le 1 + \frac{1.4}{v^2}$$

c_{npt}: nonprestressed neutral axis, in.

v: multiple of the cracking moment

f_{per}: bottom fiber stress ratio

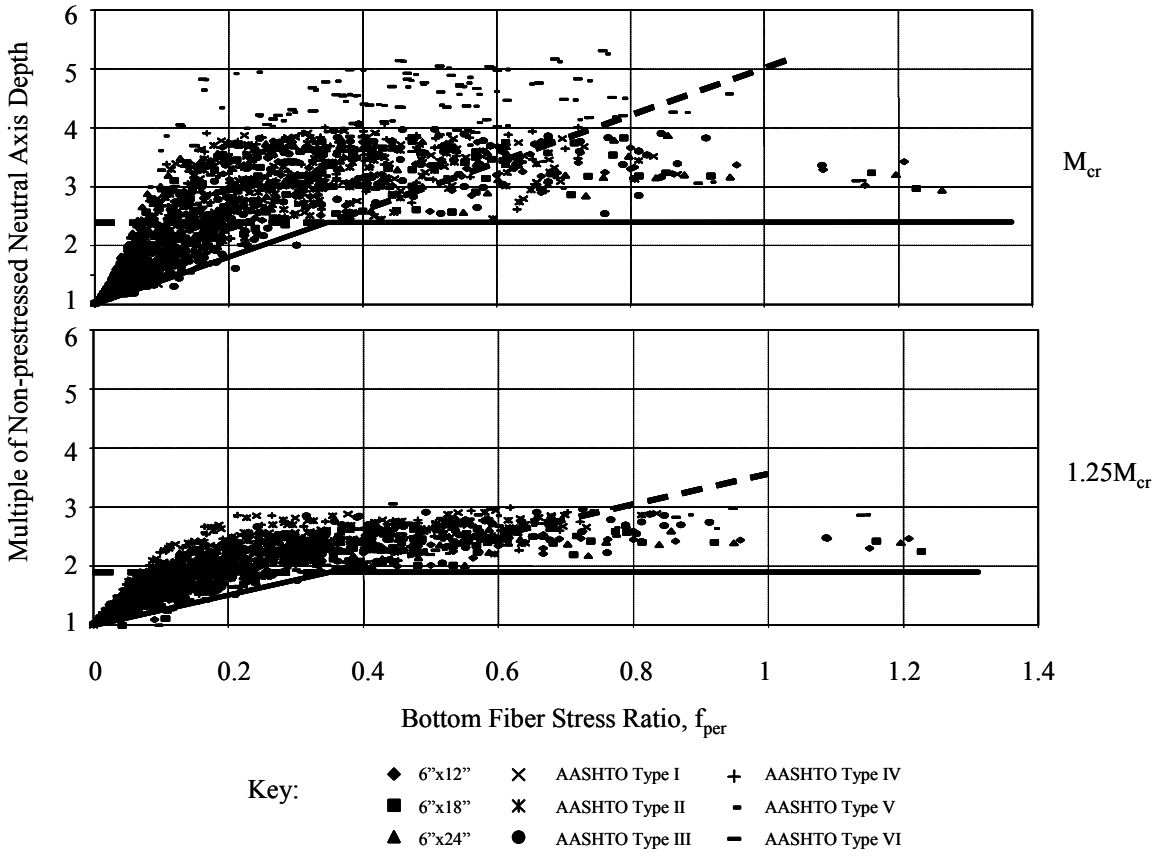

Figure 5.6(a): Parametric Study of Neutral Axis Depths for M_{cr} to $1.25M_{cr}$

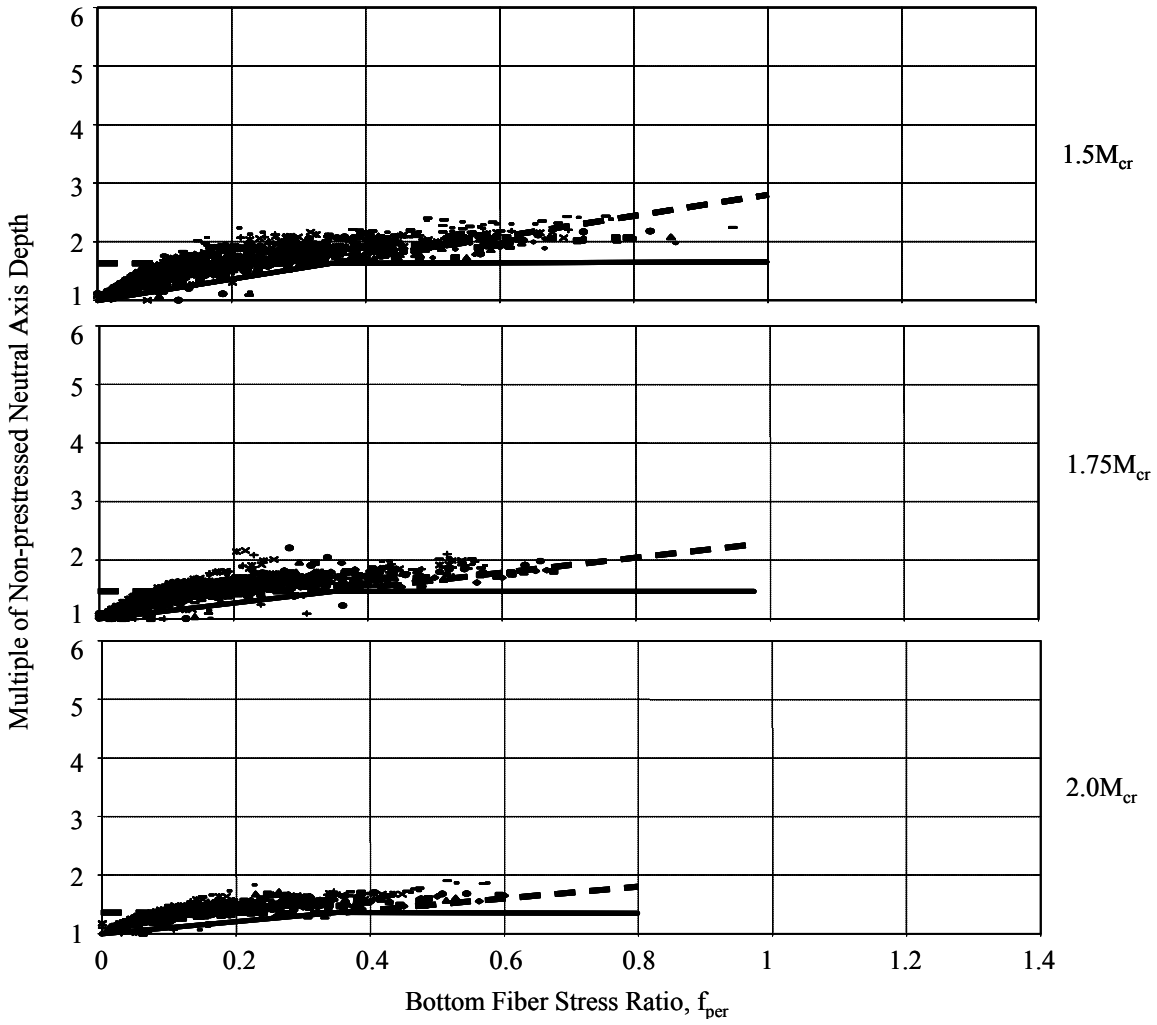

Figure 5.6(b): Parametric Study of Neutral Axis Depths for $1.5M_{cr}$ to $2.0M_{cr}$

5.3 Design of Example Beam Using Neutral Axis Depth Approximations

The example I-beam from Section 4.2 was used to clarify the design method using the neutral axis depth equation. Once again, the geometry of the section defines the flange contribution of the I-section, as shown in Figure 4.1. With the flange contribution known, only the neutral axis depth is required to be calculated to determine the shear strength of the section at a given point along the length of the beam.

The first calculation required is the nonprestressed neutral axis depth, which because of its geometry cannot be calculated using Equation 2.6. In order to calculate the nonprestressed neutral axis depth, the first moments of the compression zone and the transformed area of steel are taken to determine the neutral axis depth. For this particular case, the nonprestressed neutral axis lies just below the top flange, at 7.40 in. from the top of the section.

To calculate the cracking moment, the initial precompression of the bottom fiber must be calculated using Equation 5.2. To calculate the bottom fiber stress ratio, Equation 5.2 must be divided by the concrete strength, forming Equation 5.3. For this beam, the bottom fiber stress is 2.60 ksi, with a corresponding bottom fiber stress ratio of 0.52. By definition, the cracking moment is the moment required to overcome the initial compression and reach a bottom fiber stress of $7.5\sqrt{f_c'}$ in tension, which corresponds to the modulus of rupture. The calculated cracking moment for this beam is 1215 k-ft.

The applied moment from Figure 4.1 is used to calculate the neutral axis depth using Equation 5.4. Table 5.2 summarizes the calculations involved in calculating the shear strength using the neutral axis depth approximation. The shear strength is plotted along with the applied shear in Figure 5.7. The web-shear strength, which is shown in Figure 5.7, was calculated according to the alternate method of ACI 318, as explained earlier.

Table 5.2: Calculations of Shear Strength Using Neutral Axis Depth Approximations

Location from Left End (ft)	Nominal Shear, V_u (k)	Moment M_u (k-ft)	Multiple of Cracking Moment, v	Equation 5.4 - Neutral Axis Depth, c (in.)	Flexure-Shear Strength, V_{ci} (k)
0.00	138.3	0	N/A	N/A	N/A
14.9	79.5	1215	1.00	17.8	51.9
17.0	71.1	1335	1.10	16.0	48.4
19.0	63.2	1436	1.18	14.8	46.2
21.0	55.3	1525	1.26	14.0	44.5
23.0	47.4	1602	1.32	13.4	43.3
25.0	39.5	1667	1.37	12.9	42.4
27.0	31.6	1720	1.42	12.6	41.7
29.0	23.7	1762	1.45	12.3	41.3
31.0	15.8	1792	1.47	12.2	41.0
33.0	7.9	1809	1.49	12.1	40.8
35.0	0.0	1815	1.49	12.0	40.8

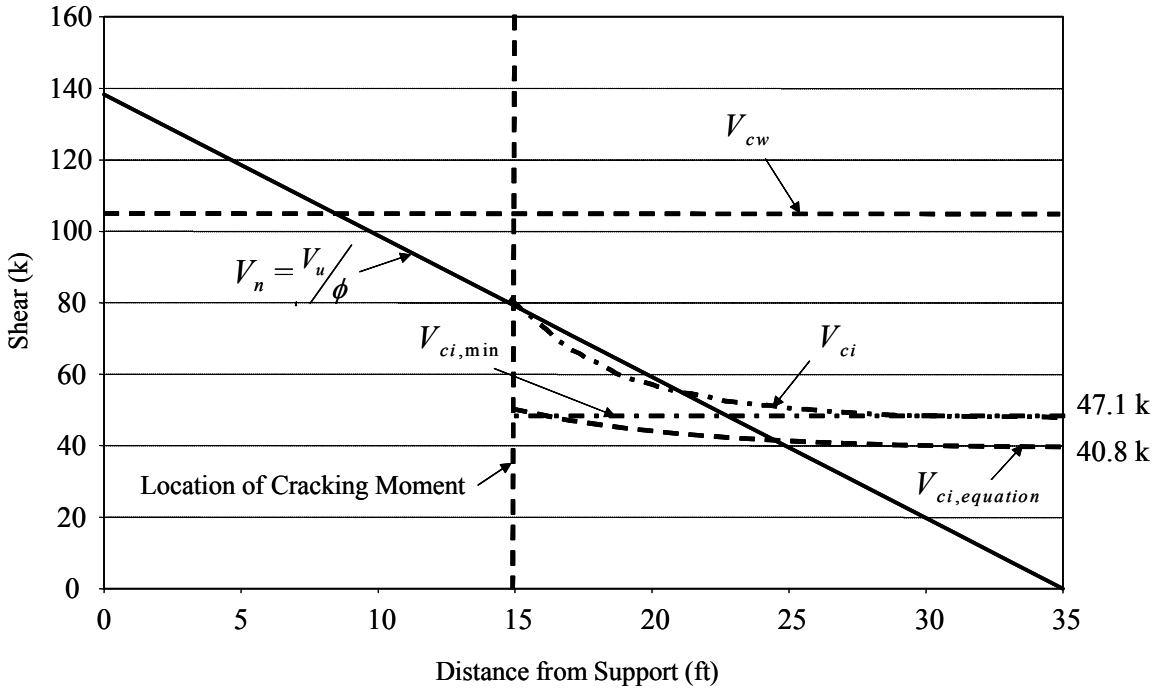

Figure 5.7: Shear Strength Diagram Using the Simplified Neutral Axis

There are three flexure-shear strengths plotted in Figure 5.7. V_{ci} represents the flexure-shear strength calculated using the actual neutral axis depth, found from a strain-compatibility analysis. $V_{ci,min}$ represents the minimum shear strength calculated for V_{ci}. Both of these shear strength curves were previously presented in Figure 4.4. The third flexure-shear strength curve, $V_{ci,equation}$ was determined using the neutral axis depth calculated from Equation 5.4.

The equation for the neutral axis depth approximation calculates a lower bound value for the neutral axis depth, which was based upon a multitude of sections. Therefore, by using Equation 5.4 there is added conservatism to the effective shear area. Consequently, the flexure-shear strength curve calculated using this approximation is more conservative than the curves using the actual neutral axis depth.

5.4 Evaluation of Prestressed Database with Neutral Axis Depth Approximation

In this section, the prestressed beam database was evaluated to determine how the approximation of the neutral axis depth affected the performance of the simplified shear model. Figure 5.8 shows the results of the simplified shear model using the approximated neutral axis depth. Table 5.3 presents the statistical results of the application of the approximate neutral axis depth to the simplified shear model. Along with the statistics for this method, the statistics for the previous three methods to determine shear strength are shown. The calculated values for flexural strength, web-shear strength and flexure-shear strength for each specimen in the prestressed database are given in Appendix B.

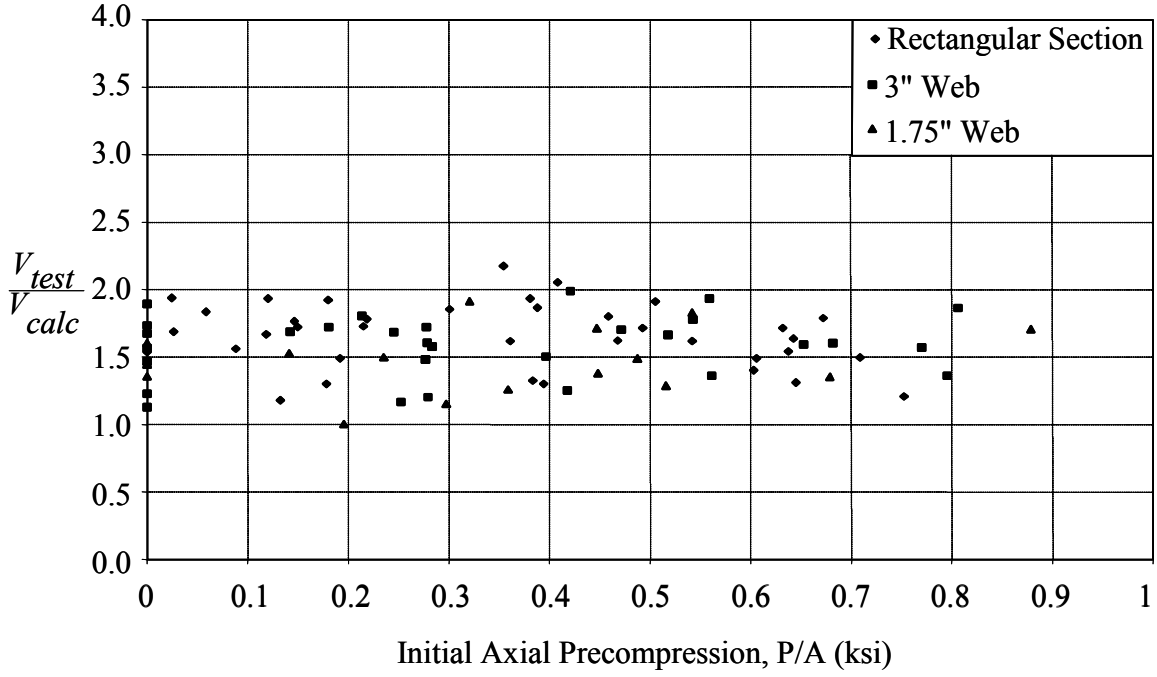

Figure 5.8: Performance of the Neutral Axis Approximation

Table 5.3: Performance of Various Design Methods

	Statistic	ACI 318	Shear Model	Design Equation – Actual N/A	Design Equation – N/A Equation
All	**All Sections**				
	Average	1.91	1.15	1.47	1.60
	ST DEV	0.508	0.203	0.221	0.244
	Correl	0.802	0.897	0.933	0.925
Section Shape	**Rectangular Sections**				
	Average	1.72	1.11	1.49	1.66
	ST DEV	0.461	0.160	0.215	0.241
	Correl	0.751	0.913	0.924	0.912
	I-Sections				
	Average	2.05	1.19	1.46	1.55
	ST DEV	0.500	0.226	0.227	0.238
	Correl	0.895	0.874	0.933	0.925
Prestress Level	**Prestressed Sections**				
	Average	1.75	1.11	1.48	1.66
	ST DEV	0.444	0.162	0.217	0.243
	Correl	0.783	0.875	0.919	0.907
	Nonprestressed Sections				
	Average	2.08	1.14	1.61	1.53
	ST DEV	0.743	0.209	0.234	0.222
	Correl	0.179	0.424	0.699	0.704

5.5 Conclusions of Neutral Axis Depth Approximations

In this chapter, an equation was developed to approximate the neutral axis depth based on two calculations: the nonprestressed neutral axis depth and the bottom fiber stress ratio. Using this equation, the shear strength of a prestressed concrete section can be easily determined. However, because of its derivation, the equation for the approximate neutral axis depth provides added conservatism to the shear strength design equation.

Ideally, it is recommended to calculate the shear strength based on the actual neutral axis depth for a given moment. However, if determining the actual neutral axis depth is impractical due to the number of calculations involved, the neutral axis depth can be approximated using Equation 5.4. Also, a single flexure-shear strength equal to the minimum shear strength calculated using the actual neutral axis depth provides a conservative, reasonable value for shear strength. As shown on Figure 5.7, the use of Equation 5.4 to calculate the neutral axis depth at numerous locations does not provide

better accuracy than using a single shear strength, $V_{ci,min}$. Therefore, the use of the approximate neutral axis depth can require more calculations and provide a less accurate shear strength than using $V_{ci,min}$.

CHAPTER 6
SUMMARY AND CONCLUSIONS

6.1 Introduction

Design methods for the shear resistance of reinforced and prestressed concrete beams are based on empirical evidence. As a result, different equations are used to calculate the shear strength of nonprestressed and prestressed beams. Research by Tureyen has proposed a model for the evaluation of shear strength based on equilibrium and principal stresses, where the entire shear is carried by the concrete compression zone. The application of this method to reinforced concrete has resulted in a simple, accurate approach for the determination of shear strength.

The objective of this research was to explore the applicability of this shear model to prestressed concrete and to investigate if a common design method could be developed for reinforced and prestressed sections.

6.2 Shear Model

The shear model was used to analyze a database of 84 specimens which were tested in shear. The combination of flexural and shear stresses in the compression zone of the cracked section were calculated and principal tension stresses were determined to evaluate the shear strength of the section. Through the analysis, it was concluded that the shear model is applicable to prestressed concrete sections and provides a method to calculate the flexure-shear strength of prestressed concrete. Consistent results were obtained over a range of initial axial precompression stresses.

6.3 Design Equation

Although the shear model is applicable to prestressed concrete, it is not a practical procedure for the calculation of shear strength. Several analyses were performed to simplify the model for rectangular and irregular cross-sections. The following conclusions were made from these investigations:

1) An average shear stress of $5\sqrt{f_c'}$, distributed over the compression zone, can be used to calculate the flexure-shear strength of prestressed sections. Therefore, the flexure-shear strength of prestressed concrete can be calculated according to:

$$V_{ci} = 5\sqrt{f_c'}A_{eff} \qquad \text{(Eq. 6.1)}$$

where:

f_c': compressive strength of concrete, psi

A_{eff}: effective shear resistance area, in^2

2) The effective shear resistance area (A_{eff}) accounts for the contribution of the flanges of I and T-sections to shear strength. The effective shear area is calculated using the web portion of the compression zone plus an additional effective overhang, as shown in Figure 6.1. The effective overhang flange width on each side of the web should not exceed 0.5 t_f.

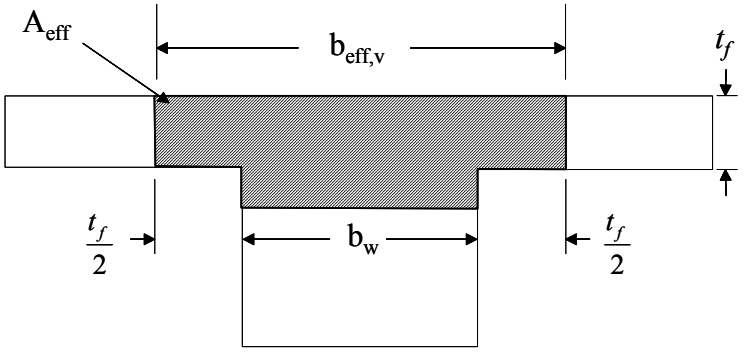

Figure 6.1: Definition of the Effective Shear Resistance Area

3) Analysis of the prestressed database indicates that the simplified design equation (Equation 6.1) accurately and consistently calculates the shear strength of prestressed sections for a wide range of effective prestress levels. This equation matches the equation proposed by Tureyen for the design of nonprestressed sections. Therefore, this research indicates that a single design equation can be used to evaluate the shear strength of both reinforced and prestressed concrete members.

6.4 Design Examples

An example beam design is presented in Chapter 4 to illustrate the design procedure using the proposed equation. For comparison, the example beam was also designed for shear using the current ACI 318 provisions. The following conclusions were made from this comparison:

1) The proposed shear model consistently calculates higher shear strengths than ACI 318. Therefore, the proposed design equation requires less transverse reinforcement than the current ACI provisions.
2) Although ACI 318 states that flexure-shear cracking is initiated by flexural cracking, the calculation of shear strength using ACI 318 provisions is not consistent. Using ACI 318, flexure-shear strength can control design even in portions of the beam which have a factored applied moment less than the cracking moment. Using the proposed design equation, flexure-shear strength is only calculated at sections where the factored applied moment exceeds the cracking moment.

6.5 Neutral Axis Calculation

For prestressed concrete sections, it is not practical to calculate the neutral axis depth by hand. To simplify this calculation, a parametric study was performed to investigate if a simple method could be obtained to estimate the neutral axis depth for a section at a given bending moment. The following conclusions were made from the parametric study:

1) The neutral axis depth is a function of several variables. Although each variable influences the neutral axis depth, the irregularity of cross-sectional shapes makes it virtually impossible to determine a single closed-form equation which encompasses all sections.
2) Equation 6.2 was developed which calculates a lower-bound value for the neutral axis depth based on the nonprestressed, cracked section neutral axis (c_{npt}) and bottom fiber stress ratio (f_{per}). Although this equation provides a simple method to calculate the neutral axis depth of a section at a given moment, because of its lower-bound empirical derivation, it can provide additional conservatism when used in design.

$$c = \lambda c_{npt} \qquad \text{(Eq. 6.2)}$$

where:

$$\lambda = 1 + \frac{4}{v^2} f_{per} \le 1 + \frac{1.4}{v^2}$$

c_{npt}: nonprestressed neutral axis

v: multiple of the cracking moment

f_{per}: bottom fiber stress ratio, $\frac{f_{pe}}{f_c'}$, ksi

6.6 Design Recommendations

It is recommended to calculate the flexure-shear strength using Equation 6.1 at multiple points along the length of the beam based upon the actual neutral axis depth calculated using a strain-compatibility analysis. If design simplification is desired, two alternative methods can be used to limit the number of calculations.

1) A single, uniform shear strength can be used for each point where the applied moment exceeds the cracking moment. This shear strength should be calculated based upon the neutral axis depth at the largest applied moment.
2) Using Equation 6.2, the neutral axis depth at points along the length of the beam can be approximated based upon the applied moment. The shear strength can be calculated based on the approximated neutral axis depths. Although conservative, it provides a simple method which can be easily calculated by hand.

Where the applied moment does not exceed the cracking moment, the current ACI 318 provisions can be used to calculate the web-shear strength of the section. These provisions are consistent with the development of the flexure-shear provision proposed here.

6.7 Future Work

The primary focus of this research was an analytical investigation of the proposed shear model considering existing data. Future research should investigate verification of the theories and simplifications used to determine the recommended design equation. Experimental studies of the impact caused by varying the neutral axis depth could prove useful in determining whether the majority of the applied shear is in fact resisted by the compression zone.

In addition, fabrication of prestressed sections using materials not considered in existing test data could prove useful to verify that the proposed shear model is not limited in its range of application. Recent materials, such as high strength concrete or fiber reinforced polymer bars (FRP), were not included in the original data which were the basis of the current ACI 318 and AASHTO 16th Edition provisions. As the proposed design method is based on mechanics, it is expected that this equation would be applicable to this extension. Therefore, construction of specimens with these differences should illustrate the range of applicability of the proposed design approach.

REFERENCES

AASHTO 16th Edition Specifications, 1996, "Standard Specifications for Highway Bridges," American Association of State Highway and Transportation Officials.

AASHTO LRFD, 1998, "AASHTO LRFD Bridge Design Specifications," American Association of State Highway and Transportation Officials.

ACI 318, 2002, "Building Code and Commentary (ACI 318-02)," American Concrete Institute, Farmington Hills, MI.

ASCE-ACI Committee 445, 1998, "Recent Approaches to Shear Design of Structural Concrete," *Journal of Structural Engineering*, Vol. 124, No. 12, American Society of Civil Engineers, Dec 1998, pp. 1375-1417.

Farmer, L., E. and Ferguson, P., M., 1967, "T-Beams under Combined Bending, Shear, and Torsion," *ACI Journal*, Vol. 64 No. 11, pp. 757-766.

Kani, M. W., 1979, *Kani on Shear in Reinforced Concrete*, Department of Civil Engineering University of Toronto, 225 pp.

Laupa, A., Siess, C., P. and Newmark, N., M., 1953, "Strength in Shear of Reinforced Concrete Beams," *Engineering Experiment Station Bulletin*, No. 428, University of Illinois.

Lyn, T.Y and Burns, N.H., 1981, *Design of Prestressed Concrete Structures*, Third Edition, John Wiley and Sons. 646 pp.

Placas, A. and Regan, E., P., 1971, "Shear Failure of Reinforced Concrete Beams," *ACI Journal, Proceedings*, Vol. 68, No. 10, pp 763-773.

MacGregor, J.G., 1997, *Reinforced Concrete: Mechanics and Design*, 3rd Edition, Prentice-Hall, Inc., New Jersey, 939 pp.

NCHRP Project 12-61, FY 2002, 2002 "Simplified Shear Design of Structural Concrete Members," National Cooperative Highway Research Program http://www4.nationalacademies.org/trb/crp.nsf/All+Projects/NCHRP+12-61.

Reineck, K.H, Kuchma, D.A., Kim, K.A, and Marx, S., 2003, "Shear Database for Reinforced Concrete Members without Shear Reinforcement," *ACI Structural Journal*, Vol. 100, No. 2, pp. 240-249.

Sozen, M.A., Zwoyer E.M. and Siess, C.P., 1959, "Strength in Shear of Beams without Web Reinforcement," *Engineering Experiment Station Bulletin*, No. 452, University of Illinois, 69 pp.

Tompos, E.J., 2000, *Influence of Beam Size and Stirrup Effectiveness on the Shear Strength of Reinforced Concrete Beams*, Master's Thesis, Purdue University, 84 pp.

Tureyen, A.K., 2000, *Influence of Longitudinal Reinforcement Type on the Shear Strength of Reinforced Concrete Beams without Transverse Reinforcement*, Ph.D Dissertation, Purdue University 185 pp.

Tureyen, A.K and Frosch, R. J., 2003, "Concrete Shear Strength: Another Perspective," ACI Structural Journal, (In Press).

APPENDIX A:
Prestressed Beam Database Properties

Title	Concrete Strength f'_c (psi)	Effective Depth d (in.)	Ultimate Load P_u (k)	Steel Area A_s (in2)	Shear Span a (in)	Effective Prestress f_{se} (ksi)	Web Width b_w (in.)	Web Height h_w (in.)	Overall Height h (in.)	Flange Width b_f (in.)	Flange Thickness t_f (in.)	Chamfer Depth c_d (in.)
A.11.43	6220	8.24	24.30	0.44	54	116	6	12	12	6	0	0
A.11.51	2900	8.44	13.85	0.249	54	114	6	12	12	6	0	0
A.11.53	4360	8.02	18.62	0.373	54	124.5	6	12	12	6	0	0
A.11.96	2900	8.41	18.79	0.467	54	116	6	12	12	6	0	0
A.12.23	5650	9.33	26.88	0.249	36	114.1	6.1	12	12	6.1	0	0
A.12.31	5800	8.64	26.55	0.311	36	114	6	12	12	6	0	0
A.12.34	7990	8.2	32.99	0.44	36	110	6	12	12	6	0	0
A.12.36	3440	9.19	21.52	0.232	36	113.9	6.1	12	12	6.1	0	0
A.12.42	6260	8.3	31.03	0.44	36	103.4	6	12	12	6	0	0
A.12.46	4660	8.2	27.93	0.352	36	131.4	6	12	12	6	0	0
A.12.53	3400	8.6	24.16	0.311	36	108.3	6	12	12	6	0	0
A.12.56	3790	8.59	26.39	0.362	36	120.5	6	12	12	6	0	0
A.12.69	2950	8.12	24.61	0.342	36	116	6.1	12	12	6.1	0	0
A.12.73	3550	8.44	28.04	0.44	36	104.3	6	12	12	6	0	0
A.12.81	2600	8.66	23.06	0.362	36	119.9	6	12	12	6	0	0
A.14.39	3350	8.35	28.95	0.218	24	117	6	12	12	6	0	0
A.14.44	3350	8.5	31.98	0.249	24	118	6	12	12	6	0	0
A.14.55	3320	8.53	36.25	0.311	24	117	6	12	12	6	0	0
A.14.68	2440	8.42	29.87	0.28	24	117.9	6	12	12	6	0	0
A.21.29	3350	8.45	8.00	0.156	54	61.1	6	12	12	6	0	0
A.21.39	3130	8.95	10.86	0.218	54	58.9	6	12	12	6	0	0
A.21.51	5630	8.12	17.15	0.467	54	59.1	6	12	12	6	0	0

Title	Concrete Strength f'_c (psi)	Effective Depth d (in.)	Ultimate Load P_u (k)	Steel Area A_s (in2)	Shear Span a (in)	Effective Prestress f_{se} (ksi)	Web Width b_w (in.)	Web Height h_w (in.)	Overall Height h (in.)	Flange Width b_f (in.)	Flange Thickness t_f (in.)	Chamfer Depth c_d (in.)
A.22.20	5350	8.45	14.47	0.176	36	61.2	6	12	12	6	0	0
A.22.24	3470	8.8	14.04	0.147	36	58.9	6	12	12	6	0	0
A.22.27	3850	8.38	13.86	0.176	36	60	6	12	12	6	0	0
A.22.28	3480	8.75	12.88	0.176	36	49.3	6.1	12	12	6.1	0	0
A.22.31	3530	8.06	14.91	0.176	36	89.4	6	12	12	6	0	0
A.22.34	4150	8.31	13.75	0.234	36	59	6	12	12	6	0	0
A.22.36	2890	8.35	14.7	0.176	36	88	6	12	12	6	0	0
A.22.39	2580	8.8	10.7	0.176	36	36.1	6	12	12	6	0	0
A.22.40	5790	8.2	26.39	0.381	36	72	6	12	12	6	0	0
A.22.49	4760	8.2	22.93	0.381	36	56.8	6	12	12	6	0	0
A.32.19	4990	9.03	11.34	0.176	36	0	6.1	12	12	6.1	0	0
A.32.22	4290	9.38	14.04	0.176	36	24	6	12	12	6	0	0
A.32.27	2800	9.16	12.48	0.176	36	10	6	12	12	6	0	0
A.32.37	6120	8.2	17.51	0.381	36	5	6	12	12	6	0	0
A.32.49	4760	8.2	20.9	0.381	36	34	6	12	12	6	0	0
B.11.20	4525	10.21	13.7	0.178	54	123.5	2.95	5.7	12	5.92	2.65	0.5
B.11.29	4190	10	17.14	0.239	54	124	2.95	5.7	12	5.95	2.65	0.5
B.11.40	4500	10	20.7	0.359	54	117	2.95	5.7	12	5.95	2.65	0.5

Title	Concrete Strength f'_c (psi)	Effective Depth d (in.)	Ultimate Load P_u (k)	Steel Area A_s (in2)	Shear Span a (in)	Effective Prestress f_{se} (ksi)	Web Width b_w (in.)	Web Height h_w (in.)	Overall Height h (in.)	Flange Width b_f (in.)	Flange Thickness t_f (in.)	Chamfer Depth c_d (in.)
B.12.10	5600	11.11	15.74	0.121	36	123	3.06	5.7	12	6	2.65	0.5
B.12.12	4570	11.13	16.85	0.121	36	125	3	5.7	12	6	2.65	0.5
B.12.14	3850	11.14	16.74	0.121	36	123	3	5.7	12	6	2.65	0.5
B.12.19	2890	11.09	17.18	0.121	36	122.2	2.98	5.7	12	6	2.65	0.5
B.12.26	4460	10.06	23.3	0.233	36	110	3.03	5.7	12	6.14	2.65	0.5
B.12.29	4180	9.76	25.1	0.238	36	121.7	3	5.7	12	6	2.65	0.5
B.12.34	4825	10.18	28.75	0.349	36	107.4	3.08	5.7	12	6.19	2.65	0.5
B.12.35	3210	9.99	22.78	0.238	36	121	3.08	5.7	12	6.3	2.65	0.5
B.12.50	2950	10.2	22.86	0.299	36	116	2.96	5.7	12	6	2.65	0.5
B.12.61	2980	9.9	23.86	0.359	36	114.5	3	5.7	12	6	2.65	0.5
B.13.16	5540	10.38	26.4	0.179	28	125.5	3	5.7	12	6	2.65	0.5
B.13.26	4600	10.03	28.85	0.239	28	124	2.94	5.7	12	6	2.65	0.5
B.13.41	4320	10.04	31.63	0.359	28	118.5	2.9	5.7	12	6	2.65	0.5
B.21.26	4470	10.21	12.3	0.238	54	62.3	2.96	5.7	12	6	2.65	0.5
B.22.09	6320	11.07	14.09	0.119	36	63.5	2.96	5.7	12	6	2.65	0.5
B.22.23	5120	10.03	18.6	0.238	36	55.3	3	5.7	12	6.05	2.65	0.5
B.22.30	2770	10.15	15	0.175	36	56.7	3.11	5.7	12	6.15	2.65	0.5
B.22.41	2710	10.02	17.4	0.233	36	51.2	3.16	5.7	12	6.25	2.65	0.5
B.22.65	1750	9.95	10.9	0.233	36	59.9	3.12	5.7	12	6.2	2.65	0.5
B.22.68	2670	9.9	18.87	0.359	36	59	3	5.7	12	6	2.65	0.5
B.31.15	5820	10.21	8.8	0.178	54	0	2.95	5.7	12	5.98	2.65	0.5

Title	Concrete Strength f'_c (psi)	Effective Depth d (in.)	Ultimate Load P_u (k)	Steel Area A_s (in2)	Shear Span a (in)	Effective Prestress f_{se} (ksi)	Web Width b_w (in.)	Web Height h_w (in.)	Overall Height h (in.)	Flange Width b_f (in.)	Flange Thickness t_f (in.)	Chamfer Depth c_d (in.)
B.32.11	5220	10.4	10.9	0.119	36	0	2.98	5.7	12	6	2.65	0.5
B.32.19	4330	10.21	10.5	0.175	36	0	3.12	5.7	12	6.16	2.65	0.5
B.32.31	2720	10.2	7.6	0.175	36	0	3.1	5.7	12	6.19	2.65	0.5
B.32.34	2510	10.11	9.67	0.178	36	0	3.2	5.7	12	6.26	2.65	0.5
B.32.41	3275	10.59	16	0.299	36	0	2.96	5.7	12	6	2.65	0.5
B.32.54	3200	10.38	14.45	0.358	36	0	2.78	5.7	12	6	2.65	0.5
C.12.09	6460	11.04	16.63	0.121	36	126	1.75	5	12	6	2.75	0.75
C.12.18	5310	9.69	18.09	0.187	36	113.7	1.75	5	12	6	2.75	0.75
C.12.19	6040	10.11	22.34	0.233	36	111.1	1.79	5	12	6	2.75	0.75
C.12.32	3620	9.86	16.3	0.233	36	103	1.86	5	12	6.17	2.75	0.75
C.12.33	5470	10.08	25.5	0.373	36	115.4	1.88	5	12	6.11	2.75	0.75
C.12.40	2390	9.69	12.1	0.187	36	115.5	1.75	5	12	6.1	2.75	0.75
C.12.44	2890	9.5	12.85	0.249	36	101.1	1.75	5	12	6.2	2.75	0.75
C.22.29	2490	10.4	9.25	0.116	36	60	1.84	5	12	6.19	2.75	0.75
C.22.31	2700	10.88	12.4	0.181	36	62	1.77	5	12	6	2.75	0.75
C.22.36	3300	10.23	10.9	0.241	36	60	1.86	5	12	6.07	2.75	0.75
C.22.39	2150	10.18	7.22	0.176	36	54.5	1.85	5	12	6.15	2.75	0.75
C.22.40	4620	9.85	17.99	0.373	36	88.8	1.75	5	12	6.2	2.75	0.75
C.22.46	3160	10.11	12.77	0.299	36	57.7	1.79	5	12	6.05	2.75	0.75
C.32.11	7310	11.06	10	0.179	36	0	1.77	5	12	6.14	2.75	0.75
C.32.22	3870	10	10.35	0.176	36	0	1.82	5	12	6.08	2.75	0.75
C.32.37	3060	10.01	9.28	0.233	36	0	1.83	5	12	6.14	2.75	0.75
C.32.42	2690	10.1	8.15	0.233	36	0	1.88	5	12	6.14	2.75	0.75
C.32.50	3230	10.68	10.6	0.356	36	0	1.84	5	12	6.1	2.75	0.75
C.32.80	3000	10	10.58	0.478	36	0	1.81	5	12	6	2.75	0.75

APPENDIX B:
Prestressed Beam Database Results

Table B.1: Results of Prestressed Beam Database Analyses

Title	V_{test}	V_{flex}	V_{cw}	ACI 318 V_{ci}	Shear Model V_{ci}	Design Equation V_{ci}	N/A Approx. V_{ci}
A.11.43	12.15	11.61	24.16	5.58	11.11	9.37	8.12
A.11.51	6.93	6.28	15.53	2.81	5.24	6.07	5.32
A.11.53	9.31	8.89	20.43	4.39	6.63	8.10	7.10
A.11.96	9.40	8.02	20.90	4.89	9.93	9.19	7.78
A.12.23	13.55	13.88	21.71	6.05	13.15	8.40	7.26
A.12.31	13.39	15.11	21.48	6.18	14.11	9.12	7.80
A.12.34	16.61	18.73	25.31	7.84	18.41	11.43	9.29
A.12.36	10.87	11.53	17.68	4.65	10.14	7.34	6.73
A.12.42	15.63	17.20	23.23	7.11	16.49	10.65	9.11
A.12.46	14.08	14.15	21.24	6.46	13.07	9.86	8.60
A.12.53	12.19	11.62	17.77	4.92	10.43	8.13	7.51
A.12.56	13.31	13.54	20.47	6.36	12.47	9.72	8.92
A.12.69	12.42	10.30	17.60	4.93	9.83	8.39	7.67
A.12.73	14.13	13.17	20.24	6.31	11.95	9.97	9.17
A.12.81	11.64	10.82	18.67	5.84	9.75	9.14	8.30
A.14.39	14.59	14.44	15.47	6.31	10.70	8.22	6.71
A.14.44	16.10	15.88	16.58	7.23	11.90	9.02	7.83
A.14.55	18.24	17.41	18.08	8.57	13.80	10.50	9.54
A.14.68	15.05	13.52	15.68	7.22	11.61	9.24	8.36
A.21.29	4.00	4.95	12.28	1.45	4.59	3.95	3.39
A.21.39	5.43	6.15	13.39	1.85	5.08	4.79	4.18
A.21.51	8.58	9.78	18.40	3.47	9.46	7.49	6.46
A.22.20	7.35	8.97	15.25	2.72	7.94	4.83	4.27
A.22.24	7.13	7.53	12.79	1.85	6.58	4.09	3.69
A.22.27	7.04	8.37	13.13	2.06	7.31	4.48	3.99
A.22.28	6.55	8.56	12.95	1.89	6.95	4.33	3.93
A.22.31	7.57	7.86	13.23	2.34	6.97	4.92	4.25
A.22.34	6.99	9.98	14.11	2.54	8.67	5.30	4.68
A.22.36	7.46	7.58	12.66	2.19	6.45	4.86	4.32
A.22.39	5.46	6.96	10.78	1.09	5.68	3.80	3.50
A.22.40	13.31	14.34	18.73	4.69	13.38	8.05	6.88
A.22.49	11.58	12.62	16.32	3.63	11.43	7.10	6.24
A.32.19	5.78	9.56	13.62	1.47	4.90	3.60	3.76
A.32.22	7.13	9.78	13.89	1.83	5.92	4.09	3.88
A.32.27	6.35	7.47	10.58	0.68	4.54	3.39	3.28
A.32.37	8.87	12.74	13.86	1.82	7.11	5.29	5.26
A.32.49	10.56	11.99	14.54	2.62	10.09	6.13	5.50

Title	V_{test}	V_{flex}	V_{cw}	ACI 318 V_{ci}	Shear Model V_{ci}	Design Equation V_{ci}	N/A Approx. V_{ci}
B.11.20	6.85	7.43	10.81	3.42	7.73	5.76	5.46
B.11.29	8.57	9.23	11.59	4.16	8.37	6.51	6.29
B.11.40	10.35	11.88	13.89	5.72	9.78	8.25	7.60
B.12.10	7.95	8.68	11.75	4.43	8.22	5.91	5.37
B.12.12	8.51	8.60	10.74	4.15	8.26	5.77	5.39
B.12.14	8.45	8.49	10.05	3.87	7.17	5.52	5.26
B.12.19	8.67	8.21	8.96	3.47	5.89	5.15	5.04
B.12.26	11.73	13.88	11.51	5.54	8.30	7.37	6.89
B.12.29	12.63	13.43	11.39	5.70	8.36	7.72	7.10
B.12.34	14.46	19.18	14.23	8.03	10.84	9.87	9.02
B.12.35	11.47	12.88	11.08	5.75	8.03	7.57	6.89
B.12.50	11.51	13.02	11.62	6.74	9.52	8.70	7.23
B.12.61	12.01	13.23	12.53	7.59	10.69	9.33	7.65
B.13.16	13.32	14.98	12.04	6.95	8.46	8.23	6.70
B.13.26	14.55	18.20	11.91	7.96	9.68	9.24	7.53
B.13.41	15.94	22.60	13.66	10.87	12.99	12.07	8.55
B.21.26	6.15	9.44	9.59	2.55	7.15	5.49	5.12
B.22.09	7.13	8.57	10.51	3.01	7.16	4.57	4.23
B.22.23	9.38	14.24	9.76	3.38	9.63	5.96	5.58
B.22.30	7.58	9.76	7.57	2.14	6.82	4.54	4.40
B.22.41	8.78	10.33	7.89	2.48	5.82	4.97	4.87
B.22.65	5.53	7.37	6.98	2.36	5.14	4.73	4.74
B.22.68	9.52	10.99	8.91	3.93	7.02	6.46	6.33
B.31.15	4.40	7.59	8.04	1.01	5.02	3.71	3.90
B.32.11	5.53	7.90	7.84	1.04	4.26	3.04	3.19
B.32.19	5.33	10.86	7.34	0.85	4.62	3.46	3.63
B.32.31	3.88	8.86	5.77	0.27	3.97	3.03	3.17
B.32.34	4.92	8.39	5.67	0.22	3.92	3.01	3.14
B.32.41	8.08	12.42	6.28	0.43	4.95	4.05	4.26
B.32.54	7.31	12.24	5.71	0.32	5.19	4.15	4.36

Title	V_{test}	V_{flex}	V_{cw}	ACI 318 V_{ci}	Shear Model V_{ci}	Design Equation V_{ci}	N/A Approx. V_{ci}
C.12.09	8.39	8.71	7.29	4.31	8.08	5.48	4.38
C.12.18	9.12	11.22	6.60	4.47	7.61	5.85	5.32
C.12.19	11.24	14.55	7.88	5.81	6.64	7.16	6.14
C.12.32	8.22	12.97	6.64	4.81	5.85	6.08	5.53
C.12.33	12.82	20.91	10.05	9.07	10.25	10.27	7.52
C.12.40	6.12	9.03	5.21	3.80	4.85	5.10	4.44
C.12.44	6.50	10.86	5.77	4.51	5.69	5.82	5.05
C.22.29	4.70	7.22	4.18	1.41	5.83	3.09	3.08
C.22.31	6.27	10.83	4.86	2.43	4.44	4.20	4.19
C.22.36	5.52	12.50	5.56	3.06	4.83	4.91	4.79
C.22.39	3.68	8.29	4.19	1.74	5.00	3.66	3.67
C.22.40	9.07	17.82	7.70	6.73	7.82	7.98	6.70
C.22.46	6.46	12.40	5.53	3.47	4.85	5.30	5.13
C.32.11	5.07	12.76	5.86	1.23	5.54	3.28	3.46
C.32.22	5.25	10.39	3.96	0.36	4.40	2.65	2.77
C.32.37	4.71	10.24	3.55	0.15	4.49	2.81	2.94
C32.42	4.15	9.52	3.45	0.06	4.31	2.75	2.87
C.32.50	5.37	13.26	3.91	0.24	5.28	3.55	3.73
C32.80	5.36	11.61	3.47	0.10	5.51	3.78	3.95